VALUE ENGINEERING AND COST EFFECTIVENESS OF VARIOUS FIBER REINFORCED POLYMER (FRP) REPAIR SYSTEMS

By

Sami Rizkalla
Principal Investigator

Owen Rosenboom
PhD Candidate

Anthony Miller
Graduate Research Assistant

Research Project 2004-15

Final Report

In cooperation with the

North Carolina Department of Transportation

And

Federal Highway Administration
United States Department of Transportation

Department of Civil Engineering
North Carolina State University
Raleigh, NC 27695-7908

June 2005

Technical Report Documentation Page

1. Report No. **FHWA/NC/2006-27**	2. Government Accession No.	3. Recipient's Catalog No.
4. Title and Subtitle **Value Engineering and Cost Effectiveness of Various Fiber Reinforced Polymer (FRP) Repair Systems**		5. Report Date **June 2005** 6. Performing Organization Code
7. Author(s) **Sami Rizkalla, Owen Rosenboom, and Anthony Miller**		8. Performing Organization Report No.
9. Performing Organization Name and Address **Department of Civil Engineering** **North Carolina State University** **Raleigh, NC 27695-7908**		10. Work Unit No. (TRAIS) 11. Contract or Grant No.
12. Sponsoring Agency Name and Address **North Carolina Department of Transportation** **Research and Analysis Group** **1 South Wilmington Street** **Raleigh, North Carolina 27601**		13. Type of Report and Period Covered **Final Report** **7/1/2003 – 6/30/2005** 14. Sponsoring Agency Code **2004-15**
Supplementary Notes:		

16. Abstract

Seventeen 40 year old C-Channel type prestressed concrete bridge girders and one impact damaged AASHTO Type II prestressed concrete girder were tested under static and fatigue loading to determine the cost-effectiveness and value engineering aspects of various Fiber Reinforced Polymer (FRP) repair and strengthening systems. Of the C-Channel girders, which were taken from two different 40 year old bridges in Eastern North Carolina, three were tested as control girders (one statically loaded to failure, and two tested under fatigue loading) and fourteen tested with various Carbon FRP strengthening systems (eight statically loaded to failure and six tested under fatigue loading). The fatigue loading applied to the strengthened C-Channel girders was chosen to simulate a specified increase in live load value in comparison to the control girders.

An AASHTO Type II prestressed concrete bridge girder was taken from a bridge near Fayetteville, NC which was struck by an overheight vehicle. The girder had significant damage to the concrete and one ruptured prestressing strand near midspan. The concrete section was restored and the girder was repaired with Carbon FRP. The repaired AASHTO girder survived 2 million cycles of loading designed to simulate the original service load of the girder with little degradation. The ultimate load observed during a test to failure was 13.3 percent higher than the predicted value of the original girder.

The experimental program and analysis of the test results demonstrate that FRP systems can effectively strengthen deficient prestressed concrete members and/or repair damaged prestressed girders.

17. Key Words Fiber Reinforced Polymers, Prestressed Concrete, Flexural Behavior, Repair, Strengthening, Impact Damage, Fatigue	18. Distribution Statement		
19. Security Classif. (of this report) Unclassified	20. Security Classif. (of this page) Unclassified	21. No. of Pages 201	22. Price

Form DOT F 1700.7 (8-72) **Reproduction of completed page authorized**

DISCLAIMER

The contents of this report reflect the views of the authors and not necessarily the views of the University. The authors are responsible for the facts and the accuracy of the data presented herein. The contents do not necessarily reflect the official views or policies of either the North Carolina Department of Transportation or the Federal Highway Administration at the time of publication. This report does not constitute a standard, specification, or regulation.

ACKNOWLEDGEMENTS

The authors would like to acknowledge the support of the North Carolina Department of Transportation through Project 2004-15, the National Science and Engineering Research Council of Canada and the National Council of Scientific and Technological Development (CNPq), Brazil. Several industry members made much appreciated donations: David White of the Sika Corporation, Doug Gremel of Hughes Brothers, Akira Nakagoshi of Mitsubishi Chemical America, Peter Emmons of Structural Preservation Systems and Ed Fyfe of Fyfe Corporation. Special thanks to Structural Preservation Systems and Fyfe Corporation for carrying out the strengthening and repair work. Thanks are also extended to the personnel at the NCDOT Bridge Maintenance Department, especially Dallie Bagwell and Tracy Stephenson for providing Bridge Maintenance facilities and constructing steel substructures for the repair and strengthening work. The authors would like to thank Jerry Atkinson and Bill Dunleavy, technicians at the Constructed Facilities Laboratory at North Carolina State University, for their invaluable help.

SUMMARY

Seventeen 40 year old C-Channel type prestressed concrete bridge girders and one impact damaged AASHTO Type II prestressed concrete girder were tested under static and fatigue loading to determine the cost-effectiveness and value engineering aspects of various Fiber Reinforced Polymer (FRP) repair and strengthening systems. Of the C-Channel girders, which were taken from two different 40 year old bridges in Eastern North Carolina, three were tested as control girders (one statically loaded to failure, and two tested under fatigue loading) and fourteen tested with various Carbon FRP strengthening systems (eight statically loaded to failure and six tested under fatigue loading). The fatigue loading applied to the strengthened C-Channel girders was chosen to simulate a specified increase in live load value in comparison to the control girders.

An AASHTO Type II prestressed concrete bridge girder was taken from a bridge near Fayetteville, NC which was struck by an overheight vehicle. The girder had significant damage to the concrete and one ruptured prestressing strand near midspan. The concrete section was restored and the girder was repaired with Carbon FRP. The repaired AASHTO girder survived 2 million cycles of loading designed to simulate the original service load of the girder with little degradation. The ultimate load observed during a test to failure was 13.3 percent higher than the predicted value of the original girder.

The experimental program and analysis of the test results demonstrate that FRP systems can effectively strengthen deficient prestressed concrete members and/or repair damaged prestressed girders.

TABLE OF CONTENTS

LIST OF TABLES

LIST OF FIGURES

1 INTRODUCTION

1.1 Background

Damage due to impact of prestressed concrete bridges continues to be one of the major problems facing the Bridge Maintenance Department at the North Carolina Department of Transportation (NCDOT). The damage results in large financial burdens on the maintenance budget, negative psychological effects on highway users, long traffic delays during maintenance, potential safety hazards, and reduced service life of bridges. Additionally, many prestressed concrete bridges are in need of upgrading in order to increase their posted capacities. In response to considerable consultation with NCDOT, a research project with practical goals was initiated to evaluate the cost-effectiveness and value engineering of Carbon Fiber Reinforced Polymer (CFRP) repair and strengthening systems.

The use of CFRP began after WWII in military high performance applications. Use within the civil infrastructure, either as a retrofit material or in construction of new structures, gained popularity in the 1980's. Today, CFRP bars, strips, tendons, and wet lay-up sheets are commonly used in the repair and retrofit of concrete structures. Some of the major benefits of CFRP include its high strength to weight ratio, high fatigue endurance and the ease of fabrication, manufacturing, handling and installation. Codification of the use of CFRP in civil infrastructure is quickly catching up with the rapid growth in installations, with many code writing agencies around the world concerned with this task.

One of the most common uses of CFRP materials is to externally bond the material directly to the concrete surface. Externally bonding CFRP systems to concrete can be achieved by bonding pre-cured laminates, or applying wet lay-up sheets. The systems are typically bonded to the tension side of the members to increase the flexural strength and/or on the sides of the

member to improve the shear capacity. Installation of this technique is relatively simple and can be achieved in a very short time. The system must be designed to avoid premature failure due to possible delamination or debonding of the CFRP material from the concrete surface, a failure mode that many researchers are currently investigating (Teng et al 2001, Oehlers & Seracino 2004). In response to premature debonding failures, the use of near surface mounted (NSM) CFRP systems was introduced by many researchers (De Lorenzis & Nanni 2001b, Hassan & Rizkalla 2003, 2004). In addition to their qualities in preventing debonding failures, the embedded nature of the technique provides superior environmental performance in comparison to externally bonded techniques, as well as protection against possible accidental and intentional damage.

1.2 Research Objectives and Scope

The main objective of this research work was to address two major concerns of Bridge Maintenance Engineers of the North Carolina Department of Transportation (NCDOT). The first objective was to find the most cost-effective and efficient CFRP system to strengthen short-span prestressed concrete bridge girders in order to increase posted bridge capacities. The second objective was to explore the use of a CFRP system to repair and restore an impact damaged AASHTO Type II girder to its original capacity.

The scope of the investigation included: 1) a comprehensive literature survey of research including published reports and field applications of concrete bridge strengthening with FRP systems, 2) An experimental program involving the testing of seventeen prestressed concrete C-Channel girders strengthened with various CFRP strengthening techniques tested under static and fatigue loading, 3) Repair of an impact damaged AASHTO Type II bridge girder with an FRP system to restore its original capacity and tested under fatigue loading conditions, 4) A cost-

effectiveness and value engineering analysis of the various CFRP repair technique, 5) The development of an analytical technique to design the flexural CFRP strengthening for prestressed concrete, 6) The development of design guidelines, selection criteria and construction specifications of CFRPs for use in flexural strengthening and repair, and 7) Recommend means for technology transfer as well as future field applications with continuous monitoring.

The original project proposal called for the testing of ten prestressed concrete C-Channels. The project has completed testing on seventeen C-Channel type girders, examining various levels of strengthening and prestressed strand configurations in addition to various CFRP systems, as shown in Table 1.1.

Table 1.1 Original v. Completed C-Channel Testing Program

	Static Loading	Fatigue Loading
Original Proposal	Five girders	Five girders
Completed Work	Nine girders	Eight girders

Approval has been granted for a one year project extension of this research project. Items to be examined in the future research work include: 1) Evaluation of an additional technique for the strengthening of C-Channel girders and 2) Assessment of additional items in the restoration of impact damaged AASHTO girders, including various levels of damage and damage locations.

For comprehensive recommendations, evaluations, and complete analysis procedures of the various CFRP repair and strengthening techniques, this document should be used in conjunction with the future report.

2 LITERATURE REVIEW

2.1 Overview

An extensive literature survey was a conducted during the course of this research program. The survey included published experimental and analytical studies of structures using FRP for repair, strengthening or imbedded reinforcement conducted by many universities and research organizations around the world. This chapter provides a brief summary and highlights of the survey. Topics include: 1) Historical perspectives on the use of FRP, 2) FRP strengthening of reinforced and prestressed concrete structures, 3) Background on the behavior of prestressed concrete subjected to fatigue loading, 4) Debonding of externally bonded plates and sheets to concrete surfaces, 5) The use of near surface mounted (NSM) reinforcement, 6) Repair of prestressed concrete using FRP, and 7) Existing design guidelines for concrete structures and bridges retrofitted with FRP.

2.2 Historical Perspective

The use of fibers to increase the strength of various buildings and structures is an ancient technology – utilized when people first started using straw in clay bricks for residential walls and roofs (Nanni 1999). These early uses saw the advantage of using two materials with different material properties. After World War II, the use of fiber reinforced polymers was mainly confined to the military for boat hulls, submarine parts and aircraft components. Once it became economically feasible, industry took advantage of the excellent properties of FRP materials, manufacturing everything from fishing poles and bicycle frames to architectural components and bath tubs.

In the 1960's, FRP began to be used in structural applications mainly as a result of its non-corrosive properties. Bridge deck slabs, sea walls, and floor slabs in aggressive chemical environments were reinforced with Glass Fiber Reinforced Polymers (GFRPs) as an alternative to epoxy coated reinforcing (ACI 440 1996). Strengthening buildings and bridges using FRP was first used as an alternative to the bonding of steel plates to the soffits of reinforced concrete beams (Oehlers 1990). FRP strengthening gained popularity in Europe and Japan in the 1980's as a result of the high strength to weight ratio and easy installation of FRP materials. Throughout the 1990s, the use of FRP in North America, Europe and Asia has continued to become more prevalent with many repair and strengthening projects completed. The number of companies manufacturing FRP products has also increased, with numerous companies producing FRP sheets, reinforcing bars and pultruded laminates.

2.3 Near Surface Mounted Reinforcement

The use of near surface mounted (NSM) fiber reinforced polymer (FRP) bars and strips are emerging as an alternative technology to externally bonded FRP laminates. Advantages of using NSM systems include the possibility of anchoring the bars/strips into adjacent members, shorter installation time, and an attractive finished appearance.

Characterization of NSM FRP bars and strips as reinforcing is fairly recent, but NSM steel reinforcing has been used in Europe for over 50 years. Asplund (1949) carried out tests on concrete beams reinforced with NSM steel bars bonded using cementitious grout and found they worked similarly to reinforcing bars originally casted in concrete. This technique was used in Finland in 1949 to strengthen a bridge deck whose top layer of steel reinforcing was erroneously omitted.

Using NSM FRP for flexural strengthening of reinforced concrete members is an attractive solution (Alkhrdaji et al 2001, Hassan and Rizkalla 2004, El-Hacha and Rizkalla 2004b), especially in the negative moment region of beams and slabs where externally bonded FRP laminates would interfere with the floor finish or be exposed to environmental degradation. NSM systems can also be used for shear strengthening of concrete members (De Lorenzis and Nanni 2001a&b, Nanni et al. 2004), and strengthening of prestressed concrete structures (Hassan and Rizkalla 2002a)

Alkhrdaji et al. (2001) strengthened a reinforced concrete bridge deck span with NSM CFRP bars and tested in-place to failure. Compared with an unstrengthened span they achieved a 30 percent increase in flexural capacity with full utilization of the FRP bars (failure due to FRP rupture).

Carolin et al. (2001) tested a series of concrete beams strengthened with NSM CFRP strips. Test results demonstrated the effectiveness of the NSM technique compared to the externally bonded technique. They recommended replacing the epoxy, used in bonding the strips to the surrounding concrete, with cement mortar to improve the work environment on site.

Hassan and Rizkalla (2002a) investigated the feasibility of using different strengthening techniques as well as different types of FRP for strengthening prestressed concrete bridge decks in flexure. Large-scale models of a prestressed concrete bridge deck were tested to failure. Test results showed that the efficiency of near surface mounted CFRP strips was three times that of the externally bonded strips.

Hassan and Rizkalla (2003 & 2004) presented experimental and analytical investigations to evaluate bond characteristics of NSM CFRP bars and strips. The influence of the groove dimensions, groove spacing and the limited adhesive cover was investigated. They concluded

that the tensile stresses at the concrete-adhesive interface, as well as at the FRP-adhesive interface, are highly dependent on the groove dimensions and control the mode of failure of near surface mounted FRP bars and strips. They recommended widening of the groove to minimize the induced tensile stresses at the concrete-epoxy interface and increase the debonding loads of NSM bars. A mathematical model to find the development length of NSM FRP bars is presented along with design charts correlated to experimental results.

2.4 Fatigue of Concrete, Prestressing Strands and CFRP

To properly assess the resistance of a structure or bridge against cyclic loading, the fatigue characteristics of the constituent materials should be assessed. For most materials there exists an endurance limit, an alternating maximum stress which a material can withstand for an infinite number of cycles. Cumulative damage models are the most effective way to assess fatigue degradation of materials within a structure, but these models are beyond the scope of this report. Through experimental testing, the fatigue resistance of materials has been defined using stress ratio versus number of cycle curves, or S-N curves, which offer fatigue life predictions when the stress ratio and other parameters are known.

The fatigue resistance of concrete was first studied extensively when reinforced concrete began being used to construct railroad bridges. Defining $S = f_{\max} / f'_c$ and $R = f_{\min} / f_{\max}$, Aas-Jacobsen (1970) defined an equation for fatigue of concrete under compression-compression cyclic loading:

$$S = 1 - \beta(1 - R)\log_{10} N \tag{2.1}$$

where β=0.064 and N is the number of cycles to failure.

The performance of concrete under tension-tension cyclic loading is less known (Ahmad 2004). Saito and Imai (1983) found that there is no endurance limit for concrete in tension under

fatigue loading and that after 2 million cycles the residual strength was 73% of its original tensile strength.

The most extensive report on fatigue on reinforced and prestressed concrete constituent materials in the United States is published by the American Concrete Institute's Committee 215 (1997). From extensive experimental studies, S-N curves are presented in graphical format for concrete under compression-compression loading, in addition to the tension-tension loading of regular reinforcing bars and prestressing strands. The effects of different variables such as bar geometry, load history and rate of loading are examined.

The fatigue resistance of prestressed concrete members is often dependent on the stress ratio applied to the prestressing strands. Various equations have been proposed to estimate the fatigue life of a prestressing strand in air, two of which are:

Collins (1991): $$\log_{10}(N) = 10 - 3.6 \cdot \log_{10}(100 \cdot SR) \tag{2.2}$$

Naaman (1991): $$\log_{10}(N) = 7.07 - 8.13 \cdot (SR) \tag{2.3}$$

Both of these equations are plotted in Figure 2.1.

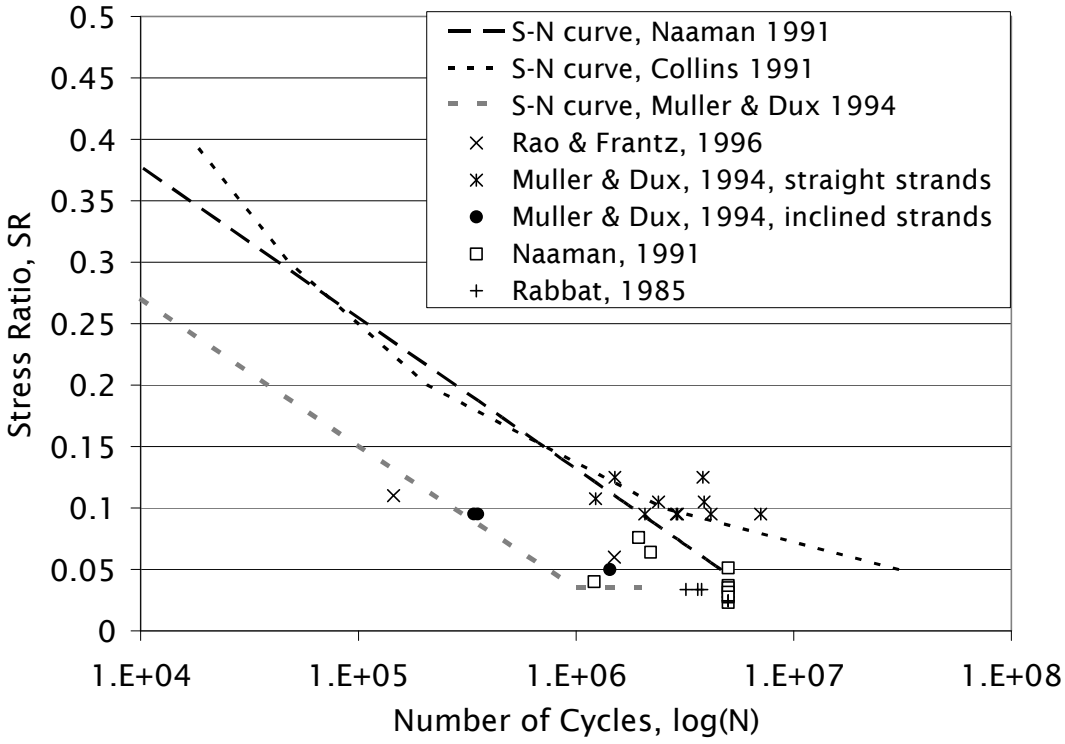

Figure 2.1 S-N Behavior of prestressing strands

Unidirectional Fiber Reinforced Polymer (FRP) materials have good fatigue resistance and very little stiffness degradation under cyclic load (Barnes and Mays 1999). Walton and Yeung (1986) found that the fatigue performance of composite materials was superior to that of other engineering materials, including steel. Adimi et al (2000) observed that for carbon fiber bars embedded in concrete cycled at a frequency of 4 Hz, the maximum stress should not exceed 35 percent of its ultimate tensile strength in order to achieve 4 million cycles of loading.

2.5 Fatigue of Prestressed Concrete

From 1950 to 1990, the fatigue of prestressed concrete bridge girders was extensively investigated. Many studies concluded that the fatigue critical component of a prestressed concrete bridge girder is the prestressing strands. One exhaustive study by Overman (1984) tested full scale precast prestressed concrete bridge girders with cast-in-place composite decks

under fatigue loading. This study and others (Rao and Franz 1996, Rabbat et al 1985) have found that if a prestressed concrete girder remains in an uncracked condition the fatigue life of the prestressing strands are infinite. The AASHTO (2004) code specifies a maximum nominal tensile stress in concrete at service load of $3\sqrt{f'_c}$ psi ($0.25\sqrt{f'_c}$ MPa) in corrosive environments and $6\sqrt{f'_c}$ psi ($0.5\sqrt{f'_c}$ MPa) in non-corrosive environments. This value is meant to maintain the service load of the girder under the cracking load so that the strands can withstand load indefinitely.

The use of inclined strands normally reduces the fatigue resistance of prestressed concrete bridge girders as a result of the fretting fatigue which occurs at the hold down points. Muller and Dux (1994) proposed an S-N curve for prestressed concrete girders with inclined strands, which is valid from 300,000 to $2 \cdot 10^6$ cycles:

$$SR = -0.12 \log_{10} N + 0.75 \geq 0.035 \tag{2.4}$$

This equation is shown in Figure 2.1.

Rabbat et al (1985) first examined the effect of draped strands in prestressed concrete girders with full size testing. Through the testing of six full-size AASHTO Type II girders under fatigue loading corresponding to a nominal bottom tensile stress in the concrete of $6\sqrt{f'_c}$ psi ($0.5\sqrt{f'_c}$ MPa), they recommended that straight strands with blanketing at the ends be employed in new constructions as their fatigue life is equivalent to that of draped strands.

A recent investigation examining the fatigue resistance of prestressed concrete was performed by Rao and Franz (1996). They conducted fatigue tests on two 56.1 ft (17.1 m), 27 year old prestressed concrete box beams. One of the beams was tested under loading designed to simulate a nominal bottom tensile stress in the concrete of $6\sqrt{f'_c}$ psi ($0.5\sqrt{f'_c}$ MPa)

corresponding to a stress ratio in the prestressing strands of $0.06 f_{pu}$. An additional test was performed on a girder to simulate a tensile stress in the concrete of $9\sqrt{f'_c}$ psi ($0.75\sqrt{f'_c}$ MPa) corresponding to a stress ratio in the prestressing strands of $0.11 f_{pu}$. The girder with the lower level of loading survived over 1.5 million cycles retaining excellent performance whereas the girder with the higher loading experienced a ruptured prestressing strand at 145,000 cycles. They recommended that all calculations to find stresses in concrete and prestressing strands be based on a cracked section analyses because of the possibility of unintentional overloads.

2.6 Reinforced Concrete Strengthened with CFRP

A wide array of research exists for the strengthening of reinforced concrete with FRP. Concrete code agencies around the world have incorporated FRP materials into their documents as viable repair or strengthening options (see Section 2.10). The static behavior of CFRP strengthened structures is well known (Carolin 2003, Arduini et al 2002, El-Hacha & Rizkalla 2004b), with predictions based on strain compatibility and equilibrium of forces within the member providing accurate predictions of failure loads and ultimate displacements. With appropriate reduction factors applied to the material properties of the FRP to account for environmental degradation, manufacturing flaws, misalignment of the fibers or debonding propensity, the desired modes of failure of concrete crushing or rupture of FRP can be achieved. With extensive research work devoted to the static behavior of CFRP strengthened reinforced concrete members, recent work has focused on the cyclic behavior of these systems. Some of the more recent studies are described in this chapter.

Barnes and Mays (1999) tested five reinforced concrete beams under fatigue loading, three strengthened with externally bonded CFRP plates. The 3.6 in x 0.048 in (90 mm x 1.2 mm)

plates were bonded to the tension surface of a 5 in x 9.2 in x 92 in (125 mm x 230 mm x 2300 mm) beam. The plate was terminated near the beam supports and mechanically anchored to the concrete by way of a steel plate bonded to the plate surface and bolted to the concrete. The results show that the fatigue performance of CFRP strengthened beams is superior to unstrengthened beams at the same level of loading due to reduced crack widths and shorter spacing of cracks. Using a criteria based on the stress ratio in the regular steel reinforcing was also deemed to give a more accurate representation of the fatigue behavior rather than applying the percent increase in ultimate capacity to the fatigue loading range.

A very similar conclusion was reached in a study by Heffernan and Erki (2004) in which 9.8 ft and 16.4 ft (3 m and 5 m) reinforced concrete beams were tested under static and fatigue loading conditions. The authors found that the stress ratio in the steel reinforcement controlled the fatigue failures and that increasing stress ratios were observed due to concrete softening during the repeated loading.

Breña et al (2005) examined the flexural fatigue behavior of ten reinforced concrete beams, eight of which were strengthened with two types of CFRP: wet lay-up sheets and pultruded laminates. The CFRP sheet strengthened specimens were 9.5 ft (2900 mm) in length and the CFRP plate specimens 10.5 ft (3200 mm) in length with cross sectional dimensions configured to give a span to depth ratio of 8.15 for both series of tests. Out of the eight strengthened beams, three failed due to the fatigue loading – one of the CFRP sheet strengthened beams due to rupture of reinforcing steel and two of the CFRP plate strengthened beams due to debonding of CFRP. Although the stress ratio in the reinforcement was identified to be an important factor in the fatigue life of the strengthened system because some of the beams failed due to debonding, the authors concluded that the stress ratio in the composite system was critical

in this case. It is possible that the detailing of the CFRP system could have prevented the premature debonding failures observed in the research.

2.7 Prestressed Concrete Strengthened with CFRP

There has been little research on the strengthening of prestressed concrete with CFRP materials. There have been some field applications using CFRP on prestressed concrete, which are be discussed in Section 2.8, yet few full scale specimens have been laboratory tested

Takacs and Kanstad (2002) showed that prestressed concrete girders could be strengthened with externally bonded CFRP to increase their ultimate flexural capacity. CFRP pre-cured laminates were applied to the bottom and side surfaces of a T-beam soffit; no transverse U-wraps were provided. Of the strengthened beams, one failed due to debonding and the other experienced a shear failure. The beams achieved an increase in flexural moment capacity of 28 and 37 percent respectively. A finite element model based on the smeared crack methodology was used for predictions of the failure loads.

Hassan and Rizkalla (2002a, 2002b) examined the flexural behavior of prestressed concrete bridge slabs strengthened with various CFRP systems. The half scale specimens were strengthened with near surface mounted (NSM) CFRP bars and strips as well as externally bonded CFRP strips and sheets. The flexural capacity of the slabs could be increased by as much as 50 percent using the CFRP strengthening, with the most cost effective solution being the CFRP sheets. A specimen strengthened with CFRP strips experienced debonding at 41 percent of the rupture strain of the material.

Reed and Peterman (2004) showed that both flexural and shear capacities of 30 year-old damaged prestressed concrete girders could be substantially increased with externally bonded CFRP sheets. Two single-tee girders were taken from an overloaded bridge, epoxy injected,

strengthened with CFRP sheets and tested to determine their shear and flexural strength. A control specimen was also tested which was not epoxy injected. Both of the girders were strengthened using the same longitudinal CFRP configuration, but one girder had provided CFRP transverse U-Wraps throughout the length of the girder whereas the other had U-wraps provided only at the supports where the longitudinal CFRP was terminated. Both strengthened girders achieved approximately a 20 percent increase in strength over the control specimen. The failure modes were different however, as one failed due to CFRP rupture and the other due to debonding of the cover concrete between the CFRP strengthening and the prestressing. Reed and Peterman encouraged the use of CFRP transverse U-wraps along the length of the girder in externally bonded systems to delay debonding failure.

2.8 Repair of Prestressed Concrete with CFRP

2.8.1 Experimental Work / Field Applications

Damage due to impact of highway bridges is a major concern of departments of transportation. Repair of the damage is often very expensive, and can result in lengthy traffic delays. Limited research has been done on the assessment of impact damage and subsequent repair methods to PC bridge girders. Several impact-damaged PC girders have been repaired in the field, but a limited number of studies have been conducted in a laboratory setting. One common repair technique is to splice the steel prestressing strands; however, this was found to perform poorly during fatigue, and in many cases is unable to restore the ultimate strength of the girder (Zobel and Jirsa 1998). The use of FRP materials is a more innovative technique that has the potential to not only restore the ultimate strength of the damaged girder, but withstand the repetitive service loadings that all bridge girders undergo. Several experimental studies have

examined the use of FRP to repair impact damaged prestressed concrete bridge girders, in addition to numerous field applications initiated by departments of transportation.

In Alabama, one span of a reinforced concrete bridge was chosen to repair damage due to aging (Stallings et al. 2000). CFRP precured laminates along with glass FRP sheets were used to restore the repaired sections past their original capacities to increase posted load restrictions. Before installation of the repair systems, load tests were performed to measure the behavior of the bridge superstructure under various static and dynamic loads. Identical static and dynamic tests were performed after the installation of the FRP repair systems to compare with the prior results. The results of these load tests demonstrated that the FRP repair system reduced girder deflections ranging between 2 to 12%, as well as reducing rebar stresses by an average of 8%. The usage of CFRP plates to repair and strengthen reinforced concrete bridge girders was successfully verified by field loading tests.

Three separate prestressed concrete bridges were repaired with CFRP systems in repair projects sponsored by the Missouri Department of Transportation. In the first project, eleven prestressed concrete bridge girders located on a bridge in Independence, MO were impact damaged due to an overheight vehicle and repaired with CFRP wet lay-up sheets (Schiebel et al., 2001). Although no prestressing strands were ruptured, all eleven girders had large cracks and spalling of concrete exposing prestressing strands. The CFRP repair system was designed using a simple section analysis procedure ensuring that the new flexural strength was equal to or greater than that of the original girder. Detailing of the CFRP repair system followed industry standards and provided transverse U-wraps at 400 mm spacing and extension of the CFRP well away from the damaged concrete area. Experimental testing was limited to bond and adhesion tests to ensure proper bond of the CFRP to the concrete substrate. In the second project, a

prestressed concrete bridge girder was repaired in-situ with CFRP wet lay-up sheets after impact damage ruptured two prestressing strands (Tumialan et al 2001). The design of the repair system was determined by the rectangular stress block approach. Two layers of CFRP sheets were applied to the tension face, extending past the damaged location. CFRP U-wraps were also applied to prevent debonding failure. Following current industry standards, the CFRP repair system was successfully installed by a contractor. Field testing was not performed, however the repaired girder is performing well in service. A third project sponsored by the Missouri DOT, repaired impact damage caused by a contractor who struck a girder during construction of a new bridge (Ludovico et al. 2003). Two prestressing strands were ruptured and a significant loss of concrete occurred. The concrete section was restored and the girder repaired using CFRP sheets in both the longitudinal and transverse directions. Load testing was not performed on the repaired section, but the girder is currently performing well under traffic loading.

The Iowa Department of Transportation has sponsored several research projects that involved the use of CFRP to repair impact damaged prestressed concrete bridge girders. In the first project, several overheight impacts damaged all the girders on a bridge (Klaiber 1999). Although no prestressing strands were ruptured, one girder had two prestressing strands which were visibly relaxed. The girders were load tested in-situ to examine their respective load-deflection behaviors. Two damaged girders were then cut out of the deck, replaced with new ones, and transported to a testing facility. The more severely damaged girder with two relaxed prestressing strands was tested to failure to observe the behavior of a beam with significant concrete loss and relaxed strands. The second girder, with only moderate damage, was then loaded to simulate service load conditions. The girder was then damaged to simulate a larger loss of concrete and rupturing of two prestressing strands. Following the simulated damage, the

girder was then repaired by first restoring the concrete section using a cementitious mortar. CFRP plates were then bonded to the bottom flange of the beam to restore the flexural capacity of the member. CFRP sheets were added in the transverse direction to prevent debonding. Load tests after the CFRP installation indicated that the repaired girder exhibited 27% less deflection than the damaged girder. The repaired girder also exhibited a higher ultimate load capacity over the control specimen previously mentioned.

In a second project sponsored by the Iowa DOT, a bridge was load tested before and after the installation of a CFRP repair system. All six prestressed concrete girders on one span of the bridge were damaged as a result of an overheight impact; however most damage only occurred to the first two girders. The first girder sustained spalled concrete as well as one ruptured prestressing strand. The second girder was damaged more significantly with a much large loss of concrete, five prestressing strands visible and two of these were ruptured. After restoration of the section was completed with patching material, CFRP plates were attached to the bottom flange of the beams. The researchers demonstrated through the before and after load tests that the midspan bridge deflections decreased following the installation of the CFRP plates. The researchers concluded that flexural strengthening of impact damaged PC girders is possible when up to 15% of the strands are severed. Higher ratios may be possible, but tests have not been performed to validate this assumption.

An experimental project was sponsored by the Florida Department of Transportation to create guidelines, standard practices, and experimental data for the repair of impact-damaged bridge girders using CFRP systems. The FDOT had previously repaired a damaged prestressed bridge girder on an active bridge, but did not have any design guidelines at the time to follow. All they had were the manufacturer's engineers to assist in the repair. In Green et al. (2004), six

44’ long AASHTO Type II girders were tested in four point bending to examine effectiveness of various CFRP systems to restore the capacity of damaged girders back to their original strengths. The experiment was comprised of one control specimen, a second control specimen with simulated damage, and four specimens with simulated damage repaired with different CFRP systems. All test results compared well with analytical predictions. The results show that one of the four repaired girders was able to achieve its original capacity. Wet lay-up CFRP sheets were used in the first repaired specimen. The girder failed prematurely, at 91% of the control specimen’s ultimate strength, due to plate-end debonding. The researchers did not provide any U-wraps along the length of the longitudinal CFRP. It is believed that the presence of U-wraps would have prevented the plate-end debonding. The second repaired specimen was repaired using pre-impregnated CFRP fabric sheets. Four layers of pre-preg sheets were installed in the longitudinal direction, along with bi-directional CFRP sheets U-wraps which were bolted into the web. The girder achieved 92% of the experimental capacity of the control girder, with failure due to adhesive failure immediately followed by rupture of the longitudinal CFRP. The third girder incorporated a spray-on FRP repair system. This system achieved 95% of the original capacity, with failure caused by FRP rupture. The researchers found after the failure that the desired thickness of the spray was 0.50 in (12.7 mm) but the actual thickness as 0.27 in (6.9 mm). The final repaired girder employed the usage of wet lay-up CFRP sheets. One transverse U-wrap was provided at the end of the longitudinal sheets to provide anchorage. The girder failed after the longitudinal FRP pulled away from the U-wraps, leading to an anchorage failure, but not until after the girder had achieved a 7% increase in strength over the control specimen. The researchers concluded that FRP can be used to restore a significant portion of the strength

capacity of an impact damaged girder, however they observed that proper detailing at termination points is critical to any FRP system.

In Di Ludovico et al. (2005), three 36.1 ft (11 m) prestressed concrete Missouri Type II bridge girders, with a 32 in (810 mm) composite cast-in-place slab, were tested monotonically to failure to assess the flexural behavior of repaired damaged sections with CFRP wet lay-up laminates. After the first girder was tested as a control specimen, the other two were damaged at midspan by removing the concrete cover and rupturing two and four prestressing strands, respectively. They were then repaired with cementitious mortar and repaired with two or three layers of longitudinal CFRP sheets below numerous transverse CFRP U-wraps. The results show that the CFRP system can restore the ultimate capacity and stiffness of the original girder, but the two repaired girders could not match the original serviceability. The failure mode observed for both of the repaired girders was rupture of a U-wrap on the undamaged girder side followed by intermediate crack debonding of the longitudinal CFRP system. The researchers provided numerous CFRP U-wraps throughout the repaired area, but they only extended around the bottom flange of the girder to the bottom of the web. It is possible that this detailing lead to the premature debonding failures at 56 and 46 percent of the ultimate nominal FRP strain. The authors also provide an analysis procedure to calculate the prestress force, the cracking moment and the ultimate moment based on strain compatibility and equilibrium. For the design of the CFRP system, they applied the bond reduction factor (κ_m) from ACI 440F (2002), but not the environmental reduction factor (C_E).

2.8.2 Analytical Work

El-Tawil and Okeil (2002) conducted a parametric study of prestressed concrete bridge girders flexurally rehabilitated with CFRP laminates. Parameters investigated in the Monte Carlo

simulations included the construction sequencing, composite action between deck and girder, and the development of a fiber section model which considered the non-linear behavior of the constitutive materials. Three different cross sections were considered corresponding to AASHTO Type II, III and IV girders with 26, 34 and 44 prestressing strands in each respectively. For each of these cross sections, three levels of damage were examined corresponding to a 10, 20 and 30 percent nominal loss of prestressing strands.

The goal of their research was to calibrate an AASHTO LRFD provision for prestressed concrete girders strengthened with CFRP by examining the different girders described above with varying amounts of CFRP repairing. They proposed using a reliability index, β, of 3.75. This is slightly more conservative than the AASHTO mandated value for prestressed concrete girders to account for the brittle nature of CFRP rupture, which was the failure mode for the girders they analyzed.

2.9 Debonding of Externally Bonded Plates

Before FRP was used as externally bonded reinforcement in concrete structures, mild steel plates were used to flexurally strengthen concrete members. The steel plates added stiffness and strength to the member but had a propensity for brittle debonding that was noted by several researchers. Oehlers (1990) provided the first quantification of the plate-end (PE) debonding failure mechanism, where he observed peeling of mild steel plates away from the concrete substrate at the plate termination point. He determined that this type of debonding failure was due to shear and flexural forces at the end of the plate as well as beam curvature at high load levels.

Malek et al (1998) observed PE debonding of externally bonded FRP plates, and provided equations to predict the failure mode of the beam by estimating the shear stress of the concrete in

the plate termination zone. He found that the debonding mechanism in FRP plated beams was due more to stress concentrations present at the plate termination point rather than the beam curvature due to the low out-of-plane stiffness of the FRP plate.

As externally bonded CFRP strengthening for concrete structures became more common, it was identified by several researchers that other debonding failure modes affected concrete strengthened with FRP more often than PE type debonding, namely intermediate-crack (IC) debonding (Teng et al 2002, Oehlers & Seracino 2004). IC debonding begins as a result of interface cracks in the concrete substrate above the FRP plate which relieve stress concentrations encountered at the flexural crack locations. As the applied load increases, the interface cracks propagate and connect between the flexural cracks. Near ultimate, the plate is only connected to the concrete at the plate ends until failure occurs when the crack propagates to the plate termination point. The slow propagation of the IC debonding results in a more ductile failure than PE debonding. Another form of FRP to concrete debonding that has been identified is critical diagonal crack (CDC) debonding (Oehlers & Seracino 2004) which occurs due to an inclined shear crack that causes the plate to debond from the root of the crack towards the plate termination point.

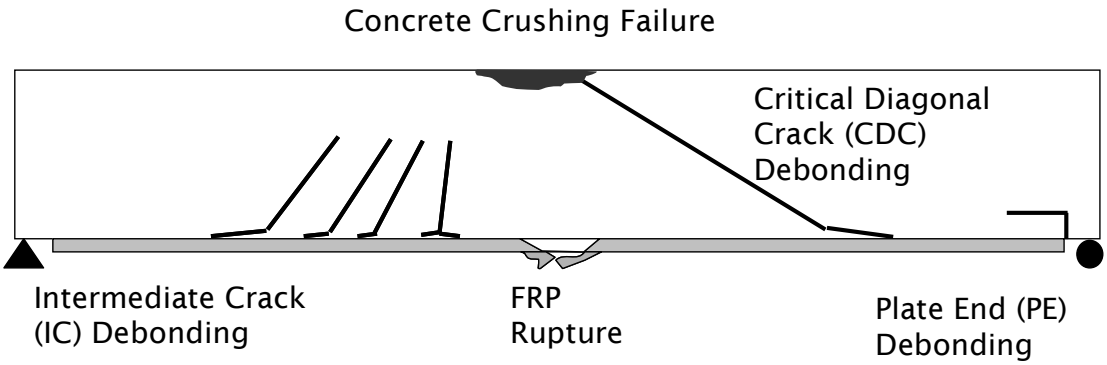

Figure 2.2 Failure modes of FRP plated beam (from Oehlers & Seracino 2004)

A comprehensive review of the published IC debonding models was presented by Smith and Teng (2002a, 2002b). They recommended the use of an equation to predict the IC debonding resistance of FRP plated reinforced concrete beam based on a fracture mechanics approach calibrated with experimental data.

The debonding of near surface mounted CFRP reinforcement has been noted by several researchers (Hassan and Rizkalla 2003, 2004, El-Hacha and Rizkalla 2004a, De Lorenzis 2002). The equations proposed by Malek et al (1998) for PE debonding of externally bonded plates were modified by Hassan and Rizkalla (2003 & 2004) to predict debonding failure loads of NSM FRP reinforcement.

2.10 Design Guidelines for Concrete Retrofitted with FRP

Various code writing organizations around the world have proposed design guidelines for the repair or strengthening of concrete structures with FRP. Some well known guidelines are presented here.

The American Concrete Institute released a document in 2002 concerning design and construction of externally bonded FRP systems for strengthening concrete structures (ACI 440F

2002). Many different aspects of using FRP are included, such as system installation guidelines, including various types of surface preparation techniques, inspection and field evaluation procedures, as well as guidelines for the repair of minor damage observed after CFRP installation. The document discussed fire endurance ratings, and strengthening limits to be used in design in the event of fire or vandalism. They recommend that an environmental reduction factor, C_E, be applied to the modulus of elasticity and the rupture strain of the FRP to account for environmental degradation over time. To reduce the propensity for debonding failures, they recommend that the rupture strain of the FRP be further reduced using a bond-dependent coefficient, κ_m, which depends on the elastic modulus, rupture strain, thickness and number of layers of the FRP system. Under sustained and cyclic load, the document recommends that CFRP materials be kept below a stress range of 55 percent. CFRP detailing concerns are also addressed in conjunction with FRP anchorage and lap splice recommendations. Design examples are also given with procedures shown for calculating reduced FRP material properties and a complete FRP flexural and shear strengthening problem.

The Concrete Society (2004) of the United Kingdom has proposed design guidance for the strengthening of concrete structures with fiber composites. A state of the art application review of various FRP installations throughout Europe and North America is first presented. Using numerous experimental studies, they propose safety factors to be applied to the FRP material properties to account for environmental degradation and misalignment of fibers. The safety factors are applied to the rupture strain, elastic modulus, and tensile strength and have values which depend on the type of material used and the method of installation. Flexural design follows from strain equilibrium and compatibility of the section. Debonding failure of externally bonded FRP systems follow a procedure based on Teng et al (2002). Design

procedures are presented to prevent debonding by limiting the maximum strain in the FRP, limiting the longitudinal shear stress outside of the anchorage region, and designing for appropriate anchorage lengths. The flexural design procedures for near surface mounted FRP reinforcement are similar for externally bonded FRP, with recommendations on anchorage design taken from Hassan and Rizkalla (2004). Under fatigue loading, a stress ratio of 80 percent is recommended as an upper limit for CFRP materials. Installation procedures, quality control and guidelines on destructive and non-destructive testing are presented.

The Swiss fédération internationale du béton, ***fib***, (2001) has published guidelines on externally bonding FRP to reinforced concrete structures. For FRP material properties, the guidelines provided safety factors to be employed for different types of material and applications to account for long term behavior. The failure modes of flexurally strengthened members are described and guidance is given to prevent various debonding failures. An entire chapter of the document is devoted to detailing rules. The anchorage of externally bonded CFRP is their primary concern, with U-wrap transverse reinforcements or other mechanical anchorages recommended at the CFRP termination points.

The Japan Society of Civil Engineers (2001) has proposed recommendations for the upgrade of concrete structures with continuous fiber sheets. They propose material safety factors to be used for safety, reliability, and serviceability. To prevent peeling of FRP sheets, the recommendation provided an equation to determine the maximum permissible stress in the sheets based on the interfacial fracture energy between the concrete and FRP as well as other material properties. Guidance is also given regarding anchorage and splice design. Detailed specifications are presented in order to experimentally determine various FRP material properties and degradation due to environmental effects.

The Canadian Standards Association (2000) published a document for the design and construction of building components with FRP. Although mainly concerned with the use of FRP materials in new constructions, the standard specifies basic design guidelines and requirements for the use of surface bonded FRP for concrete or masonry structures.

3 EXPERIMENTAL PROGRAM – C-CHANNEL GIRDERS

3.1 Introduction

This section presents the static and fatigue experimental program used to evaluate the performance of C-Channel girders strengthened with various CFRP systems. This chapter will provide specifics related to the tested girders, design of the various strengthening systems, test setup, loading scheme, instrumentation, and detailed descriptions of the individual tests. Constitutive material testing was performed on all the materials encountered, including material properties for the various CFRP systems, and these results are also included. Test results are presented in Chapter 5. The cost-effectiveness and value engineering of the CFRP strengthening systems used for the C-Channel girders are given in Chapter 6.

3.2 Test Girders

3.2.1 The C-Channel Bridge

The C-Channel prestressed concrete girder is a superstructure member commonly used for short two-span bridges ranging in length from 40 to 60 ft (12.2 to 18.4 m) in rural areas of North Carolina, typically used to span small streams or estuaries. Bridges using this type of girder were built between the late 1950's to the mid 1970's. During erection, each precast C-Channel was delivered to the bridge site, along with the bridge cap beams (which were also precast). The bridge was typically supported by a timber substructure. Once the girders were in place side by side, they were post-tensioned transversely as shown in Figure 3.1. All of the girders tested in this research project were interior girders, with no integral parapet walls connected to the deck.

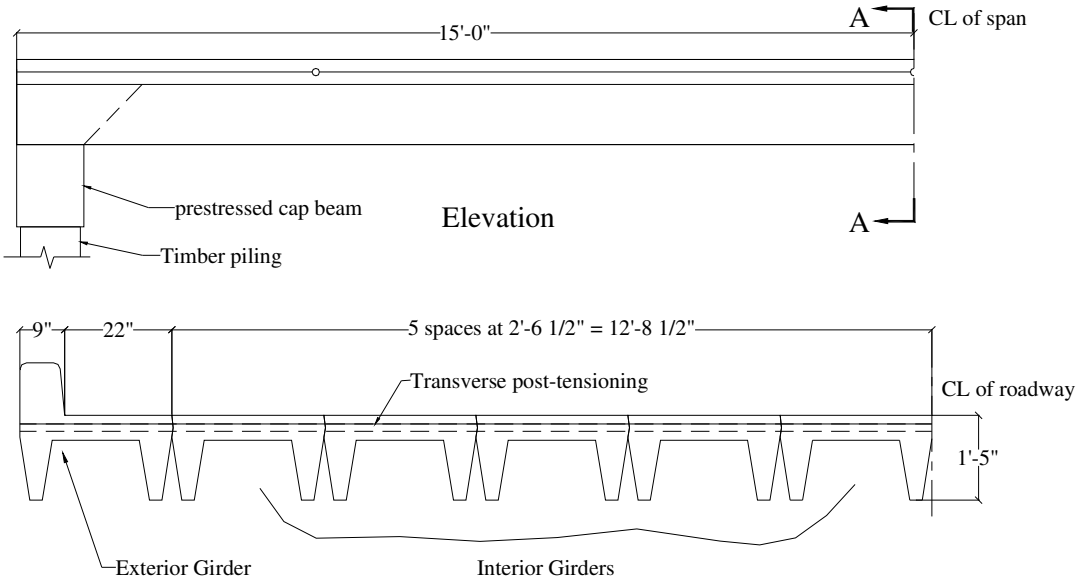

Section A-A

Figure 3.1 C-Channel bridge layout

A total of seventeen bridge girders were tested in this research program. Twelve girders had a Type I prestressing configuration with ten 250 ksi (1723 MPa) prestressing strands and came from a decommissioned bridge erected in 1961 in Carteret County, NC. The bridge was taken out of service and dismantled due to a deficient substructure supporting system. The other five girders were Type II girders, prestressed with eight 270 ksi (1862 MPa) strands and came from a decommissioned bridge in Washington County, NC. The second bridge was also decommissioned due to a deficient substructure. A typical C-Channel bridge is shown in Figure 3.2. Figure 3.3 shows a typical C-Channel substructure, which consists of a 13.5 in by 16 in (343 mm by 406 mm) prestressed cap beam supported by timber piles.

Figure 3.2 Bridge 43 in Carteret County, NC. A typical C-Channel type bridge.

Figure 3.3 Typical C-Channel bridge abutment

3.2.2 Prestressing Strands

According to the North Carolina State Highway Commission Design Standards, the C-Channel type prestressed concrete bridge girder was prestressed by various prestressing strand configurations. The configurations were used to accommodate the loads for either exterior or interior girders corresponding to spans of 20, 25 or 30 ft (6.1 m, 7.6 m or 9.14 m). All of the girders tested had a length of 30 ft (9.14 m), of which there were only two different prestressing configurations. The first twelve girders tested had a Type I prestressing strand configuration using ten 250 ksi (1724 MPa) stress-relieved 7- wire prestressing strands. The Type I configuration consisted of five strands in each web, three of which were inclined with a hold down point located at midspan. The bottom two strands were straight. The last five C-Channels tested had a Type II strand configuration using eight 270 ksi (1862 MPa) stress-relieved 7- wire prestressing strands. The Type II configuration consisted of four strands in each web, three of which were inclined with a hold down point located at midspan. The two prestressing strand configurations are shown in Figure 3.4.

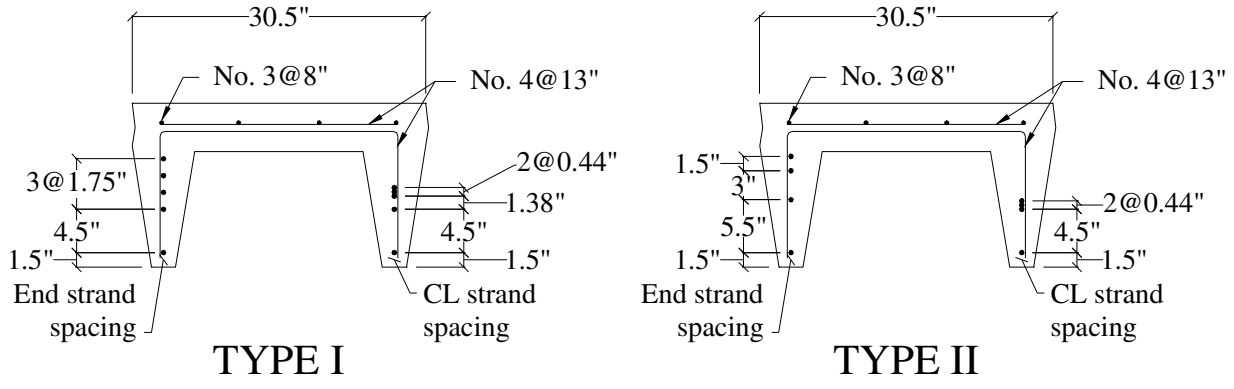

Figure 3.4 Elevation and cross section of C-Channel showing prestressing configurations

Material testing was carried out on each type of prestressing steel strands encountered in the tested Type I and Type II girders. Once testing of the girder was complete, two of the bottom

prestressing strands were extracted near the supports. Care was taken in removal of the strands to prevent any unraveling of the strands while cutting. The prestressing strand specimens after removal from the girder are shown in Figure 3.5.

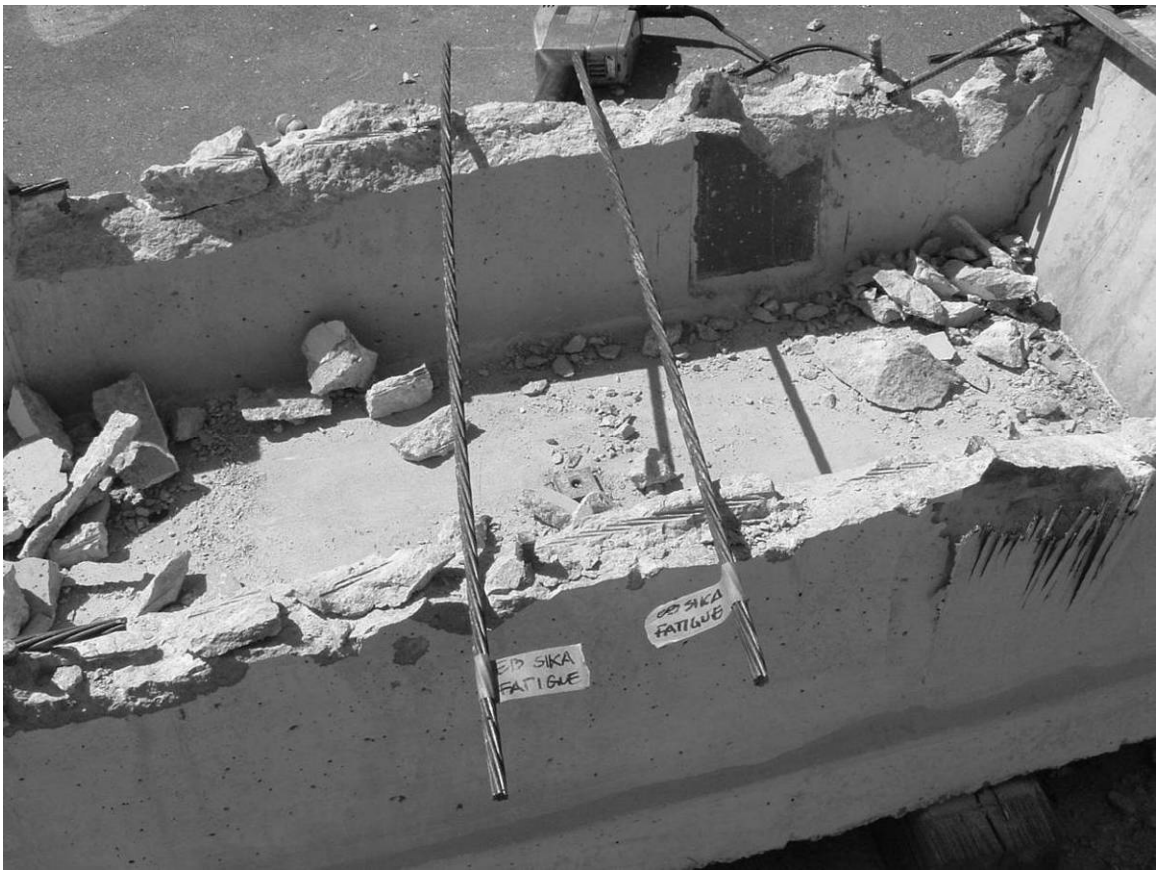

Figure 3.5 Prestressing strand extraction

The prestressing strands were tested in tension according to ASTM A416 specification using a 220 k (979 kN) MTS closed-loop universal testing machine used to apply a constant rate of displacement. The prestressing strands were clamped into the MTS grips using two 0.4375 in (11.11 mm) multiple-use super chucks provided by Prestress Supply, Inc, Lakeland, Florida. Displacement during the test was measured by a 2 in (51 mm) extensometer placed at the middle of the gauge length. The extensometer was removed prior to rupture of the strands, and the rupture strain was determined from the stroke of the MTS machine for four of the specimens.

Table 3.1 shows the yield strength, ultimate strength, modulus of elasticity and rupture strain for the tested prestressing strands.

Table 3.1 Prestressing steel properties

System Designation	f_y, ksi	f_u, ksi	f_u, %	E_{ps}, ksi
NSM1S strand 1	212	238		28971
EB3S strand 2	203	225		28884
NSM2S strand 3	207	229		27971
CF2 strand 4	207	302	6.41	30088
EB6F strand 5	232	291	3.24	30218
EB5S strand 6	228	296	5.16	28522
EB5S strand 7	228	296	5.31	28522

The Ramberg-Osgood function (Collins and Mitchell 1991) was used to match the stress versus strain behavior of the prestressing strands.

$$f_p = E_p \varepsilon_{ps} \left[A + \frac{1 - A}{\left[1 + \left(B\varepsilon_{ps}\right)^C\right]^{1/C}} \right] \tag{3.1}$$

where f_p is the prestressing strand stress, E_p is the modulus of elasticity of the prestressing strand, ε_{ps} is the strain in the prestressing strand, and A, B, C are material constants.

The constants A, B and C can be determined from the stress-strain relationships generated from the tension tests. For the Type I girders with 250 ksi (1724 MPa) strands, the average values for A, B and C were 0.025, 138.7 and 6 respectively. For the Type II girders with 270 ksi (1862 MPa) strands the average values for A, B and C were calculated to be 0.017, 106.0 and 7. Figure 3.6 shows the stress-strain behavior measured during testing and simulated using the Ramberg-Osgood formulation for the two different types of prestressing strands used.

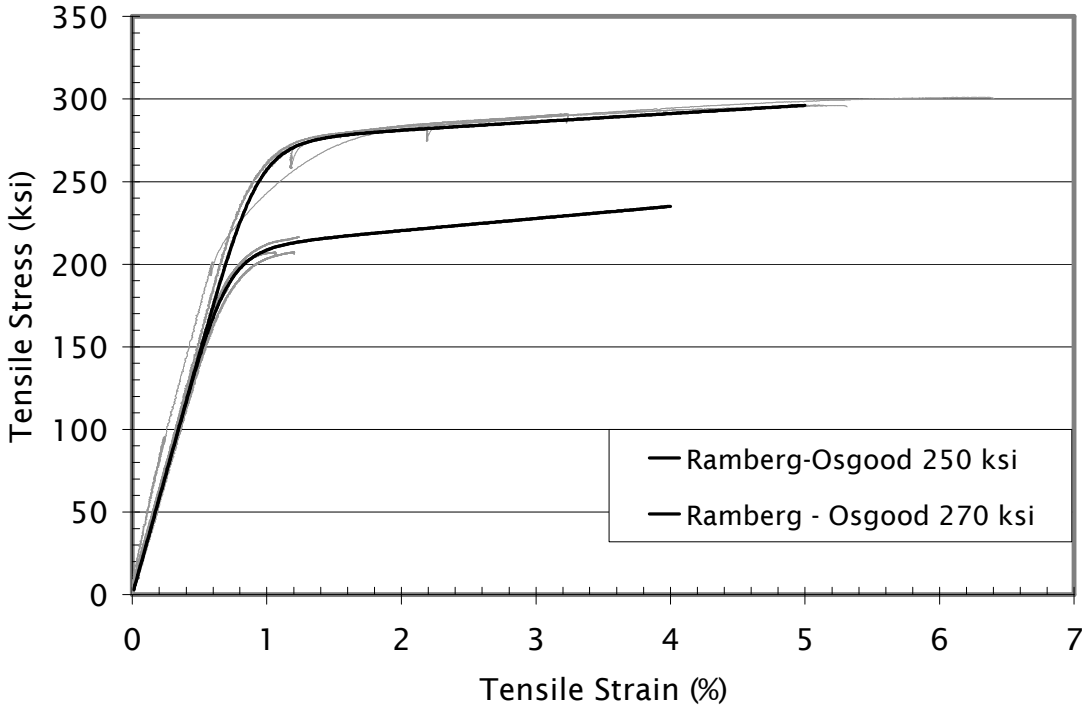

Figure 3.6 Stress-strain behavior of prestressing strands

3.2.3 Regular Reinforcing

The thickness of the deck (or flange) of the C-Channel girders was 5 in (127 mm). Shear keys were provided on both ends of the deck to achieve continuity between the girders after transverse post-tensioning. The deck was reinforced with regular reinforcing: #3 @ 7 in (D10 bars @ 180 mm) in the longitudinal direction and #4 @13 in (D12 bars @ 330 mm) in the transverse direction. Two #4 @13 in (D12 bars @ 330 mm) were used as stirrups as shown in Figure 3.4. Following the testing of each girder, two regular reinforcing bars were extracted from midspan. These bars were tested in tension using the MTS machine described in Section 3.2.2. Material properties measured during the tension tests are given in Table 3.2.

Table 3.2 Properties of non-prestressed reinforcement

Material Property	Bar 1	Bar 2
f_y, ksi	52	52
f_u, ksi	78	75
E_s, ksi	29680	--

3.2.4 Concrete

The nominal concrete strength specified for the C-Channel prestressed concrete girders was 5000 psi (34.5 MPa) at 28 days and the specified concrete strength at transfer of prestressing force was 4000 psi (27.6 MPa). During the design stage for strengthening of these girders, as described in Section 3.3, the concrete compressive strength was estimated using the following equation which accounts for the strength increases due to aging. (MacGregor 1997).

$$f'_c(t) = f'_c(28)\left[\frac{t}{4+0.85(t)}\right] \tag{3.2}$$

where $f'_c(t)$ is the concrete compressive strength as a function of time and t = time in days.

Three concrete core samples were obtained from most of the tested girders with the exception of one girder (CF2). These cores were taken by qualified NCDOT personnel, and tested in compliance with ASTM C42 specification in a Forney type compression testing machine. By inspection, it was observed that the concrete had river rock type aggregate varying in diameter from approximately 0.5 in to 1.0 in (13 mm to 25 mm). Due to the difficulty in obtaining a typical sized sample of 8 in (203 mm) long, the cores were drilled in the deck where a core of 5 in (127 mm) in length was obtained as shown in Figure 3.7. The appropriate correction factor from ASTM C42 was then applied to obtain the compressive strength of each core sample. Results of the compression tests are given in Table 3.3. Based on these results, the average

concrete strength was 9360 psi (64.5 MPa) and 7380 psi (50.9 MPa) for the Type I and Type II girders respectively.

Figure 3.7 Concrete core drilling operation for C-Channel girders

Table 3.3 C-Channel core sample test results

Specimen Designation	Compressive strength of concrete, *f'c*, ksi
CS	8.1
CF1	NA
CF2	9.7
NSM1S	10.1
NSM1F	6.9
NSM2S	9.9
NSM2F	8.9
EB1S	10.7
EB1F	7.4
EB2S	8.3
EB3S	9.8
EB4S	11.6
EB4F	8.0
EB5S	7.1
EB5F	6.7
EB6S	7.7
EB6F	8.1

3.2.5 Carbon Fiber Reinforced Polymers (CFRP)

The material used for flexural strengthening of the C-Channel girders, the main point of interest in this research project, was Carbon Fiber Reinforced Polymers (CFRPs). As mentioned in Chapter 2: Literature Review, the use of CFRPs in the built environment is gaining popularity in the United States, mainly because of its high strength to weight ratio, non-corrosive properties, and ease of installation. Three types of CFRP systems were used in this research: externally bonded wet lay-up type systems, externally bonded pre-cured laminates, and near surface mounted (NSM) systems. Explanation of each of the system types, as well as details of the installation process will be presented in Chapter 7 in conjunction with the design guidelines. The shape, type and amount of CFRP applied to the soffits of the C-Channel girder are shown in Figure 3.8. The strengthening systems NSM1 and NSM2 consisted of one CFRP bar or two CFRP strips placed in near surface mounted grooves in each soffit. Strengthening system EB1 consisted of one CFRP laminate per soffit. System EB3 consisted of two high modulus CFRP laminates per soffit. Systems EB2, EB4, EB5 and EB6 consisted of various configurations of either normal or high modulus CFRP wet lay-up sheets. Design of the CFRP systems is discussed in Section 3.3.

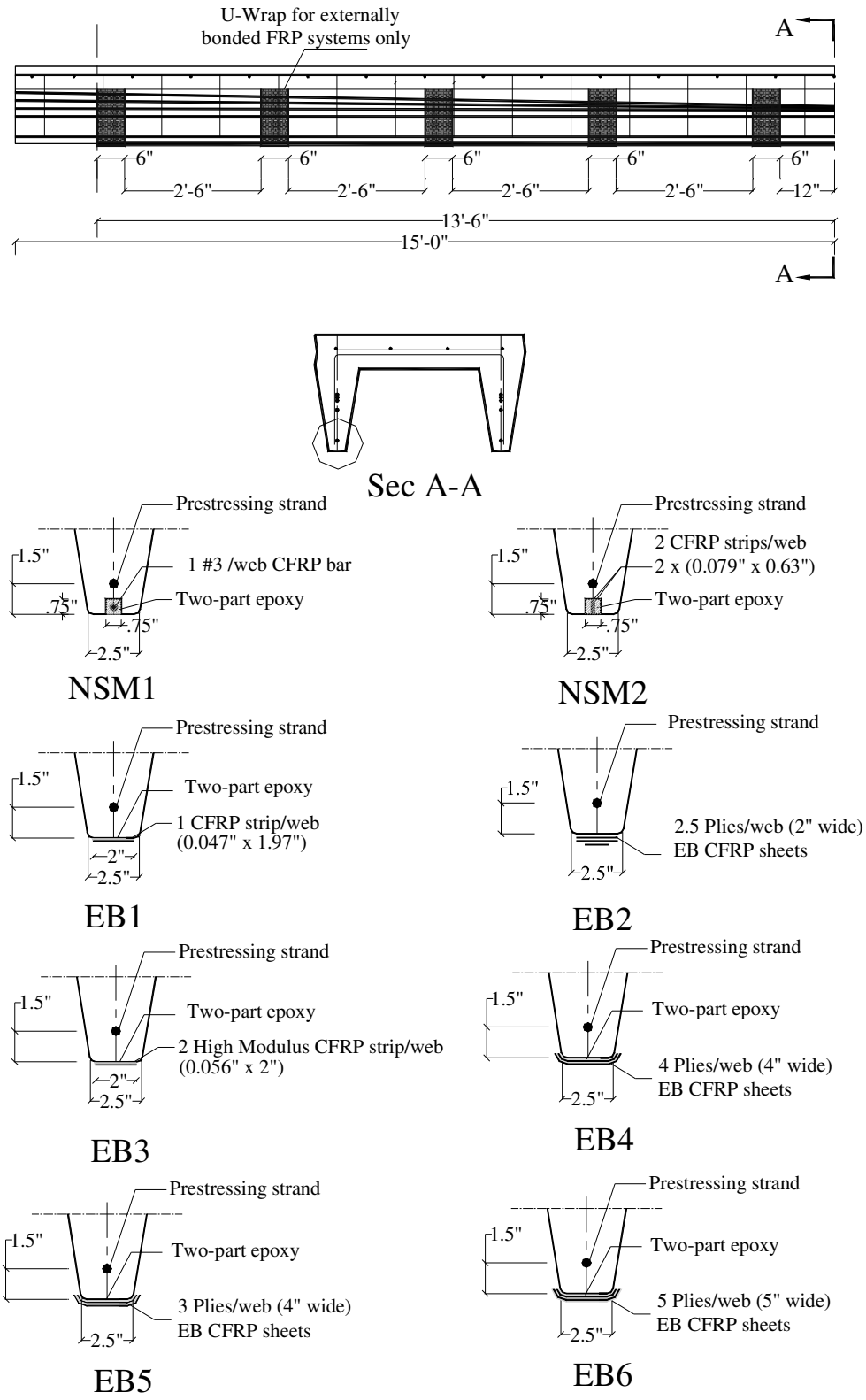

Figure 3.8 C-Channel strengthening configurations

Each type of CFRP material used in this research was tested to determine their characteristics including their tensile strength, elastic modulus, and rupture strain according to ASTM D3039 specification with the exception of CFRP bars manufactured by Hughes Brothers, where data was provided by the manufacturer. Descriptions of the various CFRP systems, along with their manufacturers, are shown in Table 3.4. The material samples for the wet lay-up CFRP sheets were taken from witness panels created at the time of strengthening and kept at the same location as the girders during the curing process. All samples were bonded to aluminum tabs using Wabo MBrace© Saturant. The width of the CFRP samples varied from 1 in to 2 in (25 mm to 50 mm) and the gauge length was kept constant at 6 in (152 mm).

Table 3.4 CFRP system manufacturers

Designation	Girders Strengthened	CFRP	Epoxy
Sika	EB1S, EB1F	Sika CarboDur pre-cured laminate	Sika Dur 30
HB.S	NSM2S, NSM2F	Hughes Brothers Aslan 500 CFRP tape	SikaDur 30
HM.PCL	EB3S	Mitsubishi pre-cured laminate K63712	SikaDur 30
VSL.1	EB2S	VSL C-200 wet lay-up sheets	VSL Type 1 & 2 resins
Fyfe.1	EB4S, EB4F	Fyfe SCH-41 wet lay-up sheets	Tyfo Type S epoxy
VSL.2	EB5S, EB5F	VSL C-200 wet lay-up sheets	MBrace system
HM.S	EB6S, EB6F	Mitsubishi wet lay-up sheets F637400	MBrace system

The prepared specimens were tested using the MTS machine described in Section 3.2.2. The strain of the CFRP was measured using a 0.236 in (6 mm) TML FLA-6-11 120 Ω electric resistance strain gauge placed at the center of the width and gauge length of the specimen. Two distinct modes of failure were observed during the tension testing. The first behavior was characterized by sudden and brittle rupture of the fibers through the CFRP matrix as shown in

Figure 3.9. The second possible mode of failure was less violent and rupture occurred through the cross section as shown in Figure 3.9. In general, failure of the pre-cured laminate strips was according to the first mode, while the wet lay-up laminates failed according to the second mode. This behavior is due to the fiber volume fraction in the pre-cured laminates which is significantly greater than the wet lay-up sheets. The only exception was the high modulus pre-cured laminates, which failed due to a smooth rupture through the cross section. If the rupture of the CFRP occurred in the vicinity of the aluminum grips the test was not included. Test results for all the CFRP tension tests are given in Table 3.5.

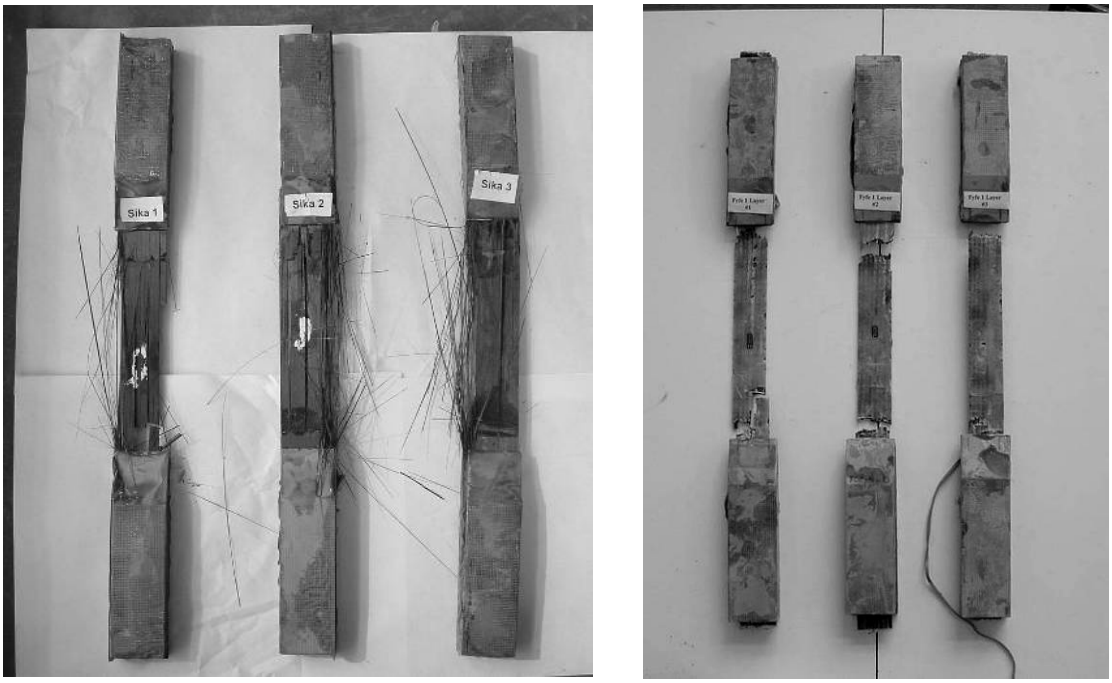

Figure 3.9 Typical pre-cured (left) and wet lay-up (right) laminate specimens after tension testing

Table 3.5 CFRP tension test results (C-Channels)

Specimen	Girders Strengthened	Thickness, in	Tensile Strength, ksi	E_F, ksi	ε_{fu}, %
Average Sika	EB1S, EB1F	0.05	400	23273	1.73
Sika Manufacturer		0.05	406	23853	1.69
Average HB.S	NSM2S, NSM2F	0.10	309	16733	1.85
HB Manufacturer		0.08	300	18995	1.70
Average HM.PCL	EB3S	0.06	145	58421	0.25
HM.PCL Manufacturer		0.04	220	53984	0.41
Average VSL.1	EB2S	0.06	97	7323	1.38
VSL.1 Manufacturer (laminate)		0.04	105	9396	1.00
Average Fyfe.1	EB4S, EB4F	0.09	49	6743	0.83
Fyfe.1 Manufacturer		0.04	143	13891	1.0
Average VSL.2	EB5S, EB5F	0.09	87	6540	1.4
VSL.2 Manufacturer		0.04	105	9425	1.0
Average HM.S	EB6S, EB6F	0.08	20	10962	0.20
HM.S Manufacturer		0.04	57	19169	0.30

3.3 Design of Strengthened Girders

The design of the strengthened girders proceeded after testing the control girder. Results of the static test on the Type I girder were assumed as the base for the design of the strengthened girders. Three different levels of strengthening were examined, the design criteria being to achieve a 20, 40 or 60 percent increase in the ultimate load carrying capacity with respect to the control girder. The design of each strengthened girder was based on a cracked section analysis program, Response 2000© (Bentz 2000). The base curve of the concrete compression model used in the cracked section analysis program was the Popovics curve, compression softening was determined using the Vecchio-Collins model and the tension stiffening was determined from the Bentz model (Bentz 2000). In the preliminary design, the compression strength of the concrete was based on the compression strength specified in the original NCDOT drawings modified

according to Equation 3.2 to account for the age of concrete at the time of testing. The compression strength used in the design was 6000 psi (41.4 MPa). The prestressing strands were all assumed to be 250 ksi (1724 MPa) for Type I prestressing configuration modeled using the Ramberg-Osgood equation with 0.030, 121 and 6 for the coefficients A, B, and C respectively (Bentz 2000). The CFRP systems used in the design were modeled as linear elastic up to failure using material properties provided by the manufacturer. The material properties used in the design of the high modulus CFRP sheets were based on extensive prior material testing conducted by another graduate student (Schnerch 2005). Discrepancies between the manufacturer's material properties and the measured properties determined at a later stage due to material testing lead to premature failures in two of the specimens tested under static loading, EB2S and EB3S. This will be discussed in detail in Section 3.4.

Flexural failure, defined as rupture of the FRP or crushing of the concrete in compression, was the desired mode of failure. It was recognized that externally bonded systems are more prone to debonding failures than near surface mounted systems. According to Malek et al 1998, shear stresses developed at the FRP cut-off point for the externally bonded systems were significantly lower than the shear strength of the concrete. Therefore, plate-end debonding is not expected to occur and is not of great concern. To delay FRP delamination-type failures along the length of the girder, 6 in (150 mm) wide U-wraps were installed at 3 ft (900 mm) spacing for all externally bonded strengthened girders. This arrangement was selected to simulate typical anchorage details commonly used by the construction industry for reinforced concrete members strengthened with FRP.

As mentioned, three levels of strengthening were examined: 20, 40 and 60 percent. The six girders designed to achieve a 20 percent increase in ultimate capacity were NSM1, NSM2,

EB1, EB2 and EB3 and EB6. One girder, EB5, was designed to achieve a 40 percent increase and girder EB 4 was designed to achieve a 60 percent increase. The desired level of strengthening was achieved four girders: NSM1, NSM2, EB1 and EB4. The desired level of strengthening was not achieved for girders EB2, EB3 and EB5 due to discrepancies in the material properties provided by the manufacturer. Girder EB6 achieved a much higher level of strengthening than anticipated as discussed in detail in the following section.

3.4 Static Tests

This section discusses the behavior of nine of the seventeen C-Channel girders tested statically to failure. The remaining eight girders were tested under fatigue loading conditions and the results will be presented in Section 3.5.

3.4.1 Test Setup, Procedure and Instrumentation

All girders were tested using a 110 k (490 kN) MTS hydraulic actuator, with the exception of the control girder which was tested using a 450 k (2000 kN) MTS hydraulic actuator. The actuator was mounted to a steel frame placed at the midspan of the girder. To simulate field loading conditions, a set of truck tires filled with silicon rubber were used as a contact surface while applying the load for the Type I girders. The footprint of the two tires was approximately 10 in by 20 in (150 mm by 250 mm), the same area as the design loading area specified by AASHTO (AASHTO 2004). The Type II girders were loaded with a steel plate having the same size as the AASHTO specified design loading area.

Typical C-Channel prestressed concrete bridges constructed in the early 1960s usually have a substructure of wooden piles that is difficult to mimic in the laboratory. However, in order to simulate small displacements at the supports, the girder was supported at both ends on a

2.5 in (64 mm) thick neoprene pad which in turn rested on a 1 in (25 mm) steel plate. Hydrostone was used at the supports for leveling purposes. The width of the neoprene pad was 8.5 in (216 mm) which provided a clear span of 28.6 ft (8710 mm) for the tested girder.

The displacement behavior of the girders during testing was monitored using three sets of string potentiometers, placed at quarter spans, and two linear potentiometers to measure vertical displacement over the supports. The compressive strain in the concrete was measured using a combination of PI gauges (a strain gauge mounted to a spring plate) and two 2.36 in (60 mm) TML FLA-60-11 120 Ω electric resistance strain gauges located at midspan. PI gauges were also placed at various locations at the level of the lowest prestressing strand to measure the crack width and to determine the strain profile along the depth of the girder. The tensile strain in the CFRP reinforcement was measured using six 0.236 in (6 mm) TML FLA-6-11 120 Ω electric resistance strain gauges: two at midspan, two at 6 in (150 mm) from midspan and two at 12 in (305 mm) from midspan. Figure 3.10 shows a typical test setup for the C-Channel girders under static loading conditions.

Figure 3.10 Typical test setup for C-Channel girders tested under static loading conditions

The loading sequence of the girders began by increasing the applied load up to a load level slightly higher than the cracking load. The girder was then unloaded, and reloaded again at a rate of 0.1 in/min (2.5 mm/min) up to the load level equivalent to yielding of the prestressing strands. This loading sequence was selected to determine the effective prestressing force in the girders by observing the re-opening of the flexural cracks. For the given measured load at reopening of the flexural crack at midspan, P_{ro}, the average effective prestressing strands, P_{eff}, can be determined according to the following equation,

$$0 = \frac{M_D}{S_b} + \frac{L \cdot P_{ro}}{4 \cdot S_b} - \frac{10 \cdot P_{eff}}{A_c} - \sum \frac{d_i \cdot P_{eff}}{S_b} \tag{3.3}$$

where M_D is the moment due to the dead load, S_b is the bottom section modulus, L is the span, A_c is the area of the concrete section, and d_i are the locations of the different layers, i, of prestressing strand measured from the neutral axis of the section.

When the girders were loaded beyond yielding of the prestressing strands, the rate of the applied load was increased to 0.2 in/min (5 mm/min) up to failure. The average prestress force for Type I and Type II girders was 15.7 k (69.2 kN) and 18.6 k (81.6 kN) respectively. Details of the various strengthening systems and material properties are summarized in Table 3.6.

Table 3.6 Details of strengthened girders and summarized material properties

Specimen Designation	NSM1	NSM2	EB1	EB2	EB3	EB4	EB5	EB6
Date of testing	3/04S 5/04F	3/04S 4/04F	3/04S 4/04F	4/04	5/04	6/04 S&F	3/05S 4/05F	3/05S 5/05F
Date of strengthening	-	2/04	2/04	2/04	2/04	4/04	3/05	3/05
Prestressing Configuration	Type I	Type I	Type I	Type I	Type I	Type I	Type II	Type II
Strengthening technique	NSM bars	NSM strips	EB strips	EB sheets	EB strips	EB sheets	EB sheets	EB sheets
FRP details	1 bar / web	2 strips / web	1 strip / web	2.5 plies / web	2 strips / web	4 plies / web	3 plies / web	5 plies / web
FRP shape	dia = 0.36 in	strips are 0.08 x 0.63 in	strips are 0.05 x 4 in	sheets are 0.05 x 2 in	strips are 0.06 x 2 in	sheets are 0.09 x 4 in	sheets are 0.04 x 4 in	sheets are 0.04 x 5 in
Groove size	0.75 x 0.75 in	0.75 x 0.75 in	-	-	-	-	-	-
A_{FRP}, in^2	0.202	0.202	0.184	0.567	0.448	3.040	0.959	2.000
E_{FRP}, ksi (matl testing)	18000	16733	23273	7323	58421	6743	6540	10962
f_{uFRP}, ksi (matl testing)	300	309	400	97	145	49	87	20
f'_c, ksi*	9.9	8.4	9.8	7.4	8.4	10.7	6.7	7.7

* this is the average of the girder tests performed for the specified type of strengthening

3.4.2 Control Girder

No visible flexural cracks were observed in the control girder (girder CS) upon delivery to the laboratory. There was only one shear crack located near the support that extended with approximately a 45 degree angle from the edge of the support to the deck. The measured camber of all the girders with Type I prestressing configuration was 1.25 in (32 mm).

The girder was loaded statically up to failure. The effective prestress force given in Table 3.6 was determined from the cracking load for this girder, which occurred at a load of 12.6 k (55.8 kN). After cracking, flexural cracks were evenly distributed along the length of the girder and located approximately at the location of mild steel stirrups. Yielding of the lower prestressing strands took place at a load level of 25.8 k (115 kN) according to readings of the PI gauges. Failure occurred due to crushing of concrete at a load level of 33.2 k (148 kN) at an ultimate deflection of 9 in (228 mm) as shown in Figure 3.11. Due to the confining effect induced by the loading tires, crushing of the concrete occurred first at the edge of the girder at midspan before it extended underneath the loading area.

Figure 3.11 Failure due to concrete crushing of girder CS

3.4.3 NSM CFRP Strengthened Type I Girders

Behavior of the two girders, NSM1S and NSM2S, strengthened with a NSM system using either FRP bars or strips respectively, was similar during testing including the failure modes. No cracks were observed in either girder at the time of delivery.

Flexural cracking was observed at a load level of 12.4 k (55 kN) for both girders. The initial stiffness of both girders was similar to that of the control girder, as was the post-cracking stiffness. After yielding of the prestressing strands, the presence of the CFRP reinforcement constrained opening of the cracks and consequently reduced the midspan deflection compared to the control girder. At this loading stage, the stiffness of girders NSM1 and NSM2 were almost double that of the control girder. The mild steel stirrups again acted as crack initiators, but other cracks between the stirrups were also observed. Failure of both girders strengthened with NSM

CFRP reinforcement was due to crushing of the concrete at the extreme compression zone followed by debonding of the NSM CFRP reinforcement at a load of 40.8 k (181 kN) for the NSM bars and 40.7 k (180 kN) for the NSM strips as shown in Figure 3.12. Since the ultimate strain in the concrete controlled the failure mode of both girders, the curvature and consequently the deflection at ultimate were similar. The measured compressive strain of the concrete at ultimate was 0.0035 in/in for both girders. The measured ultimate crack width at midspan was 0.007 in (0.17 mm) for NSM2S and 0.0063 in (0.18 mm) for NSM2S. Test results showed that strengthening of the prestressed girders using NSM CFRP bars and strips increased the ultimate load carrying capacity of the girder by 22.9 and 22.6 percent respectively compared to the control girder.

The manufacturer's reported rupture strain and the rupture strain measured during tension tests performed on the CFRP bars and strips were very similar (see Table 3.5). During the test, the maximum recorded tensile strain in the CFRP bars and strips at concrete crushing failure was 81 percent and 87 percent respectively of the ultimate strain reported by the manufacturer.

Figure 3.12 Failure due to concrete crushing of NSM1

3.4.4 Externally Bonded CFRP Strengthened Type I Girders

Four girders with a Type I prestressing configuration were strengthened with externally bonded CFRP systems. No flexural or shear cracking was noticed in the girders at the time of delivery to the laboratory.

The behavior of the prestressed concrete girder strengthened with externally bonded CFRP strips (EB1) matched that of the NSM strengthened girders before and after cracking. Flexural cracking at midspan was observed at a load level of 11.9 k (57 kN). With a similar value of $E_{FRP}A_{FRP}$ compared to the NSM strengthened girders (see Table 3.6), the cracking pattern and average crack width at midspan was also similar. Failure occurred due to intermediate crack (IC) debonding of the CFRP strip (see Section 2.9) at a load level of 39.6 k (176 kN) as shown in Figure 3.13. The majority of the debonding occurred within the concrete

substrate, although in several places debonding was noticed within the CFRP strip (interlaminate debonding). The maximum recorded strain in the CFRP prior to debonding was 72 percent of the rupture strain measured using tension coupon tests. Compared to the control girder, EB1 strengthened with CFRP strips achieved an increase in the ultimate load carrying capacity of 19 percent. The intermediate crack debonding was delayed by the presence of the externally bonded U-wraps spaced at 3 ft (914 mm) along the girder. This is discussed in greater detail in Chapter 5.

Figure 3.13 Failure due to intermediate crack debonding in girder EB1S

For the girder strengthened with 2.5 plies of externally bonded sheets (EB2S) to achieve a 20 percent increase in the ultimate capacity, behavior was similar to that of girder EB1S up to failure which occurred due to rupture of the CFRP sheets at midspan at a load of 36.7 k (163 kN) as shown in Figure 3.14; an increase of 10 percent compared to the measured ultimate load of the control girder. The maximum recorded tensile strain in the CFRP sheets was 1.29 percent,

similar to results obtained from the tension coupon tests. It should be mentioned that the design of the girder was performed using the dry fiber properties provided by the manufacturer at an ultimate strain of 1.7 percent. Therefore, the desired percent increase in ultimate capacity was not achieved. According to ACI 440F Section 14.1, the stiffness and strength per unit width calculated using the dry or the laminate properties should be identical. Table 3.7 shows the stiffness and strength per unit width calculated using the dry and laminate properties specified by the manufacturer along with results obtained from the tension coupon tests. There was considerable discrepancy in the stiffness and strength per unit width between the dry and laminate properties given by the manufacturer. The results from the tension coupon tests showed that the measured values of stiffness and strength per unit width of the CFRP sheets lied between the calculated values using the dry fiber and laminate properties as reported by the manufacturer. Therefore, in the absence of experimental data, design of externally bonded FRP sheets should be based on the laminate properties.

Table 3.7 Comparison between dry fiber and laminate properties of the CFRP system used in girder EB2S

	Stiffness per unit width (ksi/layer)	Strength per mm width (k/layer)
Dry Fiber Properties*	429	7.15
Laminate Properties*	376	4.20
Value from Material Testing	408	5.51

*specified from manufacturer

Figure 3.14 Failure due to rupture of CFRP sheets in girder EB2S

The girder strengthened with externally bonded high modulus CFRP strips (EB3S) to achieve a 20 percent increase in ultimate capacity, demonstrated 11 percent higher initial stiffness compared to the control girder. Flexural cracking of this girder occurred at an applied load of 14.0 k (67 kN). Post-cracking stiffness was also higher than that of the control girder, yet the girder failed due to rupture of the CFRP strips at a load of 23.1 k (103.7 kN) immediately after yielding of the prestressing strands. Figure 3.15 shows the girder after rupture of the laminate. The maximum measured strain observed in the high modulus CFRP strips at failure was only 0.17 percent, which is 41 percent of the specified manufacturer's rupture strain and 74 percent of the rupture strain measured from the tension coupon tests of the same material. It is believed that the early rupture of the high modulus CFRP strips was due to the presence of flaws in the manufacturing process of this relatively new material as reported by the manufacturer.

After rupture of the CFRP strips, the test was continued until concrete crushing occurred at a load of 29.1 k (129 kN). The lower level of maximum measured load in comparison to the control girder could be due to the sudden failure of the CFRP material imparting an impact load on the girder.

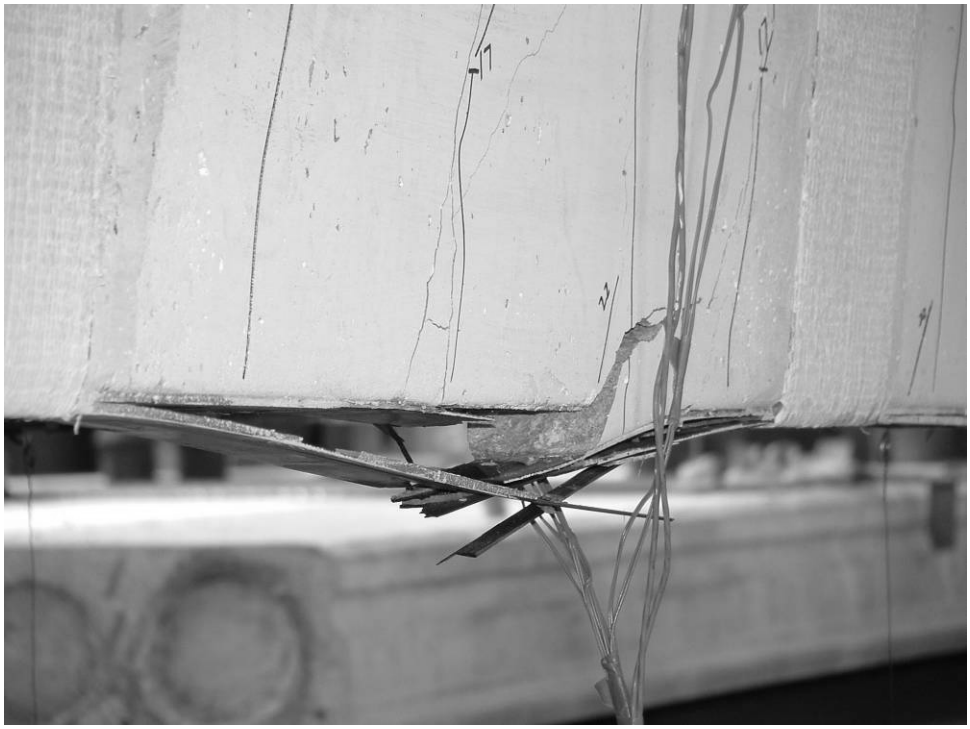

Figure 3.15 Rupture of high modulus CFRP strips in girder EB3S

The fourth girder strengthened with an externally bonded system (EB4S) was designed to achieve an increase of 60 percent in the ultimate load carrying capacity compared with the control girder. The girder was designed using the laminate properties as provided by the manufacturer. The initial stiffness of this girder was similar to that of the control. Flexural cracking occurred at a load of 13.0 k (57.6 kN). Failure was due to rupture of CFRP sheets at a load of 53.1 k (236 kN) providing an increase of 60 percent over the ultimate load of the control girder. Rupture of the CFRP sheets was observed just outside the location of the U-wrap and

occurred throughout the four layers at the same location as shown in Figure 3.16. No debonding was noticed before rupture of the CFRP sheets.

Figure 3.16 Failure due to rupture of CFRP sheets in girder EB4

3.4.5 Externally Bonded CFRP Strengthened Type II Girders

Two girders with a Type II prestressing configuration were tested under static loading conditions. Girder EB5S was strengthened with 3 layers of externally bonded CFRP sheets to achieve a 40 percent increase in ultimate strength, and girder EB6S was strengthened with 5 layers of externally bonded high modulus CFRP sheets to achieve a 20 percent increase in ultimate strength. Both girders were in good uncracked condition at time of delivery. The camber due to prestressing of all Type II girders was 1.25 in (32 mm). The strengthening for both girders was designed assuming a Type I prestressing configuration, as explained in Section 3.3. No control girder with a Type II prestressing configuration was tested under static loading

conditions. However, a control girder with the Type II pattern was tested under fatigue loading conditions (CF2). This girder, as will be explained in Section 3.5.2, had very little degradation due to the cyclic loading at 2 million cycles. Therefore, the best estimate of a control girder with the Type II prestressing pattern is the final static test of this girder tested under fatigue loading. This is explained in greater detail in Section 5.4.1.

The prestressing strand configuration was not known at the time of testing of girders EB5S or EB6S. When the tests began and the applied load reached a level of 16.4 k (72.9 kN) and no flexural cracking was visible, it was decided to unload the girder instead of increasing the load to a point where the cracking load could be determined from visual inspection. As a result of this, the cracking loads for EB5S and for EB6S were determined based on changing of the stiffness measured by PI gauge readings at midspan.

Flexural cracking of girder EB5S occurred at a load of 13.9 k (61.8 kN). At a load of 45 k (200.2 kN), the applied load suddenly dropped to zero as a result of operator error. The residual displacement at zero load was 0.5 in (12.7 mm). The girder was subsequently reloaded, and at an applied load of 45 k (200 kN) very little change in stiffness could be noticed in comparison to the first cycle of loading. After this reloading occurred, interfacial debonding was initiated at the location of the flexural cracks at midspan spread to cause intermediate crack (IC) debonding between the U-wraps located on either side of midspan. The debonding did not cause failure, but occurred due to crushing of the concrete at a load of 55.3 k (246.0 kN) as shown in Figure 3.17. The energy released upon crushing of concrete led to peeling of the U-wraps from the webs of the girder, but did not cause the CFRP to rupture. Girder EB5S achieved an increase of strength of 72.8 percent in comparison to the ultimate strength measured during the final static test of the Type II girder tested in fatigue (CF2). The measured performance of the girder

exceeded the design values due to a high rupture strain measured in the CFRP during the test, which was 18.8 percent higher than the value reported by the manufacturer.

Figure 3.17 Failure of girder EB5S due to concrete crushing

Flexural cracking of girder EB6S strengthened with high modulus CFRP sheets occurred at a load of 14.3 k (63.6 kN). At a load of 33.7 k (149.9 kN) failure occurred due to rupture of the CFRP sheets at midspan, which provides an increase of only 5.3 percent in comparison to girder CF2 during the final static test. A typical CFRP sheet rupture is shown in Figure 3.18. The tensile strain in the CFRP achieved during this test was 13.3 percent lower than the value reported by the manufacturer. After rupture of the CFRP, the test was continued until ultimate failure occurred due to a combination of progressive CFRP rupture and concrete crushing close to the values of ultimate load and displacement of the control girder.

Figure 3.18 Rupture of high modulus CFRP sheets at midspan in girder EB6S

3.5 Fatigue Tests

Eight C-Channel girders were tested under cyclic load: five girders with Type I prestressing strand configuration and three girders with Type II prestressing configuration. This chapter will provide details and descriptions of the individual tests. Full test results are discussed in Section 5.3.

3.5.1 Test Setup, Procedure and Instrumentation

The test setup and instrumentation for the girders tested under fatigue loading conditions was similar to that of the girders tested under static loading conditions with the following exceptions: 1) a 10 in by 20 in by 1 in (254 mm by 508 mm by 25 mm) loading plate was used in lieu of the loading tires to ensure adequate stability during the cyclic loading, and 2) two 6 in

(152 mm) linear potentiometers were placed at midspan to measure displacement instead of string potentiometers due to their superior performance in fatigue. After completion of the fatigue loading, string potentiometers were used for the final static test.

The initial applied loading for the girders tested in fatigue was also identical to that of the girders tested statically to failure: the girder was loaded up a load equal to the cracking load, unloaded and reloaded in order to determine the effective prestressing force in the girder. The range of typical frequencies used for fatigue loading of concrete structures is 2 Hz to 5 Hz. Due to the large scale of the C-Channel girders, they were loaded at a frequency of 2 Hz.

3.5.2 Fatigue Load Determination

The fatigue load range used for testing the C-Channel girders was designed to simulate typical loading of an actual bridge under service loading conditions. The range varies from a minimum load equivalent to the dead load and a maximum equivalent to the dead load plus the live load. For the tested C-Channel girders, the minimum load, in addition to the girder's own weight, included a load producing a moment equivalent to the moment due to an asphalt wearing surface typically used for these types of bridges. Assuming a wearing surface thickness of 4 in (102 mm) and density of 150 lbs/ft^3 (23.56 kN/m^3), the dead load was calculated as:

$$\omega_{DL} = (4)(30.5)(150) = 0.127 \text{ k/ft } (1.862 \text{ kN/m})$$

$$M_{DL} = \frac{(0.127)(30)^2}{8} = 14.34 \text{ k-ft } (19.46 \text{ kN-m})$$

Thus, the minimum concentrated load, P_{DL}, can be calculated as,

$$P_{DL} = \frac{(14.34)(4)}{30} = 1.91 \text{k } (8.51 \text{ kN})$$

A value of 2 k (8.9 kN) was used.

The maximum load was determined based on a truck configuration specified by AASHTO HS-15 type loading depicted in Figure 3.19. The axle load of 24 k (106.8 kN) was multiplied by the impact factor and the distribution factor according to AASHTO specifications (2004). The impact factor used was 1.33 as specified by AASHTO Article 3.6.2.1. The load distribution factor was determined from Table 4.6.2.2.2b-1 of the AASHTO specifications. Based on a two lane bridge 30.5 ft (9.3 m) wide supported by twelve C-Channel girders, the distribution factor used was 0.24.

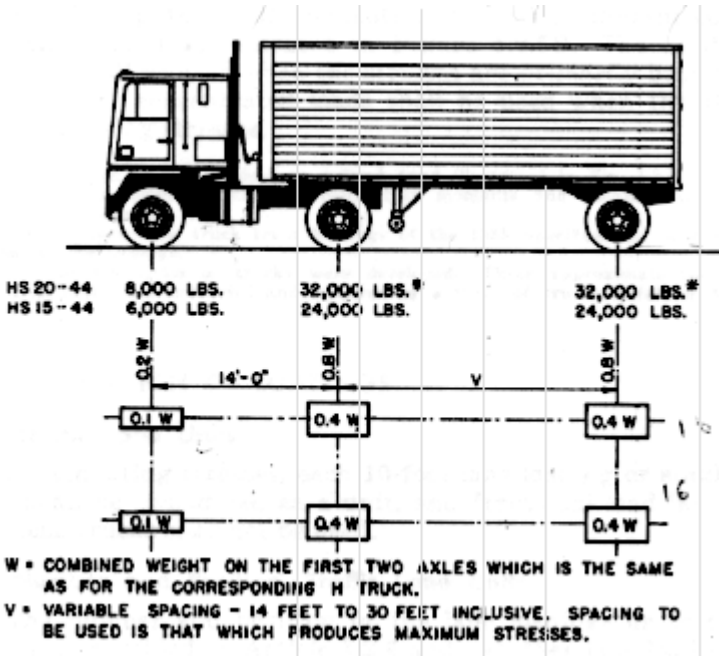

Figure 3.19 AASHTO Design Truck

Applying the appropriate factors to the middle and rear axle loads can be determined as:

(Axle Load)(Impact Factor)(Distribution Factor)=

$$(24)(1.33)(0.24) = 7.66 \text{ k (34.1 kN)}$$

When the design axle loads were applied as moving truck loads along the girder span of 30 ft (9.14 m), the maximum moment occurred when the middle axle was at a distance of 11.5 ft (3.50 m) from the right support and the rear axle was at a distance of 25.5 ft (7.77 m) from the

right support. The analysis indicates that the front axle of the truck would be acting on an adjacent span. Based on the maximum moment induced by the truck loading, the equivalent concentrated load at midspan was determined to be 9.0 k (40 kN) as shown in Figure 3.20.

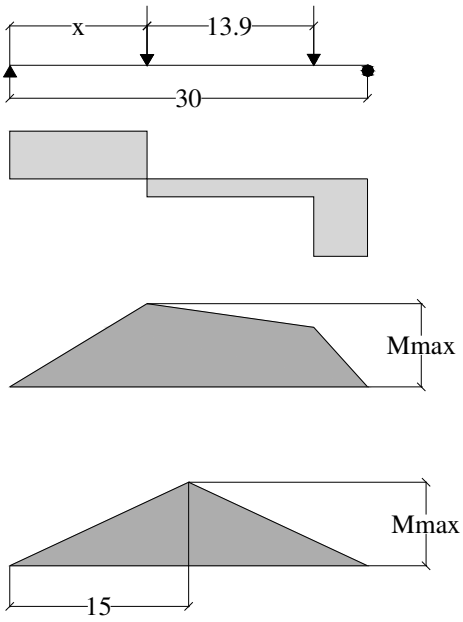

Figure 3.20 Shear and moment diagram for moving AASHTO axle loads

In June 2005 a more clear copy of the 40 year old Standard Specification for C-Channel Girders (the original design document) was obtained. It was noticed that the HS-15 type loading was specified only for girder spans of 20 ft (6.10 m) or 25 ft (7.62 m). For girders with a 30 ft (9.14 m) span, HS-13 type loading was the specified design loading. Applying the impact, distribution, and moment correction factors discussed above to the HS-13 loading, the equivalent concentrated load simulating the live load is 7.8 k (34.7 kN) which is 13.3 percent less than the HS-15 type loading originally used.

3.5.3 Control Girders

Two girders were tested as control specimens. The first was prestressed with a Type I prestressing configuration (CF1) and the second was prestressed by a Type II configuration (CF2).

At the initial stage of loading of C-Channel girder CF1, a sudden load of approximately 23 k (100 kN) was applied to the girder due to problems related to the load control system of the actuator. The load was large enough to cause flexural cracking. Following the unfortunate incident, the girder was loaded statically to determined the load causing reopening of the crack to determined the effective prestress forces as described in Section 3.4.1, the measured value of which was 9.0 k (40.0 kN), which corresponds to a loss of prestress of 14.3 percent, comparable to the level measured for the other girders. The fatigue cycles varied between an upper and lower load levels of 2 k and 11 k (8.9 kN and 49.0 kN) respectively which corresponds to HS-15 type loading, or 15.4 percent higher than HS-13 loading. The girder failed due to a ruptured lower prestressing strand after completion of 1,076,000 cycles, therefore the girder was not tested by the typical final static loading test.

Cracking of the control girder prestressed with a Type II configuration, CF2, occurred at a load level of 12.5 k (55.6 kN). After unloading and reloading, the flexural crack at midspan reopened at a load of 10.2 k (45.4 kN), which shows an approximate loss of prestress of 13.8 percent. After the initial loading cycles, the girder was cycled between the load levels 2 k and 11 k (8.9 kN and 49 kN) which was the same level used during the testing of girder CF1. CF2 survived 2 million cycles with very little degradation. The girder was then loaded to failure, which occurred at a load of 32.0 k (142 kN) which was 3.6 percent less than the ultimate strength achieved in the static test of the control girder prestressed by a Type I C-Channel prestressing

configuration (CS). Failure of the girder was due to crushing of the concrete as shown in Figure 3.21.

Figure 3.21 Concrete crushing failure of girder CF2 during final static test

3.5.4 NSM CFRP Strengthened Girders

Two girders were strengthened with NSM systems and tested in fatigue. The first was strengthened with NSM bars (NSM1F) and the second was strengthened with NSM strips (NSM2F). The two girders were identical to the two girders tested under static loading conditions, NSM1S and NSM2S. Upon receiving the girder, no initial damage was noticed for either girder. The measured camber due to prestressing for both girders was 1.5 in (38 mm).

Based on the initial loading applied to the two girders, the cracking load of the NSM bars and strips strengthened girders occurred at loads of 12.1 k (54 kN) and 11.5 k (51 kN)

respectively. After the initial loading, the strengthened girders were tested at a frequency of 2 Hz and load range of 2k to 11 k (8.9 kN to 57.6 kN), which corresponds to a live load 41 percent higher than HS-13 loading. For both girders, the largest degradation in stiffness occurred during the first 10,000 cycles. After completion of 2 million cycles, very little degradation was observed for either girder. The girder were tested up to failure and showed little difference in their behavior and the behavior of the girders tested under static loading conditions. For girder NSM1F, failure was due to crushing of the concrete at a load of 40.2 k (178 kN) as shown in Figure 3.21. The girder tested under static load (NSM1S) failed at a load of 40.8 k (181 kN). Girder NSM2F also failed due to crushing of concrete at a load of 36.9 k (163 kN), compared to the statically tested girder which failed at a load of 40.7 k (180 kN). Typical concrete crushing failure of the NSM strengthened girders during the final static test after the fatigue cycling is shown in Figure 3.22.

Figure 3.22 Concrete crushing failure of girder NSM2F during final static test

3.5.5 Externally Bonded CFRP Strengthened Type I Girders

Two girders strengthened with externally bonded CFRP systems were tested in fatigue: one girder strengthened with externally bonded strips (EB1F) and another girder strengthened with externally bonded sheets designed to increase the flexural capacity by 60% in comparison to the control, girder EB4F. These two girders were identical to the two girders that were tested under static loading conditions. By inspection it was observed that girder EB4F had one shear crack which began within the end of one web near the supports and extended to a location in the deck, similar to the damage noted for girder CS. In order to ensure flexural failure, an additional CFRP U-wrap was installed prior to testing across the crack to provide shear reinforcement at the end.

The measured cracking load of the girder strengthened with externally bonded strips (EB1F) was 12.1 k (54 kN). The girder was cycled between the load range of 2 k and 11 k (8.9 kN and 57.8 kN) which corresponded to a 41 percent live load increase over HS-13 type loading. After 10,000 cycles, the behavior of the strengthened girder was quite different from the behavior of the NSM strengthened girders. After completion of 625,000 cycles a large flexural crack was noticed near midspan which led to localized delamination of the CFRP sheets from the concrete substrate. This crack was due to rupture of one of the prestressing strands as shown in Figure 3.23. The test was continued and catastrophic failure occurred after completion of 908,000 cycles due to progressive rupture of the prestressing strands followed by debonding of the CFRP strips. Gradual degradation of the bond between the concrete and FRP due to the fatigue loading caused a loss of girder stiffness and consequently an increase in stress ratio in the lower prestressing strands precluding failure. It should be mentioned that after failure, corrosion was

observed in the lower prestressing strand – which could be a possible additional cause of the early fatigue rupture.

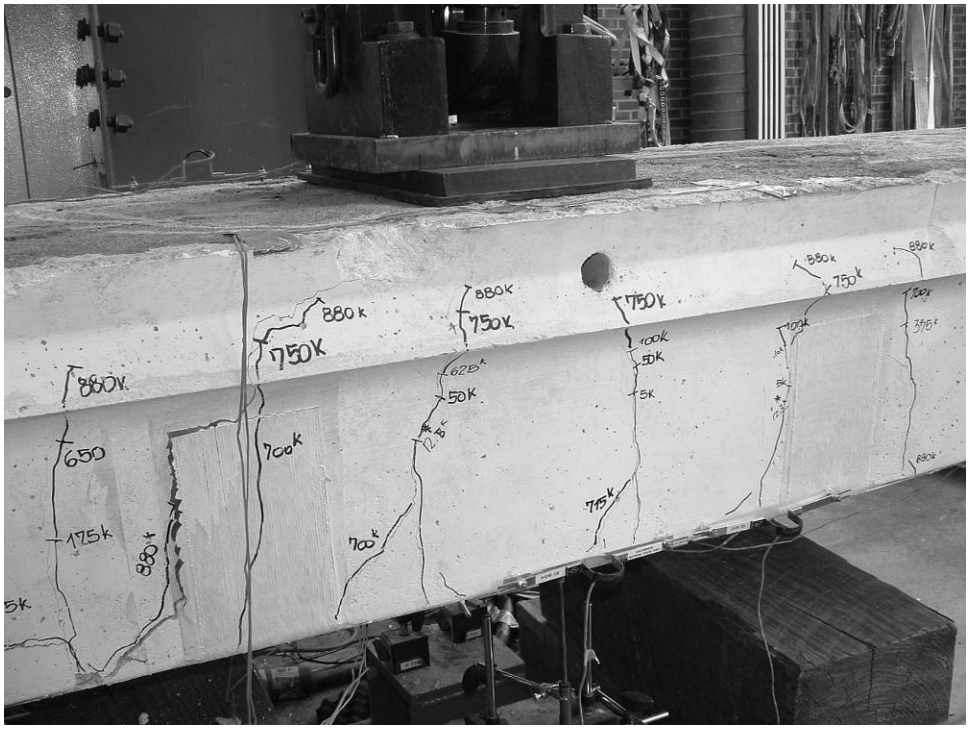

Figure 3.23 Girder EB1F after failure due to rupture of prestressing

A girder strengthened with externally bonded CFRP sheets designed to achieve a 60% increase in the ultimate load carrying capacity in comparison to the control girder, EB4F, was tested in fatigue. The cracking load of this girder was measured to be 15.7 k (70 kN), which was higher than any of the previously tested girders due to a higher effective prestressing force. The measured crack reopening load was 9.0 k (40.0 kN). This girder was tested identically to the other strengthened girders in fatigue, a load level corresponding to a 41 percent increase in HS-13 truck loading. Very little degradation was noticed between the initial loading sequences up until 1 million cycles. At this stage it was decided to increase the load range to 2 k to 11 k (8.9 kN to 72.7 kN), representing a 84.6 percent increase of the load equivalent to HS-13 truck

loading. A static test performed at one million cycles showed very little change in stiffness up to 16.4 k (72.7 kN). After 1,250,000 total cycles, a change in stiffness was observed as a result of the flexural cracks opening at midspan.

Between 1.25 million cycles and 2 million cycles very little change was observed in the cracking pattern or the load-deflection behavior. After completion of 2 million cycles, the girder was tested statically to failure. Failure was due to rupture of the CFRP sheets followed by crushing of concrete as shown in Figure 3.24. Due to the higher prestressing force observed in this girder, the girder tested in fatigue failed at a load of 55.1 k (245 kN), greater than the ultimate load observed for girder EB4S.

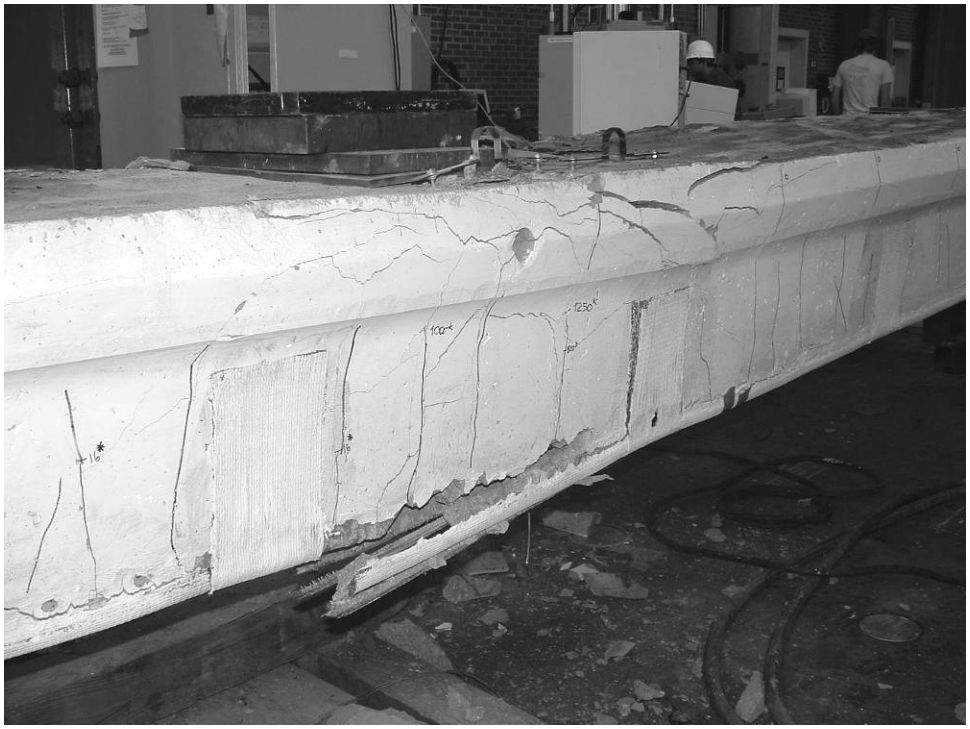

Figure 3.24 Girder EB4F after failure due to concrete crushing followed by rupture of CFRP

A post mortem investigation of the girder showed numerous ruptured wires in the top inclined prestressing strand located at the hold down point at midspan. Although this was

established after the final static test was performed, it is possible that the rupture of some of these strands lead to the significant change in stiffness noticed after 1 million cycles.

3.5.6 Externally Bonded CFRP Strengthened Type II Girders

A girder designed to achieve a 40 percent increase in ultimate flexural capacity using externally bonded CFRP wet lay-up sheets, EB5F, was tested in fatigue. A similar girder, tested under static loading conditions (EB5S) failed due to concrete crushing at an ultimate load equivalent to a 72.8 percent increase in comparison to the control girder (CF2 for this Type II girder). Visual observation indicated that the first instance of flexural cracking occurred at load level of 18.0 k (80.1 kN); however, upon inspection of the measured load deflection relationship the cracking load was determined to be 13.5 k (60.1 kN).

Girder EB5F was subjected to fatigue loading with a maximum load corresponding to a 84.6 percent increase in comparison to HS-13 truck loading, similar to the second fatigue loading regimen used for girder EB4F. After the first 5,000 cycles considerable flexural cracking was noticed at midspan. No new cracks or crack extensions were noticed until 500,000 cycles, at which time a flexural crack at midspan was noticed to be extending into the top flange of the C-Channel. At 1 million cycles, new flexural cracks were noticed. One crack on the front side and three cracks on the back side were noticed. The girder failed at 1,075,000 cycles due to the rupture of one (or possibly two) lower prestressing strands at midspan.

A final static test was performed after completion of 1,075,000 cycles. The residual displacement prior to testing was 0.51 in (13.0 mm). The loss of stiffness compared to the other girders tested under static loading conditions was very noticeable. The reduced capacity of the girder was due to the loss of the lower prestressing strand (or strands) during the fatigue test, which caused an increase in load being distributed to the CFRP system. As a result, at a load of

17 k (75.6 kN) signs of debonding began appearing. Interface cracks in the concrete just above the CFRP sheets expanded at locations of the flexural cracking. These interface cracks joined between the flexural cracks and the debonding propagated from midspan towards the supports, peeling off a layer of cover concrete between the lower prestressing strand and the CFRP as shown in Figure 3.25. The slow debonding of the CFRP sheets due to the presence of the transverse U-wraps provided a ductile failure as shown in Figure 3.25. The maximum load level observed was 31.1 k (138.3 kN).

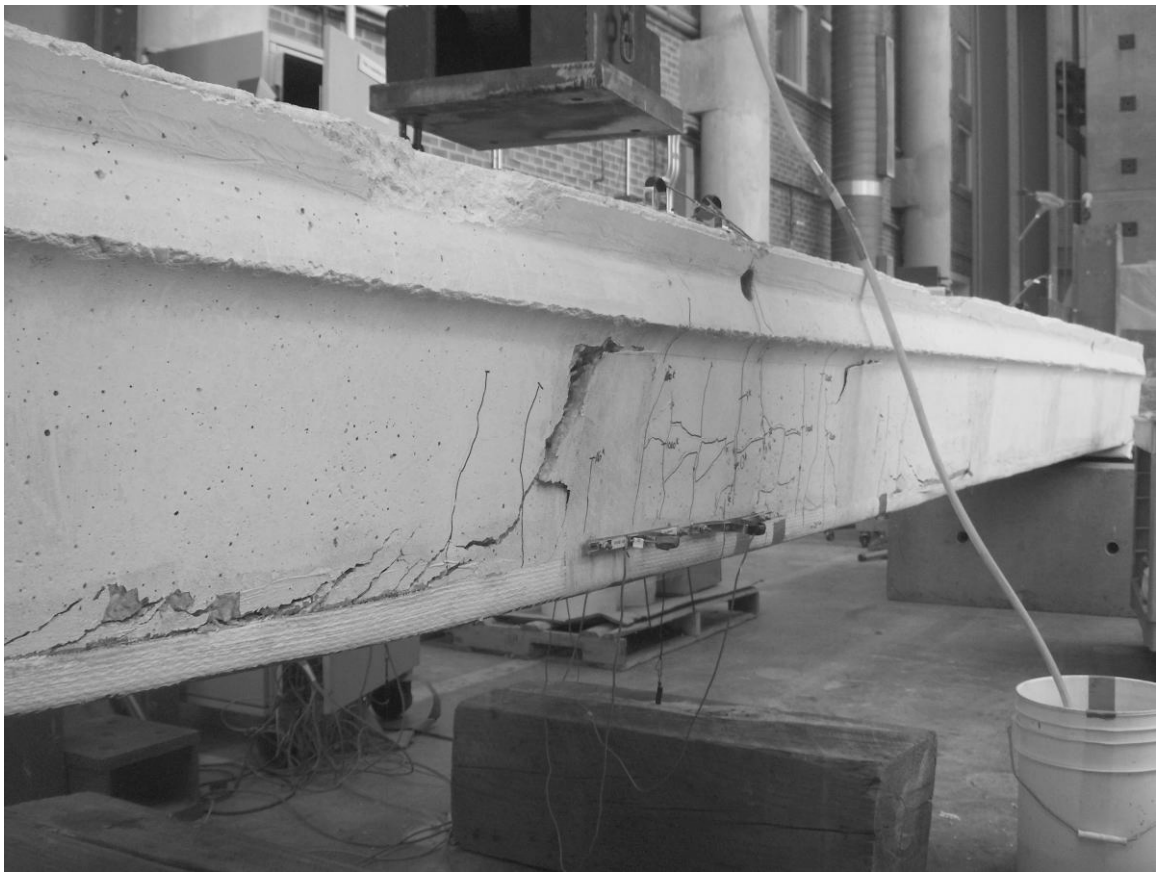

Figure 3.25 IC debonding in girder EB5F during final static test

A girder strengthened with five layers of high modulus CFRP sheets was tested under fatigue loading (EB6F). During the test of an identical girder under static loading conditions (EB6S), an increase of only 5.3 percent was achieved while the design called for an increase of

20 percent. As a result of an increase in the stiffness obtained due to the installation of the high modulus material (11 percent greater initial stiffness than the control girder), it was decided to cycle the girder up to a load value corresponding to a 41 percent increase in comparison to an equivalent HS-13 truck loading. The load levels used ranged between 2 k and 13 k (8.9 kN and 57.8 kN). During the initial static test, cracking was observed at a load level of 14.3 k (63.2 kN), very close to the cracking load observed in girder EB6S.

Although a change of stiffness was noticed in the test data from the PI gauges placed at midspan, no visible cracking was noticed at the beginning of the fatigue loading. After two million cycles of fatigue loading, no visible cracks were observed. A final static test was performed, and rupture of the HM CFRP sheets occurred at a load of 30.0 k (133.4 kN) as shown in Figure 3.26. The rupture strain of the HM material observed during the test was 0.24 percent comparable to the 0.26 percent observed in the static test on girder EB6S. Both were below the 0.30 percent value given from manufacturer. The small difference in rupture strain between girder EB6S and EB6F could be due to slight degradation of the CFRP material from the fatigue loading. After rupture of the sheets at midspan, the girder lost 23 percent of the applied load. The applied load at which rupture of the high modulus sheets was first observed was exceeded at a higher value of displacement. This shows that the high modulus material had a significant effect on the stiffness of the girder, even when not continuous throughout its length. After progressive rupture events, the girder followed the approximate load path of the control girder and the test was terminated after crushing of the concrete in the compression zone at a displacement of 7.6 in (193 mm).

Figure 3.26 Rupture of high modulus CFRP sheets

4 EXPERIMENTAL PROGRAM – AASHTO GIRDER

4.1 Introduction

In October 2003, a truck and trailer carrying excavating equipment impacted a prestressed concrete bridge superstructure of Robeson County, NC Bridge 169, Green Springs Road (SR 1718) over Interstate 95 (Figure 4.1). The bridge, originally built in 1959, consisted of four 55 ft (16.8 m) spans. Each span was comprised of four AASHTO Type II prestressed concrete girders located at 7 ft (2.13 m) spacing. The impact event heavily damaged the first exterior girder, missed two of the interior girders, and moderately damaged an opposite exterior girder.

The bridge had been hit numerous times in its lifetime and the decision was made by NCDOT bridge maintenance engineers to replace the girders in the eastern span with cored slab units to provide a shallower section and prevent potential future impacts. The bridge girders were identified by the research team and transported to Raleigh, NC for future repair work. The moderately damaged exterior girder was repaired for this phase of the research project. Repair of the other three girders will be performed as part of a project extension up to June 2006.

The concrete section of the impact damaged AASHTO Type II girder described above was restored and the section repaired using CFRP wet lay-up sheets. This chapter presents the design of the CFRP strengthening system along with an experimental program associated with the testing of the first girder. Complete test results are given in Section 5.3. Chapter 6 provides the cost-effectiveness and value engineering analysis of the repaired AASHTO girder.

Figure 4.1 Undamaged eastern span of SR 1718 over Interstate 95

4.2 Test Girder

The AASHTO Type II girder had sixteen 0.5 in (12.7 mm) diameter 270 ksi (1862 MPa) straight prestressing strands as shown in Figure 4.3. The total length of the girder was 54.84 ft (16.71 m). The girder before repair had damage as shown in Figure 4.2 and schematically in Figure 4.3. The damage extended 11.9 ft (3.63 m) on the front side and 6.0 ft (1.83 m) on the back side with approximate volume of damaged concrete equal to 4.8 ft^3 (0.1 m^3). On the front side, one prestressing strand was ruptured on the bottom layer. The composite deck of the girder ranged in width from 16.9 in (430 mm) to 13.9 in (353 mm) with an average width of 14.9 in (378.5 mm). Extraction of the cast in place diaphragms resulted in transverse cuts approximately 0.4 in (10 mm) wide in the composite deck at multiple locations.

From design drawings provided by NCDOT, the specified 28 day concrete strength for this girder was 5000 psi (34.5 MPa) and the specified concrete strength at transfer of prestressing

force was 4000 psi (27.6 MPa). Testing of the first girder was performed in June 2005, therefore the material testing of the concrete cores and prestressing are not presented in this report and will be included in the report for the project extension.

The CFRP used in the strengthening was Fyfe© SCH-41 sheets with Tyfo© Type S epoxy. Witness panels of the CFRP laminates used in strengthening were tested according to ASTM D3039 specification to determine material characteristics. The values obtained from testing compare well to the manufacturer's provided data and to testing of identical material used in the strengthening of C-Channel girders as shown in Table 4.1.

Table 4.1 CFRP tension test results (AASHTO girder)

Specimen	Girder Strengthened	Thickness, in	Tensile Strength, ksi	E_F, ksi	ε_{fu}, %
Average Fyfe.1	AASHTO	0.08	76	6351	1.2
Fyfe.1 Manufacturer		0.04	143	13891	1.0

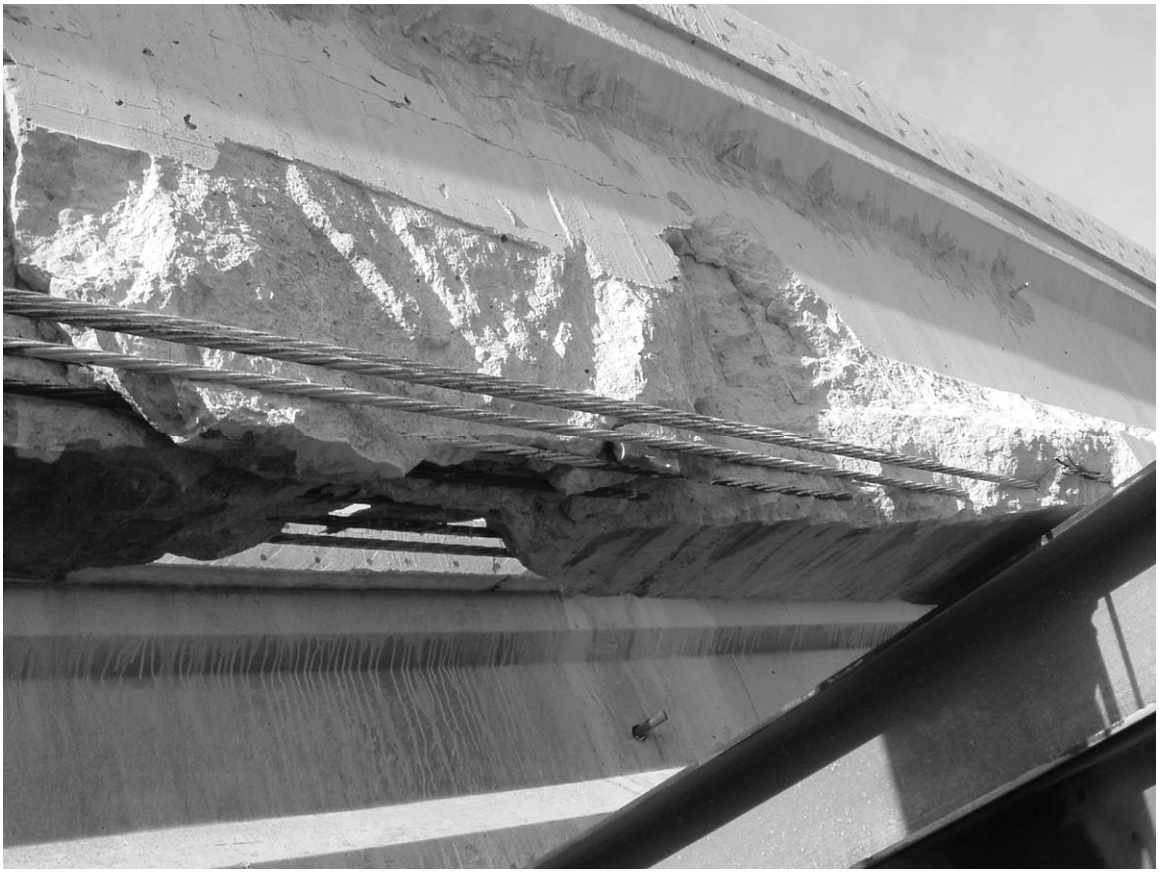

Figure 4.2 AASHTO girder prior to repair work

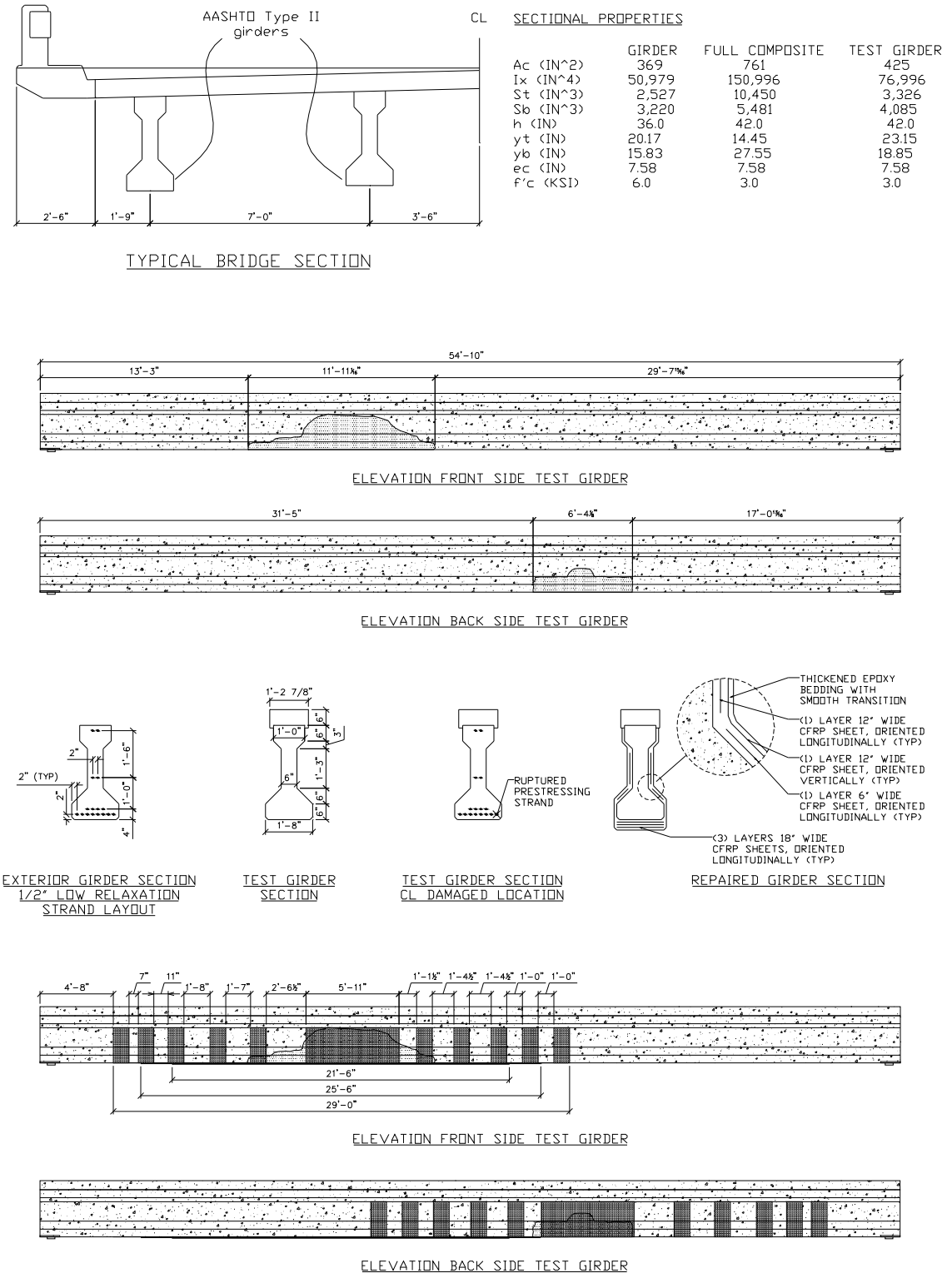

Figure 4.3 AASHTO girder cross section, elevation and CFRP design drawings

4.3 Design of Repair System

Unlike the C-Channel girders tested in an earlier phase of this research project and described in Chapter 3, the purpose of applying CFRP in this phase was mainly to repair the impact damaged AASHTO girder to restore its original ultimate flexural strength. The decision not to test a control girder, which was approved by NCDOT, was due to the limited number of girders available. Analysis procedures were used to estimate the behavior of the undamaged girder.

The repair mortar used in restoration of the lost concrete was determined in consultation with the contractor. Tyfo© Type P, two-component, quick setting, polymer modified cementitious mortar, was selected based on its good bonding performance to sound concrete and fast setting properties. During the restoration operation, the contractors exhausted their supply of this material and it was agreed to continue the repair using a similar material produced by the Sika Corporation, SikaTop© 123 Plus. The average compressive strength of the SikaTop© 123 Plus material was 6300 psi (43.4 MPa) at the time of testing. Due to the formation of shrinkage cracks, which appeared during the surface preparation stage of the installation, more careful consideration of the repair material is suggested as discussed in detail in Section 7.3.2.

The choice of a CFRP repair system to restore the original flexural capacity of the girder was based on experience gained from the test results, cost-effectiveness and value engineering analysis of the CFRP strengthening systems applied to the C-Channel girders. It was decided to use externally bonded CFRP wet lay-up sheets as the repair system due to their proven record in strengthening the C-Channel girders as well as their performance in the cost-effectiveness analysis as discussed in Section 6.2. Also, a preliminary analysis using a NSM system showed that the number of NSM CFRP bars required to restore the original capacity was high and

perhaps unpractical for this type of application. In addition, it was apparent that the damaged concrete section to be restored was large and deep into the girder cross section and therefore needed transverse CFRP wet lay-up U-wraps to stabilize crack growth in this region. These needs and concerns lead to the use of a wet lay-up system as the main longitudinal repair reinforcing. The type of wet lay-up system used was identical to the one used in strengthening the C-Channel girder EB4S and EB4F: Fyfe© CH-41 composite and Tyfo© S two part epoxy.

Due to the large damaged portion of the concrete section, it was relatively easy to determine the prestressing strand configuration and compare it with the original design plans for the girder, provided by NCDOT bridge maintenance personnel. The longitudinal repair system to restore the original strength of the girder was based on cracked section analysis program, Response 2000© (Bentz 2000). The base curve of the concrete model used in the cracked section analysis program was the Popovics curve including compression softening which was based on the Vecchio-Collins model and the tension stiffening was based on the Bentz model (Bentz 2000). The compression strength of the concrete at 28 days was determined from NCDOT design specifications as 5000 psi (34.5 MPa). The 270 ksi (1862 MPa) prestressing strands were modeled using the Ramberg-Osgood function (Equation 3.1) for low relaxation strands. The CFRP system material properties were taken from data provided by the manufacturer:

Ultimate Tensile Strength for design laminate:	107, 950 psi (745 MPa)
Laminate thickness:	0.04 in (1 mm)
Tensile Modulus:	8.9×10^6 psi (61.5 GPa)

By inspection it was found that one prestressing strand located on the most heavily damaged side of the girder was ruptured due to the impact load. The damaged region of the girder is shown in Figure 4.2, over which the prestressing strands were exposed. To account for

corrosion damage of the strands due to their exposure for six months prior to concrete restoration, one additional prestressing strand was considered to be missing in the design of the repair system. According to Klaiber et al (1999) and Shanfelt and Horn (1980), no additional prestress losses in the exposed strands were assumed in the design of the repair system. It should be noted that their reports dealt with girders that had not been removed from a bridge, and were in composite action with the deck. Shanafelt and Horn (1980) recommended also that the bridge be pre-loaded with a truck during concrete restoration. This recommendation is based on the concept that the truck load would induce tensile stresses at the bottom surface of the prestressed concrete girder which would in turn induce compression in the restored concrete zone after removal of the truck load from the bridge.

The amount of longitudinal CFRP reinforcement to restore the original ultimate flexural strength of the girder was determined using a Response 2000© cracked section analysis program with the assumption that the damage occurred at the midspan section. Using a procedure similar to the one described in Appendix A, the design called for three layers of CFRP sheets 16 in (405 mm) wide. Proper strengthening required that adequate development length of the CFRP sheets be provided to utilize their full strength and strain capacity. The CFRP reinforcement should also be designed to provide sufficient strength to prevent the initiation of new cracks in the non-prestressed damaged region.

In order to ensure adequate development of the CFRP flexural reinforcement, the following detailing was used:

1) The three layers of CFRP longitudinal reinforcement were extended beyond the location of the ruptured prestressing strand by 6 ft (1829 mm). This length was

selected based on the full development length of the 0.5 in (11.1 mm) diameter prestressing strands.

2) To prevent possible plate-end debonding, the termination points for the CFRP longitudinal reinforcements were staggered at a distance of 2 ft (610 mm) from each other. This detail was determined in consultation with the design engineer of the contractor who was very experienced with the properties of the CFRP wet lay-up system.

3) Transverse U-wrap CFRP wet lay-up sheet reinforcements were provided throughout the length of the repaired region on top of the main longitudinal sheets. 12 in (304 mm) U-wraps were provided at the termination points for each longitudinal CFRP sheet (6 locations) and at two locations between the first cut-off point for the longitudinal CFRP and the damaged region. The U-wraps extended around the bottom flange and extended the full depth of the web and top flange on each side of the girder. The purpose of the U-wraps was to prevent the possible debonding failures discussed in Section 2.9.

To control crack initiation of concrete in the restored region, the following details were considered in the design of the CFRP repair design:

1) Since the concrete used for the restoration was not prestressed, it was expected to crack at the service load level. In order to control the growth of cracks within this region under fatigue loading, three 2 ft (610 mm) wide CFRP transverse U-wraps were used to completely encapsulate the repaired concrete area. The width used was equal to the rolls of the CFRP sheets. Since the main objective for providing U-wraps at the damaged area was to control crack growth, the sheets were

overlapped by 1 in (25 mm) to provide continuity and prevent the formation of cracks between the sheets. Moisture build-up beneath the CFRP reinforcing could be a concern if the length of the damage was very long, therefore completely encapsulating the entire length of the girder should be avoided.

2) To control transverse shrinkage and flexural cracks, two additional CFRP sheets were provided longitudinally along the length of the repaired area: two 6 in (152 mm) wide CFRP sheets attached to the angled portion of the bottom flange, and two 12 in (254 mm) CFRP sheets attached to the web of the girder on each side. This reinforcing, acting as tension struts, alleviated the flexural contribution of the main longitudinal reinforcement, and acted as a crack growth inhibitor in the damaged region. In order to provide adequate anchorage, the sheets were extended beyond the damaged region to the extents of the main longitudinal CFRP reinforcing.

Figure 4.4 CFRP Repaired AASHTO girder

4.4 Test Setup and Procedure

4.4.1 Test Setup

The repaired AASHTO girder was tested under fatigue loading conditions using a 110 k (490 kN) MTS hydraulic actuator. Selection of the 110 k (490 kN) actuator was based on its large capacity servo-valve which permitted testing of the girder using a relatively high frequency of load cycles. The actuator was mounted to a steel frame which was placed at the midspan of the girder. The loading contact area was a 10 in by 20 in (150 mm by 250 mm) steel plate which is equal to the AASHTO specified design loading area (AASHTO 2004).

Neoprene pads 22 x 9 x 2.5 in (559 x 229 x 64 mm) were used between two 1 in (25 mm) steel plates to support the girder and to simulate field supporting conditions. The top plate was 11 in by 30 in (279 mm by 762 mm) and the bottom plate was 22 in by 30 in (559 mm by 762 mm). The bottom of the plates was supported by a concrete support block 4 x 4 x 2 ft (1.23 x 1.23 x 0.61 m). The girder was provided with a built in 18 in by 15 in (457 mm by 381 mm) steel plate welded to an 18 in by 6 in (457 mm by 152 mm) steel plate which rested on the top plate of the bearing system as shown in Figure 4.5.

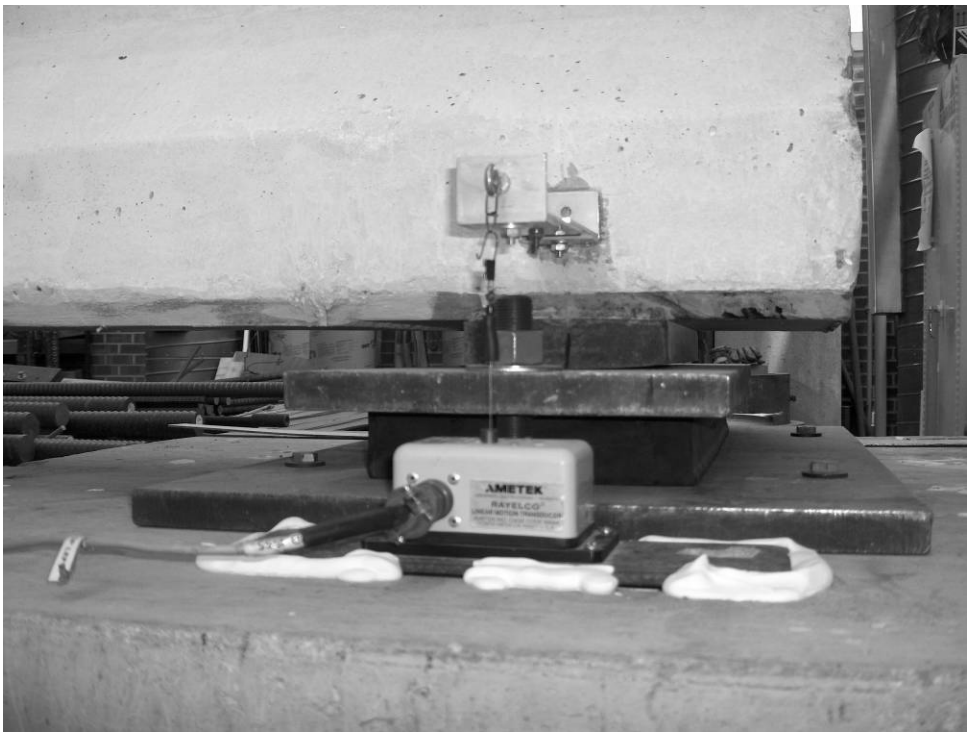

Figure 4.5 AASHTO girder support assembly

4.4.2 Fatigue Load Determination

The goal of the fatigue loading scheme was to simulate loads which would be encountered during the service life of the original girder to verify that the repaired girder could withstand a level of loading equivalent to the original girder. Two different fatigue loading schemes were considered for the repaired AASHTO girder: one which would simulate the

original AASHTO HS-15 truck design loading, and another which would simulate tensile stress in the extreme bottom of the concrete flange equal to $3\sqrt{f'_c}$ psi ($0.25\sqrt{f'_c}$ MPa), which is specified by the AASHTO code (2004) for service loading in corrosive environments. Preliminary analysis of the girder indicated that the original girder was overdesigned; meaning that using HS-15 type loading would not simulate the worst case conditions. Therefore the design of the fatigue loading was based on determining a live load level which would simulate a tensile stress in the bottom flange of the concrete equal to $3\sqrt{f'_c}$ psi ($0.25\sqrt{f'_c}$ MPa).

The test girder had a composite deck slab approximately equal to the width of the top flange, 12 in (305 mm). In the actual bridge, the width of the deck slab working in composite action with the girder was 7 ft (2133 mm). In order to determine the live load required for testing of the test girder, the following analysis was conducted:

1) Determine the live load moment which induces a tensile stress in the bottom flange of the concrete equal to $3\sqrt{f'_c}$ psi ($0.25\sqrt{f'_c}$ MPa) for the actual bridge girder with a 7 ft (2133 mm) composite deck slab. The analysis includes the effects of the prestressing and the dead loads through sequencing of the different construction stages.
2) Determine the resulting stress profile through the cross-section of the actual girder with full composite deck based on the magnitude of live load determined in Step 1. Use the profile to calculate the stress at the level of the lower prestressing strands.
3) Determine the level of the applied load that should be used for the test girder to induce a stress in the lower prestressing strand equal to the value determined in Step 2.

Step 1)

The section properties of the AASHTO Type II girder, the test girder, and the actual bridge girder with a 7 ft (2133 mm) composite deck slab are shown in Figure 4.3. Properties of the transformed section of the actual bridge girder accounting for the weaker strength concrete of the cast-in-place deck slab can be determined using the modulus ratio, η, as follows:

$$\eta = \sqrt{\frac{f'_{cdeck}}{f'_{cgirder}}} \tag{4.1}$$

$$= \sqrt{\frac{3000}{5000}} = 0.7746$$

where f'_{cdeck} and $f'_{cgirder}$ are the concrete compressive strengths of the deck and AASHTO girder respectively.

The dead loads supported by the bridge girder with and without the full 7 ft (2133 mm) deck slab can be determined as follows:

Dead Loads Supported by Girder

Girder self weight		0.384 k/ft (5.60 kN/m)
Slab		0.531 k/ft (7.75 kN/m)
Diaphragms		0.036 k/ft (0.525 kN/m)
Total dead loads supported by girder	w_{dg} =	0.951 k/ft (13.88 kN/m)
Total dead load moment supported by girder	M_{dg} =	336.0 k-ft (455.5 kN-m)

Dead Loads Supported by Composite Section

Asphalt overlay	0.306 k/ft (4.46 kN/m)
Barrier walls	0.050 k/ft (0.73 kN/m)

Curb and gutter		0.289 k/ft (4.22 kN/m)
Total dead loads supported by composite section	w_{dc} =	0.246 k/ft (3.59 kN/m)
Total dead load moment supported by composite section	M_{dc} =	86.92 k-ft (117.8 kN-m)

The effective prestress force, P_f, was calculated assuming an effective stress of 165.12 ksi (1138.3 MPa) which corresponds to an assumed 12.6 percent prestress losses and a jacking force equal to 70 percent of the ultimate tensile strength of the strands. Therefore,

$$P_f = 16 \times 0.167 \times 165.12$$

$$= 441.2 \text{ k (1961.5 kN).}$$

Using the previously specified tensile stress in the concrete of $f_{bgc} = 3\sqrt{f'_c} = 0.212$ ksi (1.46 MPa), and the following stress condition at the extreme fiber of the bottom flange:

$$f_{bgc} = -\frac{P_f}{A_g} - \frac{P_f e_g}{S_{bg}} + \frac{M_{dg}}{S_{bg}} + \frac{M_{dc} + M_{lc}}{S_{bc}} \tag{4.2}$$

where A_g is the area of the girder, S_{bg} is the section modulus below the neutral axis for the girder, and S_{bc} is the section modulus below the neutral axis for the actual bridge girder with 7 ft (2133 mm) composite deck, the live load moment for the actual bridge girder with full composite deck, M_{lc}, was determined to be 458.6 k-ft (753.0 kN-m).

Step 2)

The top compressive stress in the concrete for the actual bridge girder with full composite deck, f_{tgc}, for the given live load moment, M_{lc}, can be determined using the following equation:

$$f_{tgc} = -\frac{P_f}{A_g} + \frac{P_f e_g}{S_{tg}} - \frac{M_{dg}}{S_{tg}} - \frac{M_{dc} + M_{lc}}{S_{ic}} \tag{4.3}$$

where S_{tg} is the section modulus above the neutral axis for the girder and S_{ic} is the section modulus at the interface of the girder and the composite section above the neutral axis. The compressive stress, f_{tgc}, was found to be 1.83 ksi (12.63 MPa). Given the stress profile of the actual bridge girder with full composite deck, the stress level in the concrete at the lower prestressing strand, f_{pslc}, can be determined from:

$$f_{pslc} = \frac{d_{lps}}{h}\left(f_{tgc} + f_{bgc}\right) - f_{tgc} \tag{4.4}$$

where d_{lps} is the distance from the extreme compression fiber in the concrete to the level of the lower prestressing strands and h is the depth of the section. f_{pslc} was found to be 0.0986 ksi (0.680 MPa).

Step 3)

The live load moment that will induce the stress found in Equation 4.4 in the lower prestressing strand for the test girder, M_{ltg}, was determined by conducting the following analysis:

3.1) Determine the top and bottom stresses in the concrete, f_{tgt} and f_{bgt}, by assuming a value of M_{ltg} in the following equations:

$$f_{tgt} = -\frac{P_f}{A_g} + \frac{P_f e_g}{S_{tg}} - \frac{M_{dg}}{S_{tg}} - \frac{M_{dc} + M_{ltg}}{S_{it}} \tag{4.5}$$

$$f_{bgt} = -\frac{P_f}{A_g} - \frac{P_f e_g}{S_{bg}} + \frac{M_{dg}}{S_{bg}} + \frac{M_{dc} + M_{ltg}}{S_{bt}} \tag{4.6}$$

where S_{it} is the section modulus above the neutral axis at the interface of the girder and the composite section for the test girder and S_{bt} is the section modulus below the neutral axis for the test girder.

3.2) Determine the stress in the concrete at the level of the lower prestressing strands for the test girder, f_{psltg}, from the following equation:

$$f_{psltg} = \frac{34}{36}\left(f_{tgt} + f_{bgt}\right) - f_{tgt} \tag{4.7}$$

3.3) Perform iterations using different values of M_{ltg} until a value of f_{psltg} is determined which is equal to the value of f_{pslc} found in Step 2.

The live load moment applied to the test girder that will induce a stress in the concrete at the layer of lower prestressing strands of 0.0986 ksi (0.680 MPa) is M_{ltg} = 351.9 k-ft (477.2 kN-m). This moment corresponds to a concentrated load at midspan of 26.5 k (117.8 kN). The stress profiles of the girder with full 7 ft (2133 mm) composite deck slab, and the test girder are shown in Figure 4.6.

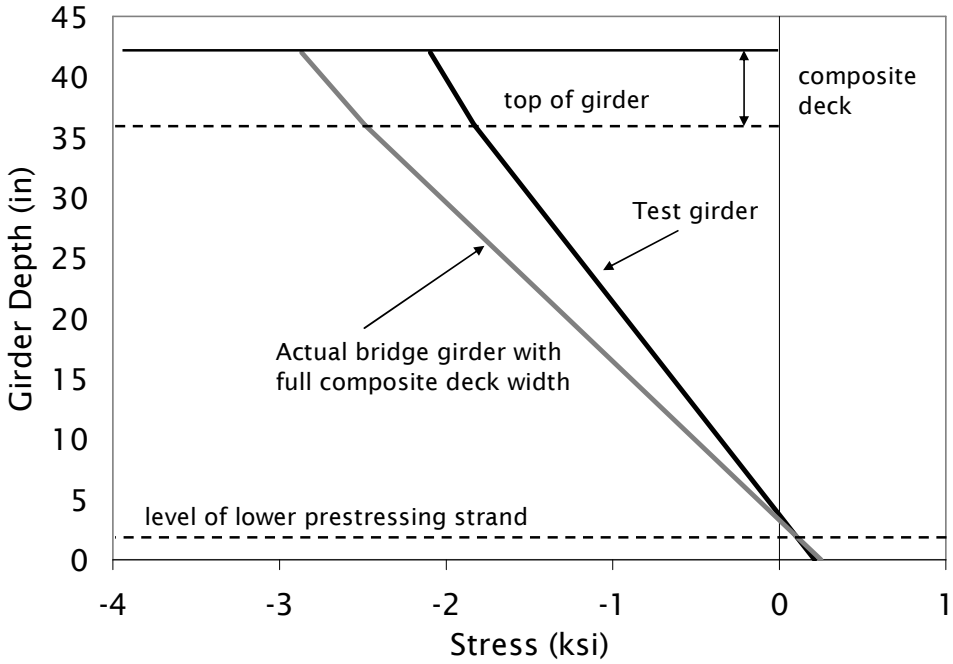

Figure 4.6 Stress profiles used in AASHTO fatigue load determination

To determine the minimum load for the fatigue loading, the following total dead loads acting on the actual bridge girder with full composite deck, M_{DLc}, were calculated as follows:

$$M_{DLc} = M_{dg} + M_{dc} \tag{4.8}$$

$$= 425.6 \text{ k-ft } (577.1 \text{ kN-m})$$

The dead load of the test girder, M_{DLg}, include the girder self weight of the girder and the weight of the 12 in (305 mm) of deck slab above the top flange of the girder. These loads correspond to a dead load moment of $M_{DLtg} = 177.0$ k-ft (240.1 kN-m). Therefore, the required applied load needed to simulate the dead loads acting on the bridge should be based on the difference between the above two moments and was found to be $M_{DLs} = 248.6$ k-ft (337.0 kN-m), which corresponds to a concentrated load at midspan of 18.7 k (83.2 kN).

Based on the above, the minimum load which should be used for the fatigue loading is 18.7 k (83.2 kN) and the maximum load, which is the summation of the dead load and the live

load, is 45.2 k (201 kN). This range simulates a level of stress in the lower prestressing strand of the test girder equal to the stress in the lower prestressing strand for the actual bridge girder in composite action with the full width of the deck slab.

As mentioned previously, the design loading of HS-15 produced a bottom tensile stress in the concrete less than the $3\sqrt{f'_c}$ psi ($0.25\sqrt{f'_c}$ MPa) value specified by AASHTO. Using the AASHTO (2004) code: for an exterior girder with bridge configuration "k", and with two design lanes loaded, the distribution factor, g_{ext}, is 0.6253. Using the distribution factor and an impact factor of 1.33, the axle loads of the HS-15 type loading were found to be: 4.99 k, 19.96 k and 19.96 k (22.2 kN, 88.8 kN and 88.8 kN). Using these loads will produce a maximum moment of 432.2 k-ft (586.1 kN-m) in the full composite bridge girder.

Using a procedure similar to the one described above, the live load which induces a stress in the prestressing strand for the test girder equal to the value found for the girder with full composite deck under HS-15 loading was found to be 24.9 k (110.8 kN). This is slightly lower than the value determined from the earlier analysis and therefore the girder was tested using the first conservative loading levels.

4.4.3 Loading Scheme

The loading of the AASHTO girder consisted of three stages: 1) initial loading, 2) fatigue loading, and 3) final static loading to failure.

Initially, the girder was loaded up to a load level of 51 k (227 kN), applied using displacement control loading. The load was selected to simulate a bottom nominal tensile stress in the concrete of $6\sqrt{f'_c}$ ksi ($0.5\sqrt{f'_c}$ MPa), in order to evaluate the observed stress ratio in the lower prestressing strand and behavior at this load level. The fatigue loading was oscillated

between the loads of 18.7 k and 45.2 k (83.2 kN and 201 kN) to simulate the dead load to the dead load plus live load as determined in Section 4.4.2. The load was applied using a 110 k (490 kN) actuator which permitted a frequency of 2 Hz to be used during the test. The fatigue test was stopped at various intervals to record data during intermediate static tests. The final test of the girder consisted of several cycles to simulate extreme overloading type conditions up to failure.

4.5 Instrumentation

The displacement profile along the length of the repaired AASHTO girder was measured using string potentiometers placed at L/8 points. The compressive strain in the concrete was measured using a combination of PI gauges (a strain gauge mounted to a spring plate) and 2.36 in (60 mm) TML FLA-60-11 120 Ω electrical resistance strain gauges. The tensile strain in the CFRP reinforcement was measured using 0.236 in (6 mm) TML FLA-6-11 120 Ω electrical resistance strain gauges. Placement of the instrumentation measuring compressive and tensile strains was carefully selected to determine: 1) The strain profile of the section at midspan, 2) The behavioral differences between the damaged and undamaged sections, and 3) The tensile strain in the CFRP to determine the bond characteristics throughout the longitudinal CFRP. A schematic drawing of the instrumentation used during the test is shown in Figure 4.7.

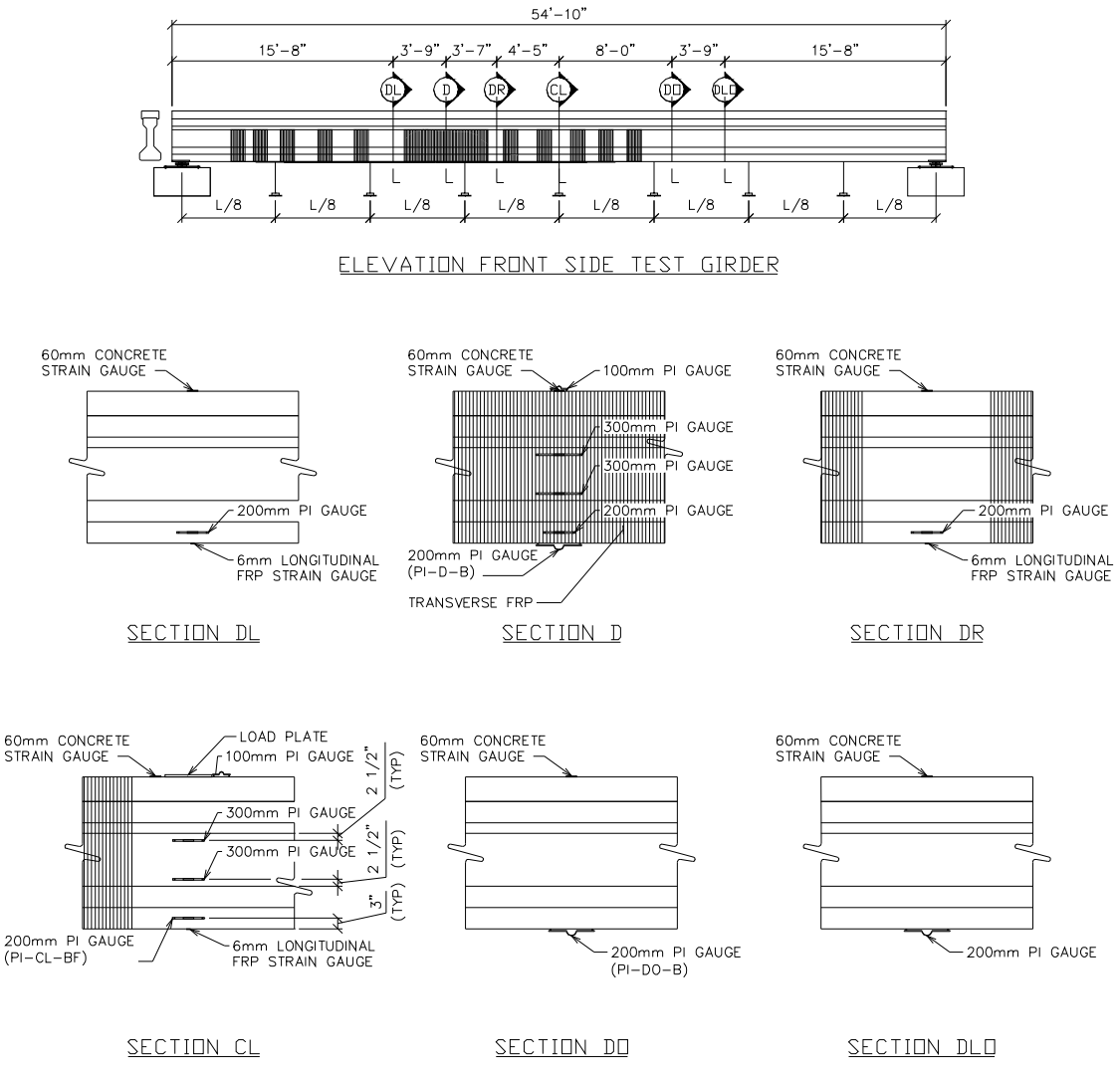

Figure 4.7 Repaired AASHTO instrumentation plan

4.6 Test Description

The first visual cracking was observed on the side of the girder with the ruptured prestressing strand and the highest degree of damage, just outside the transverse U-wraps encapsulating the damaged region at 42.0 k (186.8 kN). After the first three initial cycles, three cracks formed on the same side at both edges of the transverse CFRP U-wraps in the damaged region, and extended to the top of the bottom flange. However, it should be noted that the three cracks noticed during the initial static cycles did not grow significantly during the fatigue loading regimen. The midspan deflection of the girder at the load level of 45.2 k (201.0 kN) degraded

from an initial value of 0.771 in to 0.922 in (19.6 mm to 23.4 mm), after completion of 2 million cycles.

The girder completed 2 million cycles with a total residual deflection of 0.12 in (3 mm) due to fatigue-creep effects in the concrete (ACI 215 1997). Very little change in stiffness was observed. The test girder was loaded after the fatigue loading up to a load level of 339 kN and a total deflection of 1.5 in (38.8 mm). The flexural cracks near midspan and in the damaged region extended through the bottom flange as a result of this loading. The girder was reloaded up to a load of 90.0 k (401 kN) and total deflection of 2 in (51 mm) during the second cycle. During this cycle the cracking in the damaged area and within the limits of CFRP repair did not extend, but new cracks were noticed just outside the termination point for the longitudinal CFRP. The test was stopped since the load carrying capacity of the girder exceeded the capacity of the actuator and testing frame.

The final monotonic test to failure started after installation of the new test frame at midspan. At a load of 101 k (449.3 kN) the flexural crack just outside the CFRP repair area extended into the web. Cracks in the damaged region did not extend farther than the top of the bottom flange due to the presence of the tension strut longitudinal CFRP. At a load of 131 k (582.7 kN), crushing of the concrete was observed in two locations: 1) on either side of the loading plate at midspan and 2) above the damaged region in the compression zone at the location of a saw cut which was used to remove the cast-in-place diaphragms. The maximum measured load was 136.0 k (605.4 kN) at a midspan displacement of 5.78 in (146.7 mm). The load dropped 2.0 k (8.9 kN) after the maximum load was obtained and the loading rate was increased to 0.2 in/min (5.1 mm/min). At a displacement of 6.17 in (156.8 mm), a large flexure-shear crack suddenly formed outside the longitudinal CFRP repair area and connected to the

concrete crushing zone near the edge of the loading plate and caused catastrophic failure as shown in Figure 4.8. Complete test results are presented in Section 5.6.

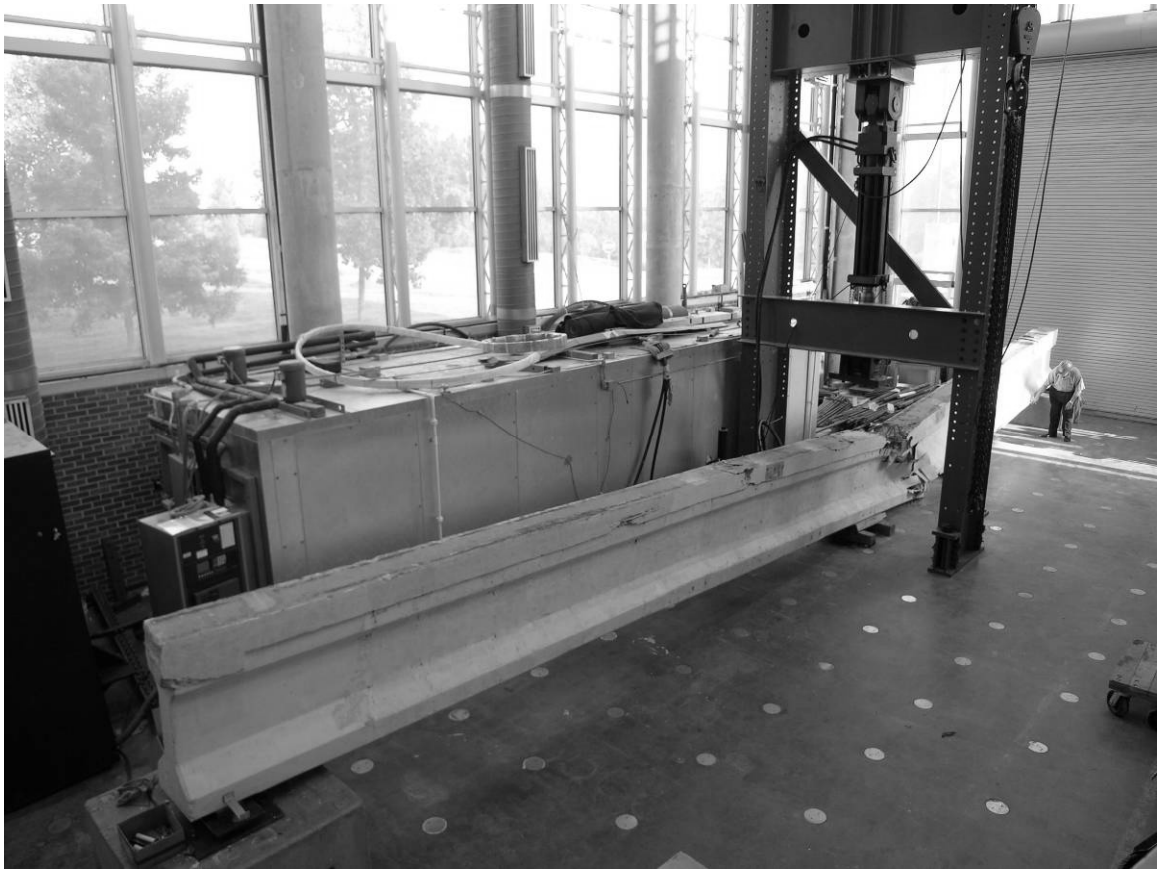

Figure 4.8 Repaired AASHTO girder after failure

5 TEST RESULTS AND DISCUSSION

5.1 Introduction

In order to present the test results along with their analytical predictions, the results of the tested girders as well as descriptions of the analytical procedures are presented in this section. Test results are presented to compare the behavior of the various strengthening systems used in this research and the capability of the analytical modeling to predict the behavior. The two types of analytical modeling used were non-linear finite element simulations using ANACAP©, and a cracked section analysis using Response 2000©. Test results for the strengthened C-Channel girders tested under static and fatigue loading are presented as well as the test results of the repaired AASHTO girder tested under fatigue loading conditions followed by static loading up to failure.

5.2 ANACAP© Finite Element Simulations

ANACAP© is a non-linear finite element program for analysis of plain, reinforced and prestressed concrete members and structures and was developed by the ANATECH Corporation. The program was used to run finite element simulations on all the tested girders with the various repair and strengthening configurations. The 3-D modeling capabilities of ANACAP©, along with advanced analytical models for the constituent materials, provide accurate predictions of the behavior of concrete structures (James 1997).

ANACAP© uses the smeared cracking methodology for modeling of concrete where cracking is assumed to be distributed over an entire element. This mechanics-based philosophy uses plasticity theory that incorporates cracking and other concrete properties. Values for the elastic modulus and nominal compressive strength of concrete were obtained from testing of the

concrete cores extracted from the tested girders described in Section 3.2. The effect of concrete confinement at different stress levels was incorporated into the analysis as well as an elastic modulus allowing for changes between the three distinct zones of the stress-strain curve of concrete – the initial linear region, strain hardening region and strain softening region. Opening and reopening of cracks can also be simulated for cyclic loading regimes and the program considers the effects of aggregate interlock and their effect in lowering shear capacity as crack widths increase at high load levels.

The stress strain characteristics of the prestressing steel was based on material testing of prestressing strands as described in Section 3.2. The ANACAP© program considers other factors inherent in the behavior of reinforcing in concrete such as: 1) Bond slip, 2) Anchorage loss, 3) Discontinuities in strain at locations of cracks, and 4) Buckling of compression reinforcement after crushing of concrete.

Characteristics of the CFRP material were also based on material testing and presented as perfectly linear elastic to failure. Since the original program was not designed for these types of materials, it was required to analyze the load-deflection response and terminate the behavior if the strain in the CFRP reached the desired rupture strain value.

The concrete cross section of the girder was modeled with 20 node elements using quadratic isoparametric displacement interpolation. The prestressing steel and the CFRP were modeled as sub-elements within the concrete section elements. Modeling the loading and supports reflected the conditions encountered during laboratory testing. The applied load was distributed at midspan over an area of 10 in x 20 in (254 mm x 508 mm), and spring supports used to simulate the behavior of the neoprene pads. The load-deflection response of the modeled girders was obtained using ANACAP© by the incremental application of the load up to failure.

At each load interval, equilibrium is obtained and the stiffness of the member recalculated to adjust for nonlinearity. Experimental verification of the accuracy of the program can be found elsewhere (Hassan and Rizkalla 2003, 2004).

5.3 Response 2000© Cracked Section Analysis

In addition to the non-linear finite element simulation, a cracked section analysis was performed for the strengthened girders using Response 2000© software. Verification of this program can be found elsewhere (Bentz 2000). Due to limitations of the geometry input of the program, the concrete section of the C-Channel girders was modeled as a single-tee type section by combining the two webs of test girders. The cross section of the AASHTO girder was directly used without modification. Strength of the concrete for each girder was based on material testing of concrete core sample (see Sections 3.2 and 4.2). The concrete behavior was modeled using the Popovics curve. Tension stiffening was included in the analysis. The prestressing steel was modeled using the Ramberg-Osgood function, using constants corresponding to the behavior observed in tension tests on samples taken from each girder. The CFRP was assumed to be linear-elastic up to failure with modulus of elasticity and rupture strain values determined from tension coupon tests.

The results from the cracked section analysis showed good agreement with the non-linear finite element analysis and the experimental results presented in the following section. Based on good agreement achieved between the cracked section analysis and the experimental results, the need for a finite element simulation to predict the behavior of such girders is not warranted. A complete design example using Response 2000© is presented in Appendix A.

5.4 C-Channel Static Tests

5.4.1 Introduction

Nine girders were tested monotonically to failure. One of these was a control specimen, and eight were strengthened with various CFRP strengthening systems. Two of the strengthened girders were Type II girders and seven were Type I girders (as designated in Section 3.2). Since it was not known prior to testing that the girders had different prestressing strand configurations, no control girder was tested for the Type II configuration. However, a Type II specimen was tested as a control girder in fatigue and showed very little degradation after 2 million cycles. It is the data from the monotonic load which was applied after completion of the fatigue loading which is being used in this context as a control girder for the girders with a Type II prestressing strand configuration. It should be noted that the behavior of the girders CS and CF2 was very similar, with ultimate loads of 33.2 k (147.7 kN) and 32.0 k (142.3 kN) for each girder respectively as depicted in Figure 5.1. As a result of different prestressing strand configurations and different ultimate strand tensile strengths, all the results are separated according to the type of girder tested.

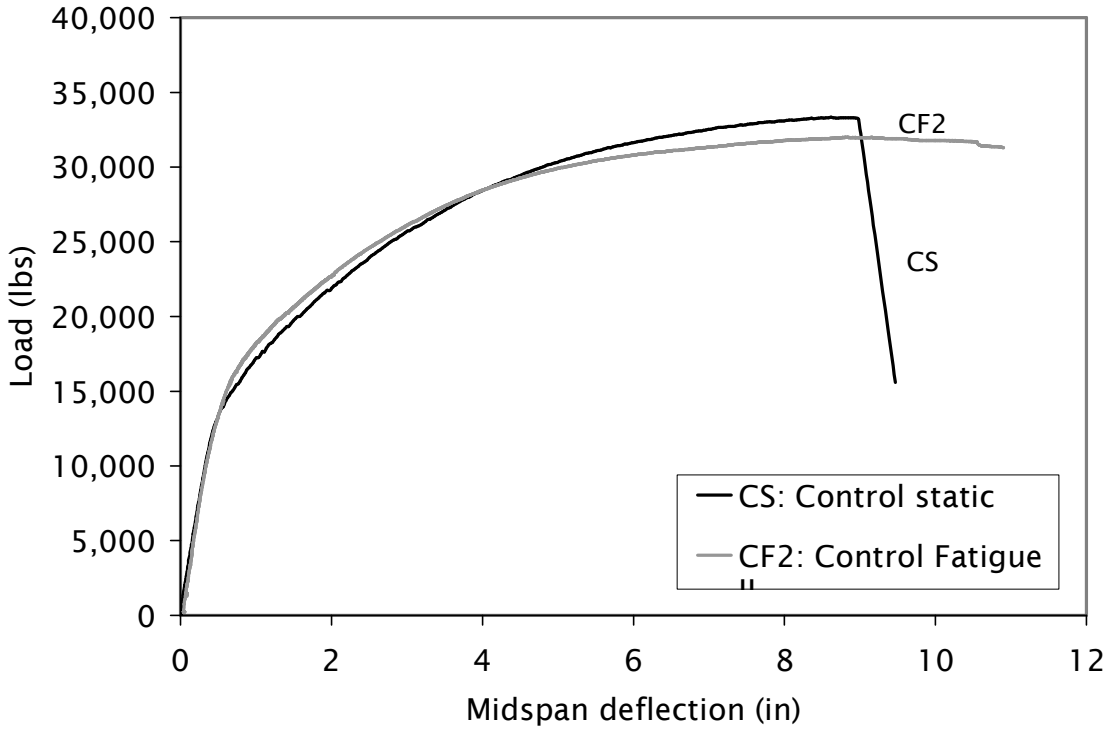

Figure 5.1 Experimental comparison between control girders

5.4.2 Type I Girders

Seven Type I girders were tested monotonically to failure, one control girder and six strengthened girders.

Crack Development – each of the girders were loaded up to the cracking load, unloaded, and reloading again to determine the cracking load and the crack reopening load (which are shown in Table 5.1). Initiation of the flexural cracks was determined either by visual inspection or by analysis of the test data. Typically, cracking occurred between the loads 11.8k to 14.0 k (52.9 and 62.3 kN). Flexural cracks were located at the bottom of the C-Channel soffit near midspan, with a length near midspan equal to the depth of the girder from the edge of the loading area. Spacing of the cracks was approximately 13 in (330 mm), as shown in Figure 5.2, which corresponds to the distance between the transverse stirrups used for the C-Channels. As the

applied load increased, all the girders developed additional flexural cracks along the span at the same spacing.

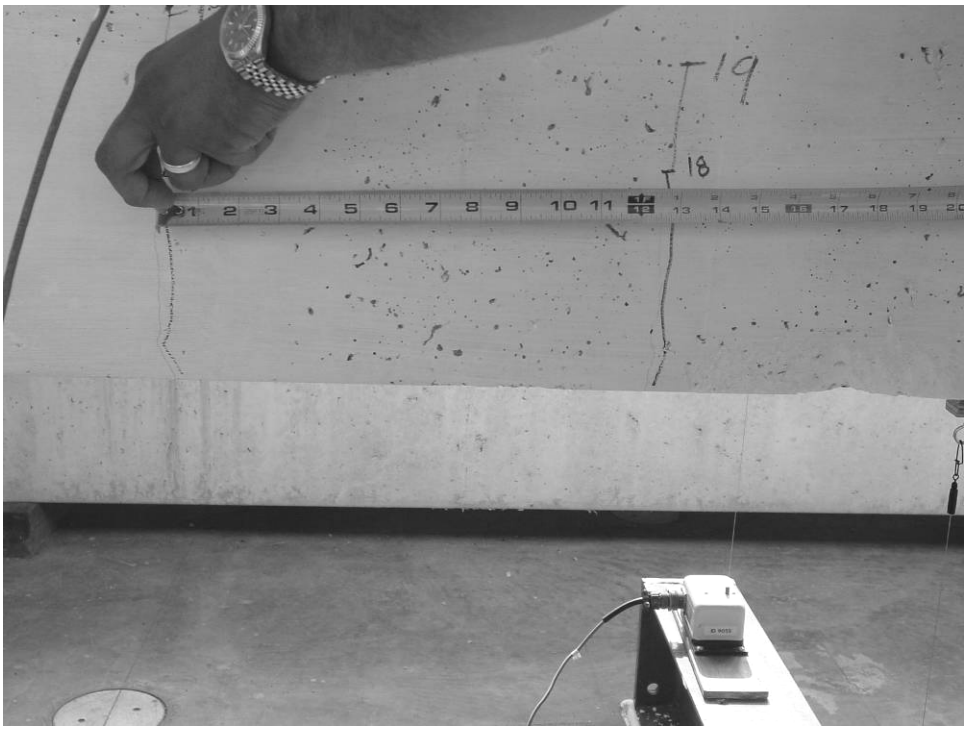

Figure 5.2 Typical flexural cracking at midspan of C-Channel girders before yielding of lower prestressing strands

Table 5.1 Summarized test results for Type I girders tested under static loading conditions

Specimen Designation	CS	NSM1S	NSM2S	EB1S	EB2S	EB3S	EB4S
Strengthening	-	NSM bars	NSM strips	EB strips	EB sheets	EB HM strips	EB sheets
P_{cr}, k	12.6	12.4	12.4	11.9	12.1	14.0	13.0
P_{ro}, k	--	8.8	8.5	9.0	8.0	8.8	8.5
P_e, k	16.0	15.9	15.6	16.2	14.9	15.9	15.6
Losses, %	15.3	14.3	13.8	15.9	18.5	15.9	17.5
P_{ult}, k	33.2	40.8	40.2	39.6	36.7	29.1	53.1
S, % increase in capacity	--	22.9	22.6	19.3	10.5	--	60
ultimate compressive strain in concrete (experimental), in/in	0.003	0.0036	0.0036	0.003	0.0026	0.0026	0.003
ultimate tensile strain in CFRP (experimental), %	--	1.34	1.45	1.22	1.29	0.17	1.17
Experimental/manufacturer tensile strain in CFRP, %	--	80.2	85.3	72.2	129	41.4	117
Failure mode*	C	C	C	D	R	R	R
Initial Stiffness, k/in**	28.4	26.6	26.7	29.0	27.6	32.5	29.5
Secondary Stiffness, k/in†	1.0	3.0	3.0	3.4	3.1	--	6.0
Structural Efficiency, %/k ‡	--	6.31	5.90	4.38	2.58	--	2.93

* C = crushing of concrete, R = rupture of CFRP, D = debonding of CFRP
** defined from 2 k to 11 k (9 kN to 44.5 kN)
† defined from 28 k to 33 k (124.6 kN to 146.8 kN)
‡ defined as (% increase in capacity) / (E_{FRP} A_{FRP})

Beyond an applied load level corresponding to yielding of the prestressing strands (approximately 22.5 k [100 kN]), the cracking pattern of the control and strengthened girders diverged. Increasing load initiated more cracks between the existing cracks. At ultimate, the flexural cracking of the control specimen extended approximately 6.6 ft (2 m) from each side of midspan. The flexural cracks of the strengthened girders extended farther at ultimate, up to 9.8 ft (3 m) from each side of midspan. The CFRP strengthening reduced crack spacing, crack width and crack growth for all of the strengthened girders with respect to the control girder. For the girders whose failure was due to crushing of the concrete, it was observed that flexural cracks within the loading area changed their direction near ultimate and extended towards the loading area and formed a compression fan. The curvature of both the control and strengthened girders at failure was not sufficient to cause the flexural cracks to bifurcate, or fork, near the compression zone. The cracking pattern and crack widths generated from a Response 2000© analysis of the control girder, a girder strengthened 20 percent, and a girder strengthened 60 percent is shown in Figure 5.3 which is representative of the crack patterns and widths observed during the individual tests. The crack pattern of a girder strengthened using NSM bars which achieved a 20 percent increase in ultimate capacity (NSM1S) is shown in Figure 5.4. The failure mode of this girder was concrete crushing followed by debonding (see Section 2.9), creating forking cracks in the concrete cover between the NSM CFRP and the lower prestressing strand.

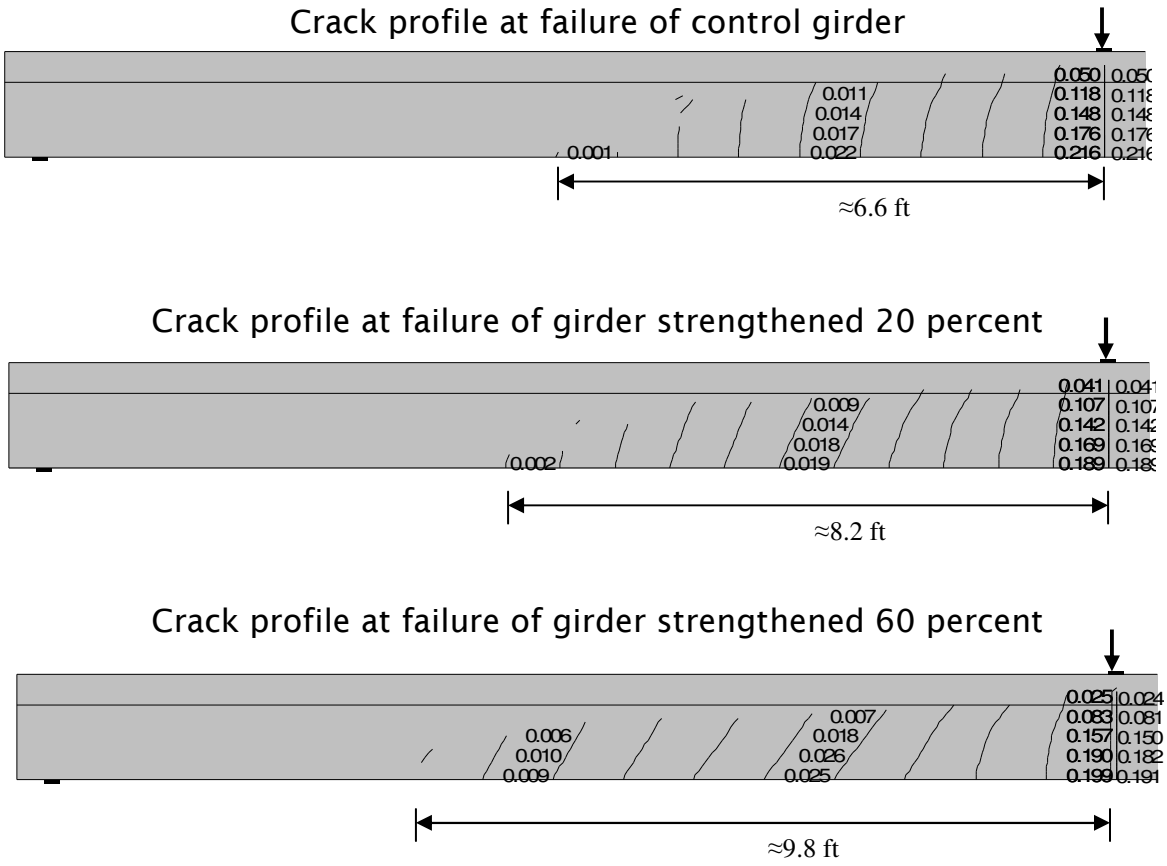

Figure 5.3 Response 2000© crack patterns and widths of control and strengthened C-Channel girders (in inches)

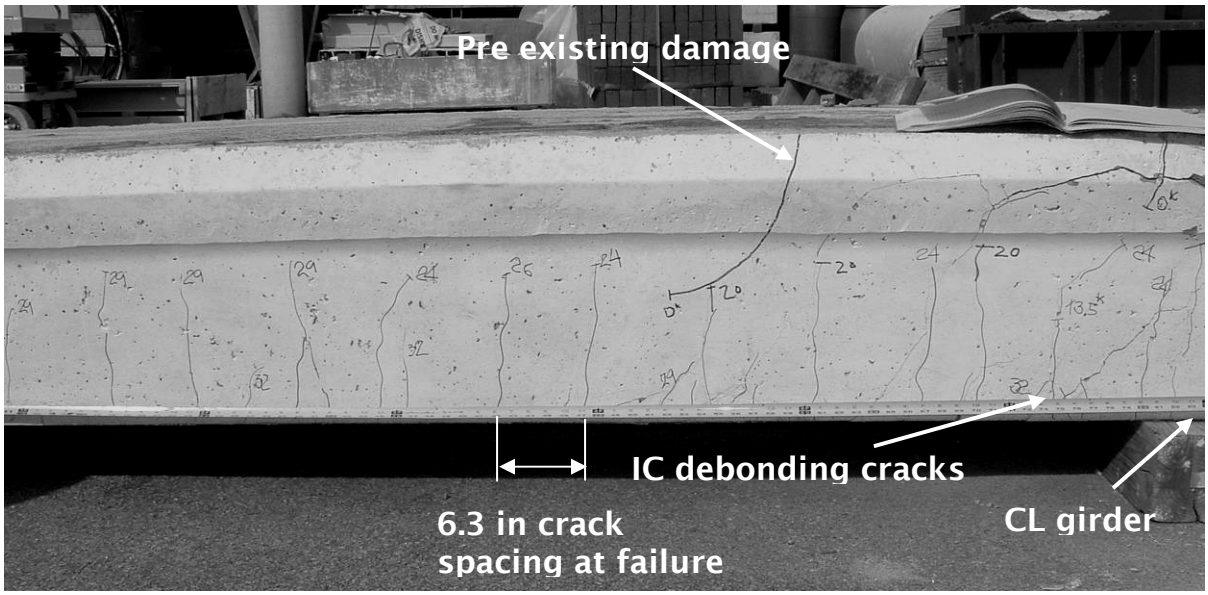

Figure 5.4 NSM bars strengthened girder NSM1S showing crack profile around midspan

PI gauges mounted near the bottom of the C-Channel soffit at midspan were used to measure the tensile strain in the concrete at various load levels. The average crack width at midspan can be calculated using the measured strains at any applied load level from the following equation:

$$CW_{ave} = \frac{(\varepsilon_{ci} - \varepsilon_{ccr}) \times l_{PI}}{n} \tag{5.1}$$

Where ε_{ci} is the measured strain at a certain applied load level, ε_{ccr} is the measured strain in the concrete at the flexural cracking load, l_{PI} is the length of the PI gauge, and n are the number of cracks observed within the PI gauge length. The load versus the average crack width at midspan for the Type I girders is shown in Figure 5.5. The figure indicates that the presence of the strengthening system restrained crack opening and growth with respect to the control girder, CS. At ultimate, the crack widths of the strengthened girders were as much as 400 percent less than the control girder.

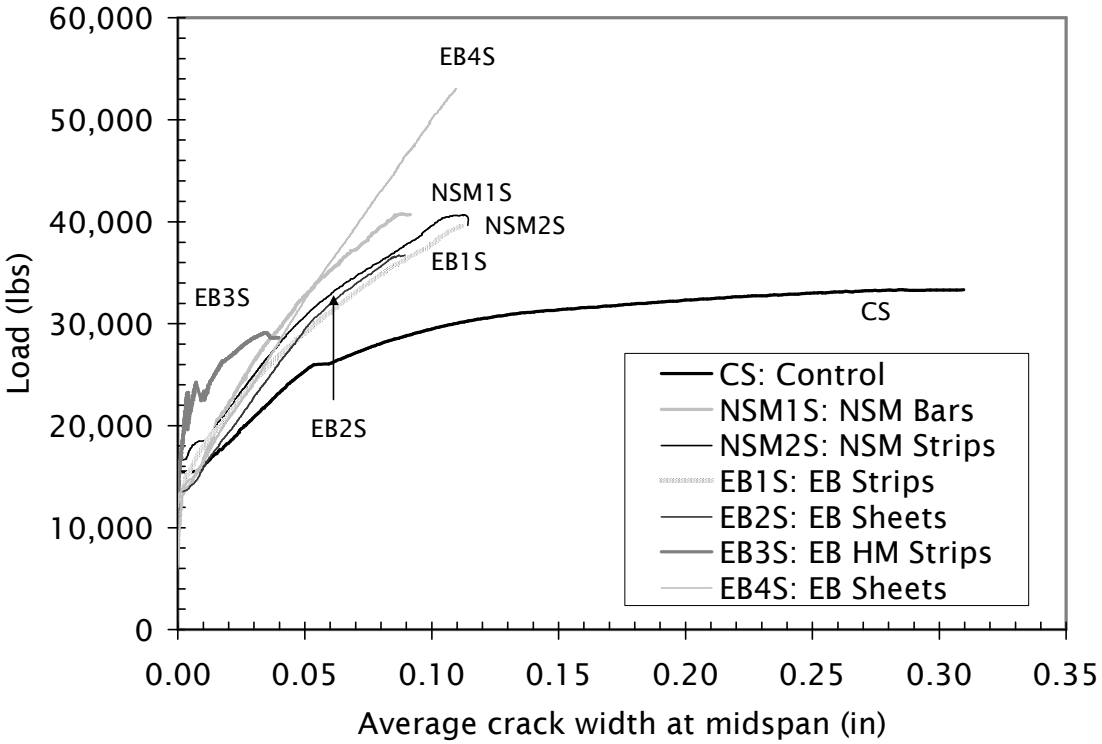

Figure 5.5 Load v. crack width for Type I girders tested under static loading conditions

Stiffness – Prior to cracking, the strengthened girder and the control girder behaved elastically. Based on the load versus displacement relationships measured during the test, the initial flexural stiffness, k_i, of the C-Channels was determined for each tested girder and shown in Table 5.1.

Comparing the initial stiffness of the strengthened girders which achieved a 20 percent increase in ultimate load capacity, with the initial stiffness of the control girder, it was obvious that the strengthening system has very little effect on the initial stiffness. However, using a strengthening system to achieve a 60 percent increase in ultimate capacity, modest increases in initial stiffness can be obtained. The girder strengthened with high modulus strips increased the initial stiffness 14.7 percent above than the control specimen.

The measured secondary stiffness, calculated within the load range 28 k to 33 k (124.6 kN to 146.8 kN) is shown in Table 5.1. This value represents the stiffness which is expected during an extreme overloading type event. Since girder EB3S did not reach loads corresponding to yielding of the prestressing strands before rupture of the CFRP, the stiffness was not calculated, although stiffness before rupture was high. As expected, the girder strengthened to achieve a 60 percent increase in ultimate capacity had the highest secondary stiffness for the Type I girders, six times the value determined for the control girder CS.

Effective Prestress – The effective prestress force in one strand, P_f, of the Type I girders was determined from the loading and unloading scheme adopted at the beginning of each test. From the crack reopening load, P_{ro}, the effective prestress can be solved from

$$\frac{10\times P_f}{A_c}+\sum\frac{P_f e_i}{S_b}-\frac{\omega_D L}{8}\times\frac{1}{S_b}-\frac{P_{ro}L}{4}\times\frac{1}{S_b}=0 \qquad (5.2)$$

where ω_D is the distributed self weight of the girder, e_i is the eccentricity of the prestressing strand with respect to the neutral axis of the section, L is the clear span length, A_c is the cross-sectional area of the girder, and S_b is the section modulus of the girder below the neutral axis. The measured values of effective prestress force per strand varied between 14.9 k and 16.2 k (66.3 kN and 72.1 kN) for girders with Type I prestressing configuration. From the C-Channel specifications, the initial jacking force was 18.9 k (84.1 kN), equivalent to $0.7 f_{pu}$, where f_{pu} was specified as 250 ksi (1723 MPa). Long-term losses calculated using the initial jacking force varied between 15.3 percent and 21.2 percent for the girders with Type I prestressing configuration. The losses determined experimentally are less than the value of 20.1 percent given in Collins and Mitchell (1991) for typical prestress losses in 250 ksi (1723 MPa) prestressing strands and the losses of 28.5 percent calculated using the AASHTO specification (2004) lump-sum method.

In some cases where the load corresponding to crack reopening was not determined, the cracking load itself was used to calculate the effective prestress in the strands by using the modulus of rupture for the concrete (AASHTO 2004) substituted for zero in Equation 5.2:

$$f_t = 7.5\sqrt{f'c} \text{ psi } (0.625\sqrt{f'c} \text{ MPa}) \tag{5.3}$$

The cracking loads, crack reopening loads and prestress losses for the Type I girders are shown in Table 5.1.

Structural Efficiency – The structural efficiency, SE, of a CFRP strengthening system was evaluated using the following expression:

$$SE = \frac{S}{E_{FRP} A_{FRP}}, \text{ \%/k (\%/MN)} \tag{5.4}$$

where S is the percent increase in ultimate flexural capacity achieved using a CFRP system compared to the control girder and E_{FRP} and A_{FRP} are the elastic modulus and area of CFRP material respecitively. Material properties of the CFRP, including thickness of the laminates, were measured for each case. The structural efficiency as defined represents how efficient the CFRP strengthening system is with respect to the amount of material and its stiffness. The results indicate that NSM systems had the highest structural efficiency, around 6 %/k (1400 %/MN). The structural efficiency of girder EB4S, which was strengthened to acheive a 60 percent increase in ultimate capacity compared to the control girder, was over two times the values measured for the NSM strengthened girders. These values are provided in Table 5.1

The NSM systems performed well under this definition as a result of the high rupture strains that were achieved during the test due to the superior bond characteristics that can be achieved for this type of system. The other CFRP systems failed earlier due to the limited strain achieved at ultimate or debonding such was the case for the high modulus material and the CFRP strips respectively. The only other system which achieved a high percentage of structural efficiency were the girders strengthened with externally bonded normal modulus sheets to achieve a 40 and 60 percent increase in ultimate capacity (EB4S and EB6S). In both of those cases, the amount of CFRP material installed using the wet lay-up system, and as a result lower values of stiffness, gave lower values of structural efficiency.

Ultimate Load and Displacement – Test results indicate that the addition of a brittle material such as CFRP, to a ductile structural member such as prestressed concrete, does not reduce the overall ductility of the member. As shown in Figure 5.6, the ultimate loads of a prestressed concrete girder can be substantially increased using CFRP materials without

sacrificing the ductility of the section. The premature failure of two of the strengthened girder is discussed in detail in Section 3.4.4.

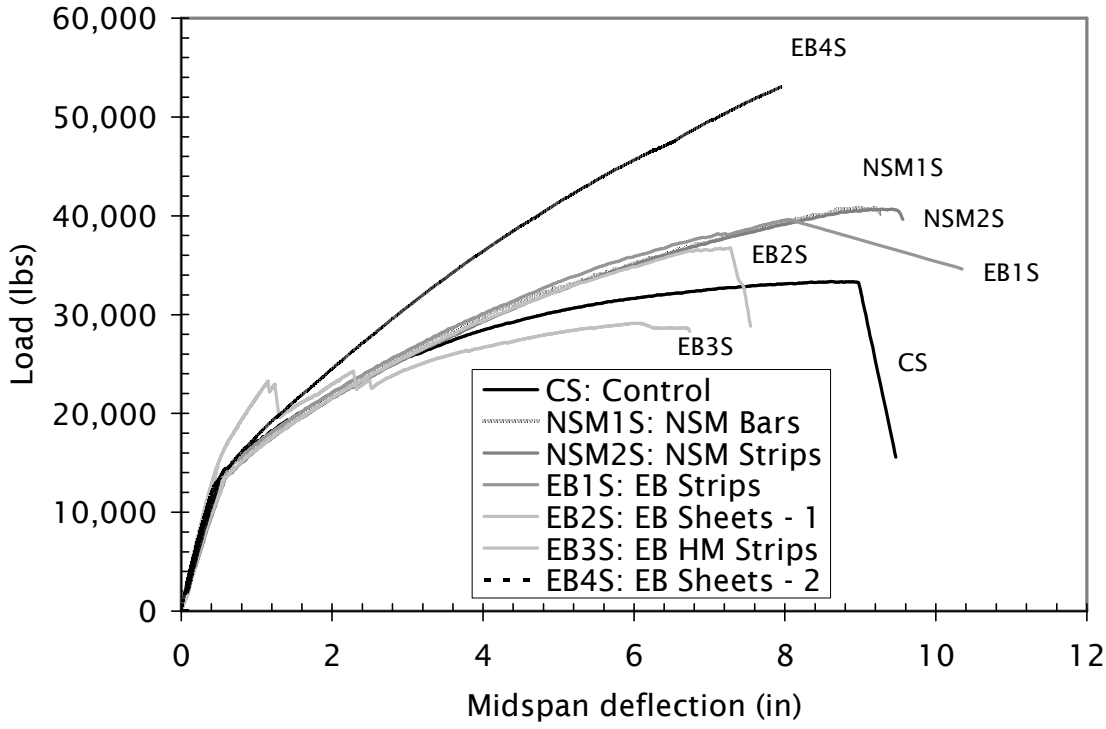

Figure 5.6 Load deflection response of Type I girders

The failure mode of two girders, EB2S and EB3S, was rupture of the CFRP material before achieving their design goals. After rupture of the high modulus CFRP strips in girder EB3S, the behavior followed closely the behavior of the control girder (CS). However, as a result of the damage imparted on the section because of the sudden rupture of the CFRP, the girder failed at an ultimate displacement lower than that of the control girder. The maximum measured concrete strain at ultimate was 0.0026 in/in.

Girder EB4S, strengthened with four layers of normal modulus CFRP sheets, failed due to rupture of the CFRP material. The rupture occurred at the location of the CFRP U-wrap closest to midspan and occurred simultaneously throughout the four layers in each web. The

measured concrete strain at ultimate was 0.003 in/in. The measured tensile strain in CFRP at ultimate was 1.17% which is 117 percent of the manufacturer's specified rupture strain.

Two of the strengthened Type I girders (NSM1S and NSM2S) experienced failure at ultimate due to concrete crushing which was the same failure mode as the control girder (CS). After crushing of the concrete, due to the sudden increase in the curvature of the girder, the NSM systems debonded from the concrete substrate. The maximum measured compressive strain in concrete at failure for both girders was 0.0036 in/in.

Predicted v. Experimental – Three of the C-Channel girders with Type I prestressing strand configuration were analyzed using finite element simulations and cracked section analysis as discussed in Sections 5.2 and 5.3. For the control girder tested under static loading conditions, girder CS, the ultimate loads obtained from the cracked section analysis and the finite element simulation were within 10.2% and 2.1%, respectively, of the measured ultimate loads observed during the experiment. The ultimate displacement observed during the finite element analysis was very close to the experimental value. The failure modes also were the same – crushing of the concrete at midspan. For the cracked section analysis however, the ultimate displacement was considerably lower than the experimental value. The concrete crushed at an earlier strain value in the cracked section analysis due to not being able to model confinement effects under the loading tires in the Response 2000© analysis. The load versus deflection curves determined from both types of analyses are shown along with the experimental data in Figure 5.7.

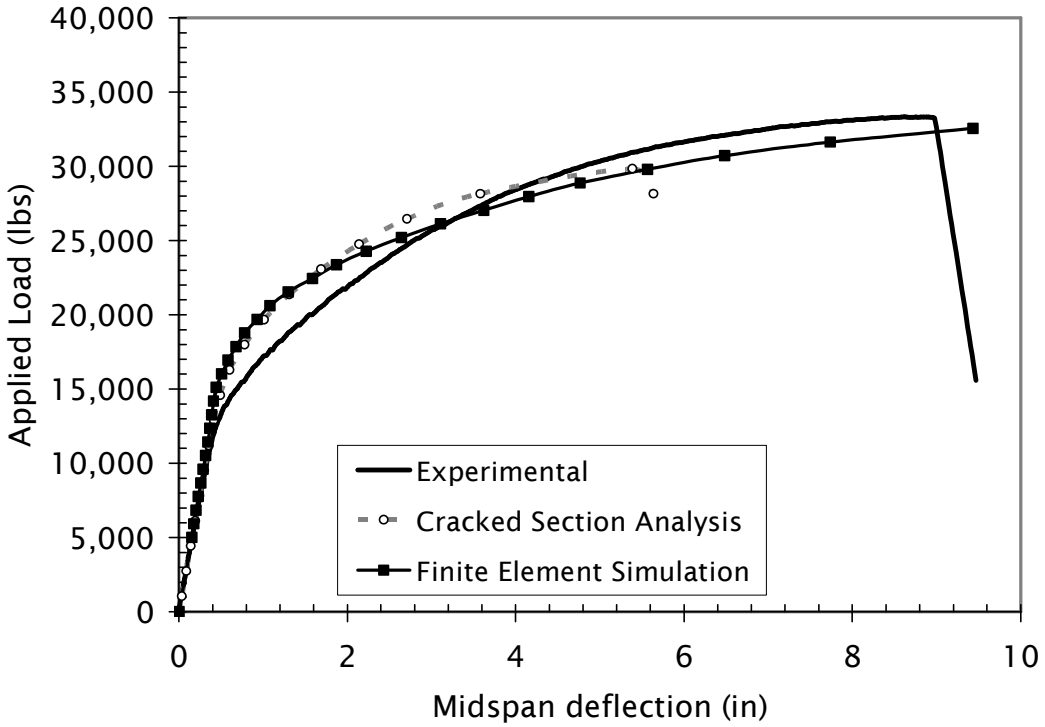

Figure 5.7 Analysis v. experimental for girder CS

Two Type I girders strengthened with CFRP were analyzed using a cracked section analysis and finite element model as shown in Figures 5.8 and 5.8. For the girder strengthened with NSM bars (NSM1S), the measured ultimate load was 40.8 k (181.5 kN), whereas the ultimate load determined from cracked section analysis and the finite element model was 40.3 k and 41.6 k (179.3 kN and 185.0 kN) respectively, a difference of -1.2% and 1.9%. For the girder strengthened with four plies of externally bonded sheets (EB4S), the ultimate loads from the cracked section analysis and the finite element simulation deviated 6.9% and 8.7% respectively compared to the experimental values.

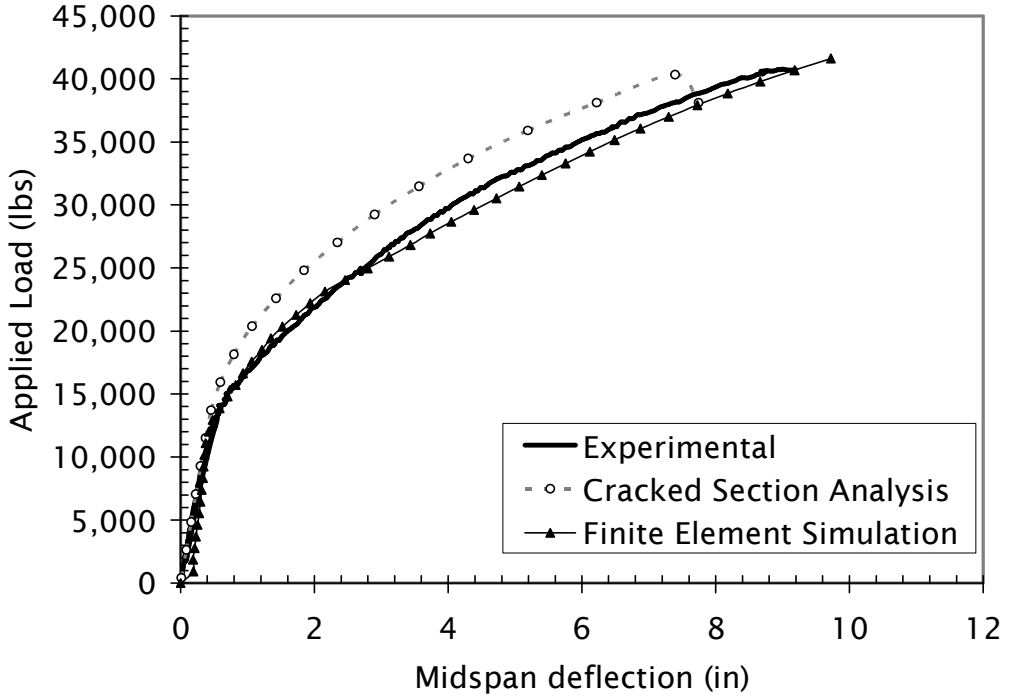

Figure 5.8 Analysis v. experimental for girder NSM1S

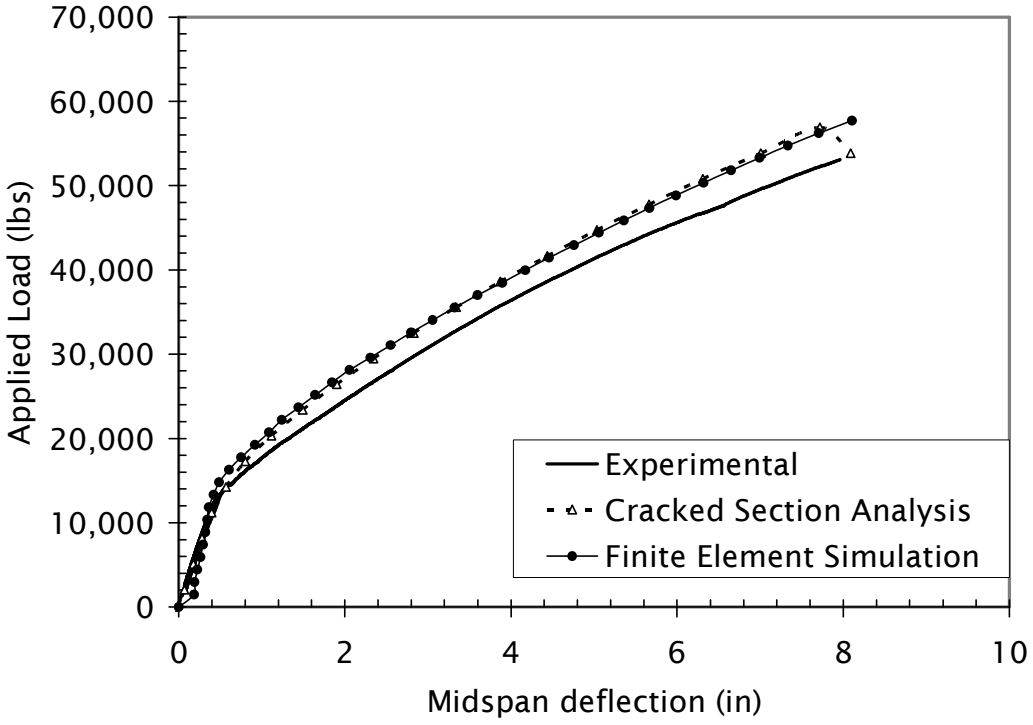

Figure 5.9 Analysis v. experimental for girder EB4S

5.4.3 Type II Girders

Two strengthened girders with a Type II prestressing strand configuration, EB5S and EB6S, were tested under static loading conditions. The static testing to failure of the unstrengthened girder CF2 after 2 million fatigue cycles was used as a control girder, as explained in Section 5.4.1.

Crack Development – Due to the fact that the behavior of C-Channel type girders with Type I and Type II prestressing strand configurations are very similar, the cracking pattern both before and after yielding of the prestressing were similar for the control girder and for the strengthened girders. The transverse reinforcing stirrups were located at similar spacing in both the Type I and Type II prestressing configurations. Therefore the spacing of the flexural cracks was similar for both types of girders. The eccentricity of the prestressing was slightly higher for the Type II configuration. In addition, the strain at which yielding of the prestressing occured was greater for the Type II configuration due to the use of higher strength strands with an ultimate tensile strength of 270 ksi (1862 MPa). As a result, the flexural cracking observed for the Type II girders extended slightly farther away from midspan section at failure due to the higher curvature which occurred at failure.

The cracking load, P_{cr}, and crack reopening load, P_{ro}, were substantially higher for the Type II girders than for the Type I girders due to the larger prestressing eccentricity even though the two types had approximately the same total effective prestress force. These values, along with other test results are given in Table 5.2.

Table 5.2 Summarized test results for Type II girders tested under static loading conditions

Specimen Designation	CF2‡	EB5S	EB6S
Strengthening	--	EB sheet	EB HM Sheets
P_{cr}, k	12.9	13.9	14.3
P_{ro}, k	--	--	--
P_e, k	18.7	18.7	18.4
Losses, %	13.8	13.8	15.2
P_{ult}, k	32.0	55.3	33.7
S, % increase in capacity	--	72.8	5.3
ε_c, ultimate compressive strain in concrete (exp), in/in	0.0032	0.0029	0.0025
ε_t, ultimate tensile strain in CFRP (exp), %	--	1.33	0.26
Experimental/Manufacturer tensile strain in CFRP, %	--	133	86.7
Failure mode*	C	C	R
Initial Stiffness, k/in**	30.6	33.1	34.2
Secondary Stiffness, k/in†	1.1	6.6	12.5
Structural Efficiency, %/k ¬	--	6.34	0.14

* C = crushing of concrete, R = rupture of CFRP, D = debonding of CFRP
** defined from 2 k to 11 k (9 kN to 44.5 kN)
† defined from 28 k to 33 k (124.6 kN to 146.8 kN)
‡ the control in this case is defined as the final static test on girder CF2
¬ defined as (% increase in capacity) / (E_{FRP} A_{FRP})

The crack widths of the Type II girders, calculated using Equation 5.1, were less than their equivalent Type I girders. Substantial reduction of crack widths compared to the control girder were observed for Type II girders strengthened with CFRP, similar to the behavior of the strengthened Type I girders.. The largest crack width reduction was measured in the girder strengthened with five layers of high modulus CFRP sheets, EB6S, prior to rupture of the CFRP as shown in Figure 5.10.

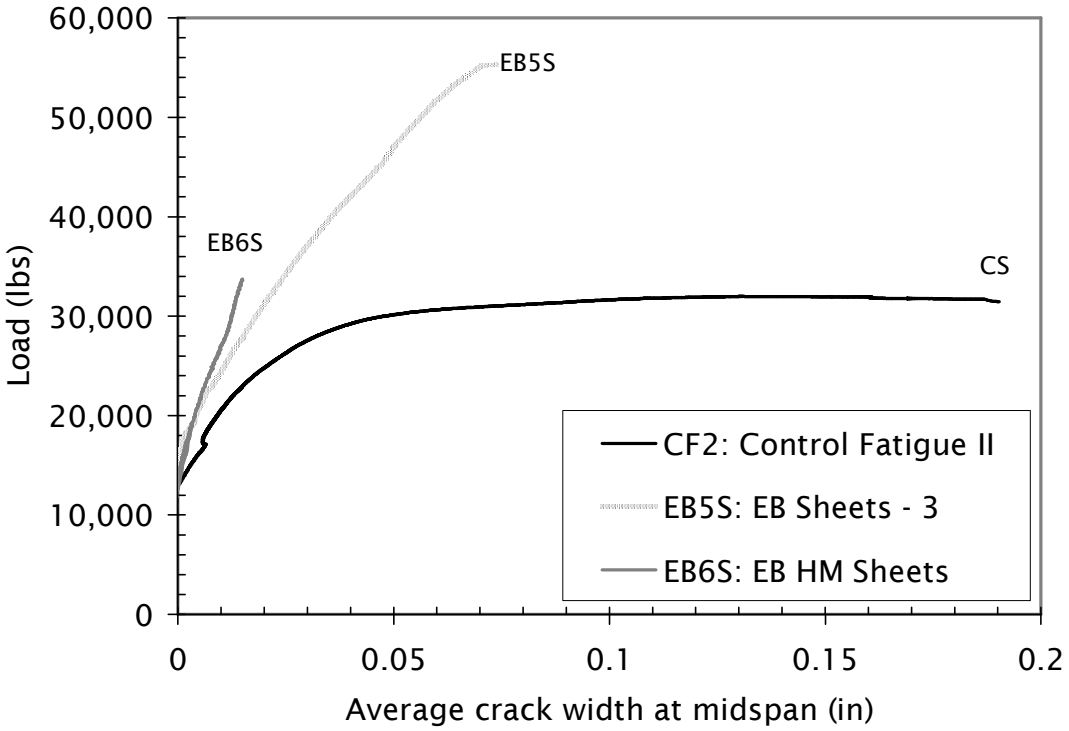

Figure 5.10 Load v. crack width for Type II girders tested under static loading conditions

Stiffness –The initial stiffness of the strengthened Type II girders was 9 percent and 11 percent higher than the control girder for girders EB5S and EB6S respectively. The secondary stiffness was considerably larger for the strengthened girder compared to the control. The girder strengthened with the high modulus material has a secondary stiffness nearly double the girder with normal modulus material.

Effective Prestress – The effective prestress per strand for the Type II girders was greater due to the larger strand area and higher strength of the strands. The effective prestress, as calculated from experimental data using Equation 5.5, varied between 18.4 k and 18.7 k (81.8 kN and 83.2 kN). The average of the Type I effective prestress forces per strand were 18 percent lower than the Type II girders. The jacking force was the same as the Type I girders, equivalent to 70 percent of the ultimate strength of the strands, which was 22.1 k (98.1 kN). The prestress

losses varied between 13.2 and 13.8 percent, slightly lower than the losses observed in the Type I girders. These values were less than a value of 20.1 percent recommended for prestress losses from Collins and Mitchell (1991) and a value of 27.1 percent calculated using the AASHTO (2004) specification lump-sum method.

Structural Efficiency – The structural efficiency of the strengthened Type II girders was calculated using Equation 5.7. For the girder strengthened with high modulus CFRP sheets, the structural efficiency was very low due to the early rupture of the CFRP material before achieving the design goal. The girder strengthened with normal modulus sheets had a structural efficiency comparable to the Type I girders strengthened with NSM systems – yet the efficiency of NSM systems applied to Type II girders is not known.

Ultimate Load and Displacement – The ultimate load versus deflection of the Type II girders tested under static loading conditions is shown in Figure 5.11. The ductility of the prestressed concrete section was maintained in girder EB5S with the installation of normal modulus CFRP sheets. The ultimate load was 72.8 percent higher than the control girder, and the ultimate displacement was only 16 percent less than the control. It should be noted that since girder EB5S was unloaded at a load level of 50.0 k (222.4 kN) (see Section 3.4.5), there might be added ductility due to the benefits of aggregate interlock under cyclic loading. The failure mode of girder EB5S was due to crushing of concrete, similar to the control girder. The maximum measured compressive strain in concrete at failure was 0.0029 in/in, slightly lower than the observed value for the control girder of 0.0032 in/in. The maximum tensile strain measured during testing of girder EB5S was 133 percent of the manufacturer recommended rupture strain.

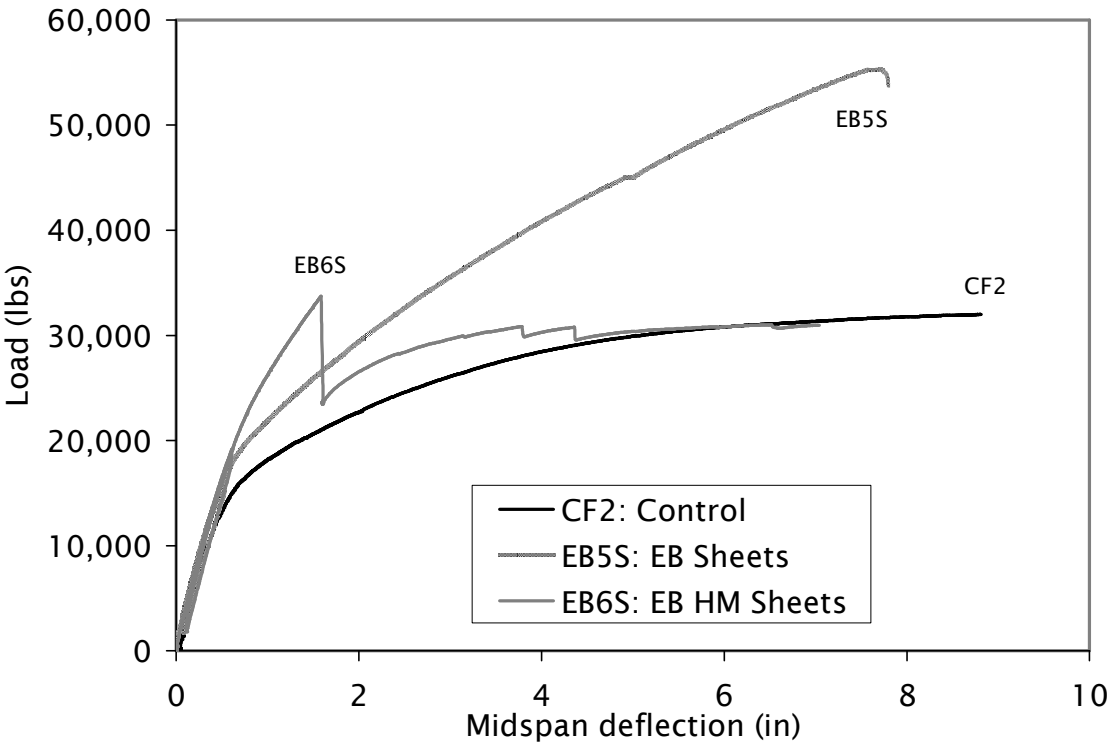

Figure 5.11 Load deflection response of Type II girders

Girder EB6S failed due to rupture of CFRP material at a load of 33.7 k (149.9 kN), which represents an increase of 5.3 percent over the ultimate load measured in the testing of the control girder. The maximum measured tensile strain in the CFRP at the rupture event was 0.26 percent, which is 86.7 percent of the rupture strain used in design. Although for the NSM strengthened Type I girders, this percentage may be acceptable, for the girder strengthened with high modulus material this loss in rupture strain capacity had a large influence on the observed behavior. The high modulus material was very sensitive to fiber orientation and this could have played a role in the difference between the design and the measured rupture strain. The failure was due to concrete crushing, after numerous CFRP rupture events along the length of the girder, at a measured concrete compressive strain of 0.0025 in/in. The rupture events for girder EB6S continued far longer than the rupture events in girder EB3S, which was also strengthened with

high modulus material, due to the better bond characteristics of the high modulus sheets compared to the strips.

Predicted v. Experimental – Two of the C-Channel girders with Type II prestressing strand configuration were analyzed using finite element simulations and cracked section analysis as discussed in Sections 5.2 and 5.3. The predicted behavior of the control girder CF2 was similar to the control girder for the Type I girders. The ultimate load values obtained in the finite element analysis and cracked section analysis were lower than the measured values by 13 percent and 8 percent respectively as shown in Figure 5.12. Ductility of the control girder was not fully predicted by the cracked section analysis since the program Response 2000© doesn't take into account concrete confinement in loading area. The failure mode predicted by both analyses was due to crushing of the concrete, the same mode observed during the test.

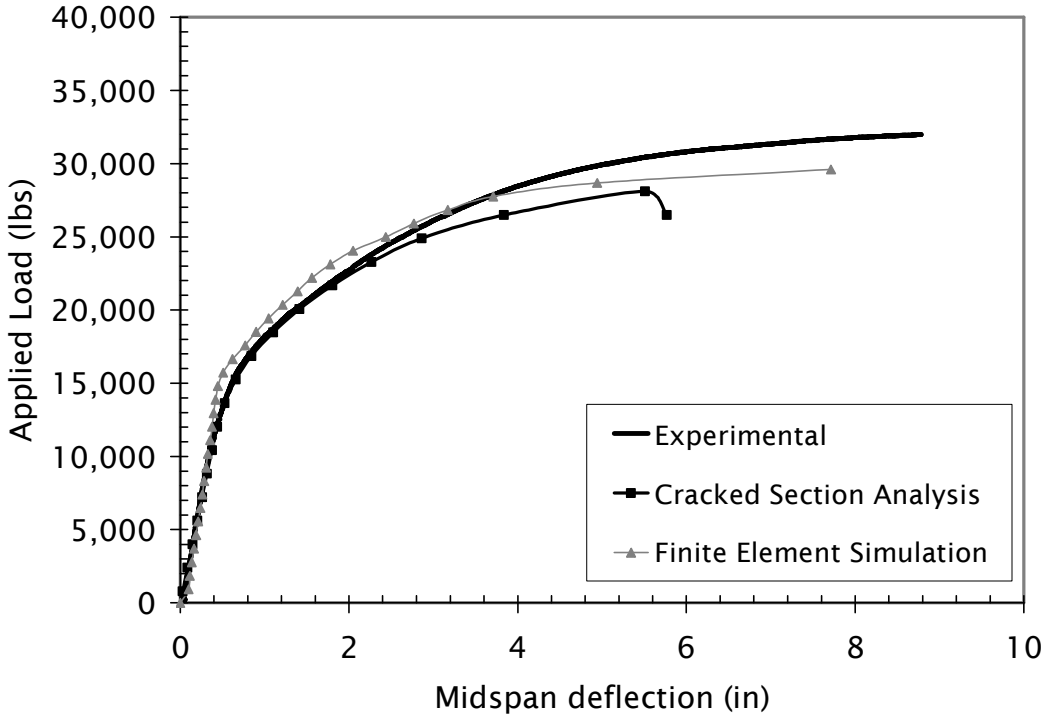

Figure 5.12 Analysis v. Experimental for final static test of girder CF2

The finite element and cracked section analysis for girder EB5S are shown in Figure 5.13. The analyses shown were conducted using design material properties provided by the manufacturer, not values obtained during material testing.

The strengthening scheme of girder EB5S was designed to increase the load carrying by 40 percent compared to the control girder. The measured ultimate capacity was increased by 72.8 percent. After the testing of the girder, it was found that the material properties provided by the manufacturer were conservative – including the stiffness and ultimate strength values which were larger than the specified values used in design.

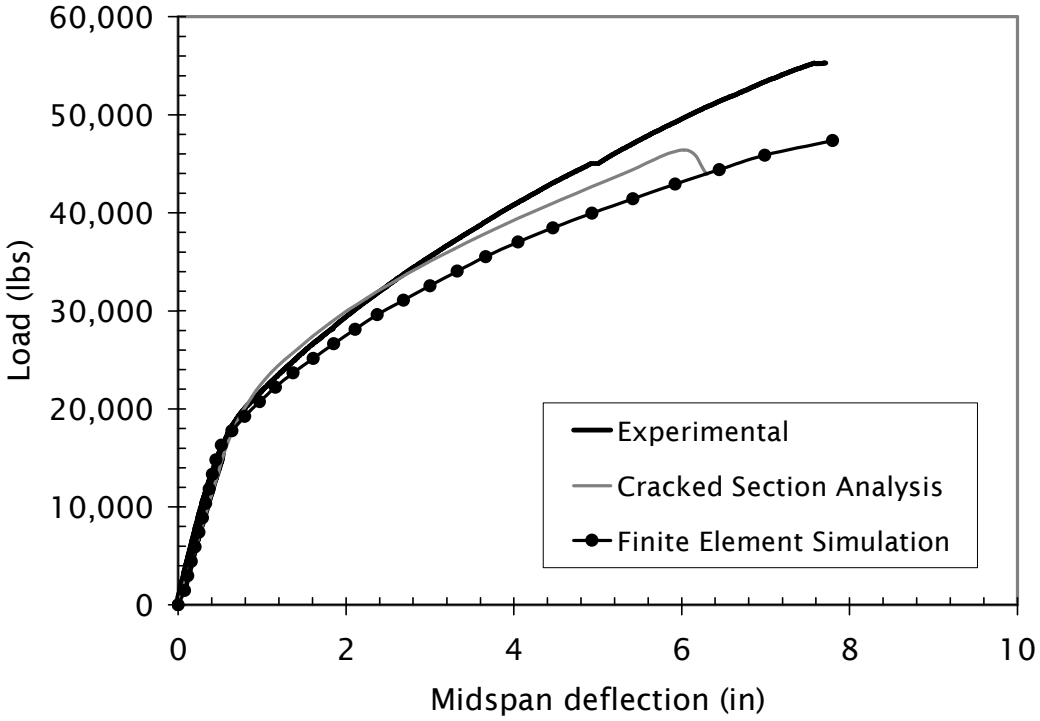

Figure 5.13 Analysis v. Experimental for girder EB5S

5.5 C-Channel Fatigue Tests

5.5.1 Introduction

Eight girders were tested under cyclic loading conditions including two unstrengthened girders used as control specimens and six CFRP strengthened girders. One of the control girders

and two of the strengthened girders had a Type II prestressing strand configuration, the rest were Type I. The results of the control girder with a Type I configuration are presented here, but due to a testing equipment error, the girder was accidentally subjected to a high load which could have altered the behavior from what is typically measured. Even though the load-deflection response and ultimate capacity of the control girders with Type I and Type II prestressing strand configuration are very similar, all the test results are separated according to each type. As discussed in Section 3.5.2, the fatigue loading applied to the girders was determined assuming that the design load was HS-15, but it was later discovered that the design load for the original girders was a HS-13 type loading. Therefore, when the specified live load for the fatigue testing was designed to represent a 20 percent increase over the assumed design load of HS15, it was actually representing a 41.0 percent increase over the original design load of HS-13. Similarly, the loading for the girders designed to represent a 60 percent increase over HS-15, was actually representing an 84.6 percent increase over the original design load of HS-13. This admittedly severe loading provides the research work with an upper limit value for the possibilities of strengthening prestressed concrete with CFRP.

5.5.2 Type I Girders

Load - Displacement Hysteric Reponse – After the completion of each fatigue cycling regime, a static test was performed. Several static tests were performed at the beginning of the fatigue cycling since most of the degradation was expected to occur early in the fatigue regimen (Ahmad 2004). The load versus displacement characteristics of three strengthened Type I girders, as well as the control girder, are shown in Figures 5.14 to 5.17. Summarized test results for the Type I girders tested under fatigue loading are given in Table 5.3.

Table 5.3 Summarized test results for Type I girders tested under fatigue loading conditions

Specimen Designation	CF1	EB1F	NSM1F	NSM2F	EB4F
Strengthening	-	EB strips	NSM bars	NSM strips	EB sheets
P_{cr}, k	--	12.1	11.5	12.1	15.7
P_{ro}, k	9.0	8.4	8.4	8.6	9.0
P_e, k	16.2	15.4	15.4	15.6	16.2
Losses, %	14.3	18.3	18.3	17.6	14.3
N, number of cycles achieved, thousands	1076	625	2000	2000	2000
Failure Mode*	RPS	D+RPS	C	C	RFRP
P_{ult}, k (residual)	--	--	40.2	36.9	55.3
% change from virgin	--	--	-1.5	-10.2	4.1
Initial Stiffness, k/in**	20.3	27.6	29.4	26.6	31.1

* C = crushing of concrete, RPS=rupture of prestressing strand, RFRP = rupture of CFRP, D = debonding of CFRP
** defined from 2 k to 11 k (9 kN to 44.5 kN)

The Type I control girder, CF1, failed due to a ruptured lower prestressing strand after 1,075,000 cycles of fatigue loading equivalent to HS-15 type loading, which is equivalent to loading 15.3 percent higher than HS-13 type loading, as shown in Figure 5.14. As mentioned previously, this girder was subjected to a sudden unmeasured load due to an error in the loading system. The initial stiffness of this girder after the sudden loading was 39.6 percent less than the initial stiffness of an identical girder tested under static loading conditions, girder CS. It is believed that the sudden and unmeasured load was high enough to cause yielding of the prestressing strands resulting in residual displacement and reduced fatigue life of this control girder.

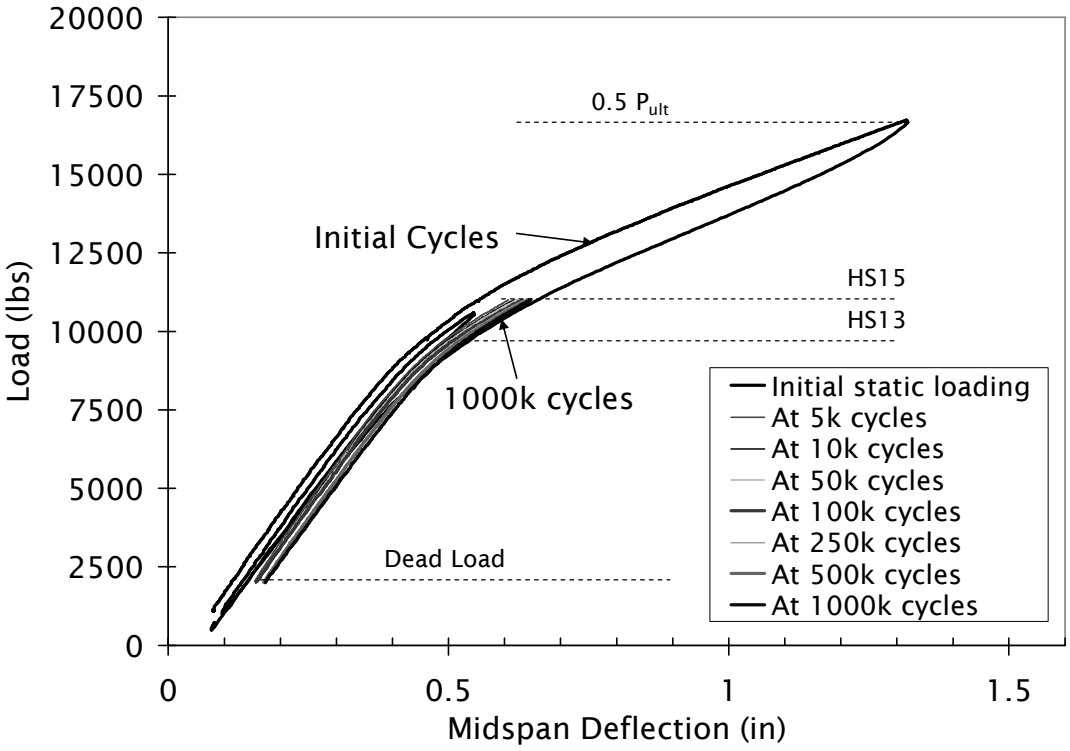

Figure 5.14 Load versus deflection for the first control girder tested in fatigue, CF1

Girder NSM1F and NSM2F, strengthened with NSM bars and strips respectively, performed very similarly to each other since both girders were strengthened with a similar area of FRP. The load versus displacement hysteresis of girder NSM1F is shown in Figure 5.15. The displacement degradation during fatigue cycling for both girders was very small, on the order of 0.08 in (2 mm), and the girder stiffness after the initial cycles remained constant up to 2 million cycles. The incremental increase of the deflection is mainly due to the fatigue creep of the concrete in the compression zone.

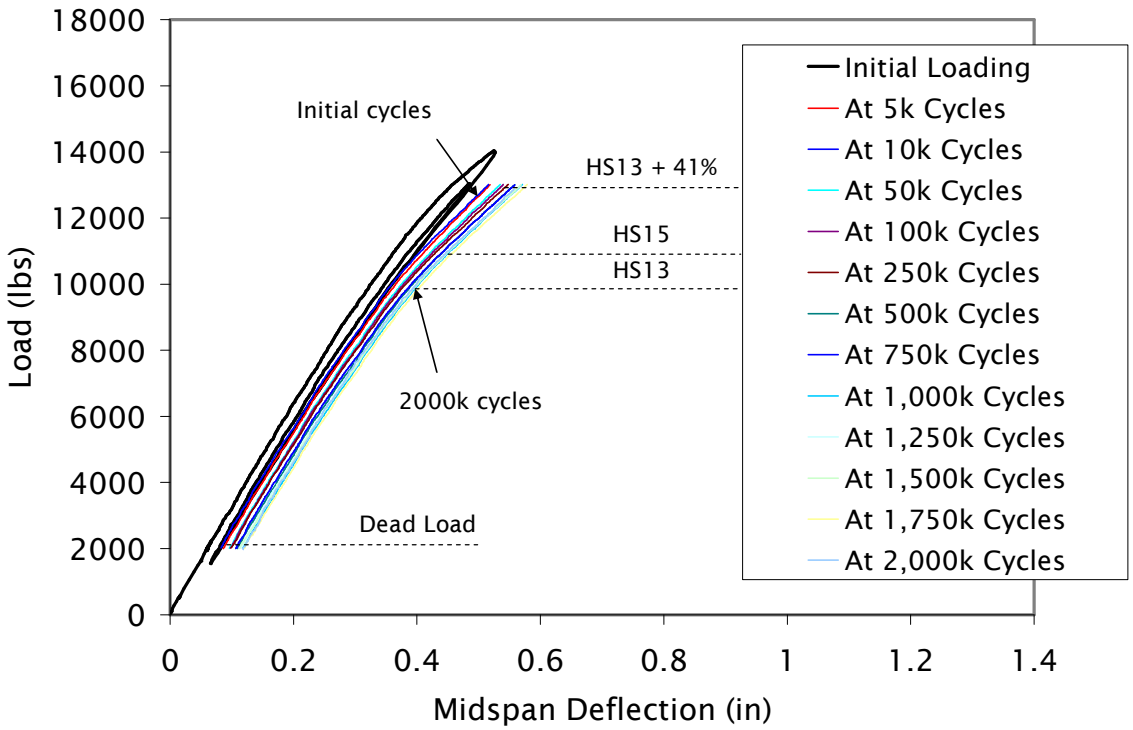

Figure 5.15 Load versus deflection for girder NSM1F

A larger amount of energy dissipation can be noticed in the first cycles of girder EB1F compared to NSM1F or EB4F. After 500,000 cycles, considerable displacement degradation was observed at the upper load level as shown in Figure 5.16. The displacement degradation at the lower load level remained nearly constant, signifying stiffness loss. At 625,000 cycles, failure occurred due to rupture of a lower prestressing strand. The test was continued and significant stiffness loss and residual displacement was observed until catastrophic failure occurred near 900,000 cycles. By inspection, it was noted that several of the strands were corroded at the lower level which could have caused the early fatigue failure girder EB1F.

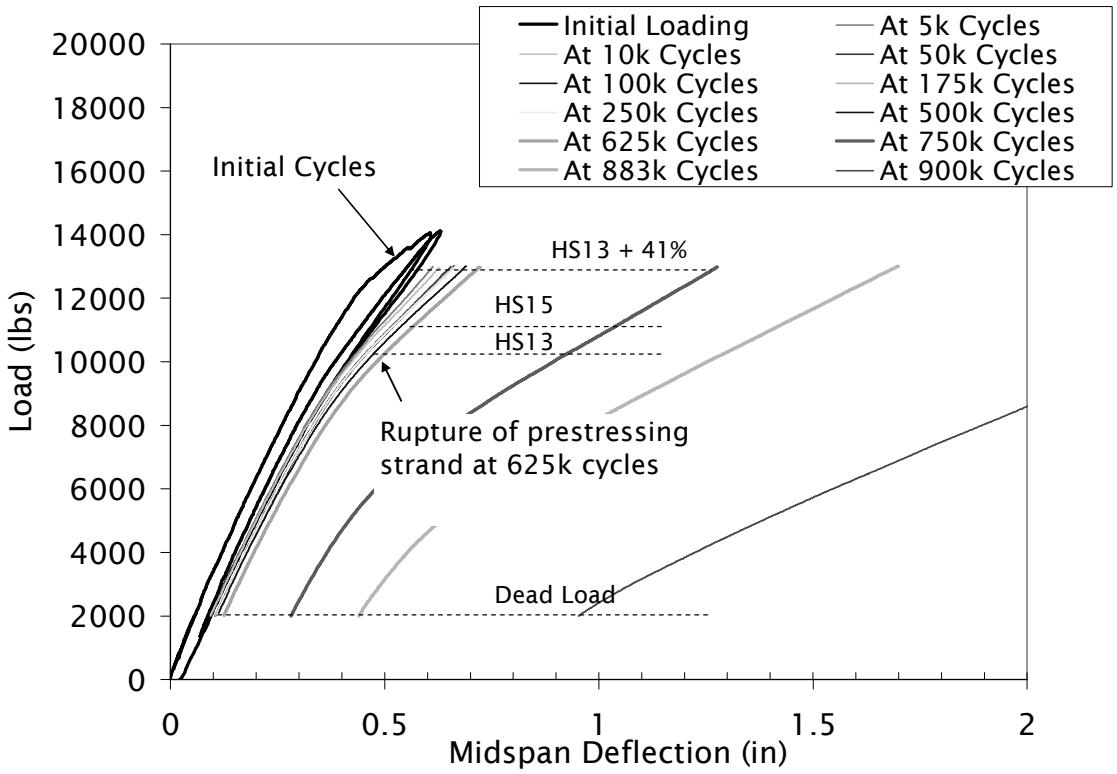

Figure 5.16 Load versus deflection for girder EB1F

Girder EB4F, strengthened with CFRP sheets, survived 2 million cycles of different loading levels as shown in Figure 5.17. After 1 million cycles with an upper load value corresponding to a 20 percent increase in HS-15 live load (a 41.0 percent increase in HS-13 live load) with little degradation, the test was continued at an upper load value corresponding to a 60 percent increase in HS-15 live load (a 84.6 percent increase in HS-13 live load). After the first cycles of the new level of loading, a large reduction in secondary stiffness was observed, yet the girder survived 2 million cycles with little additional degradation.

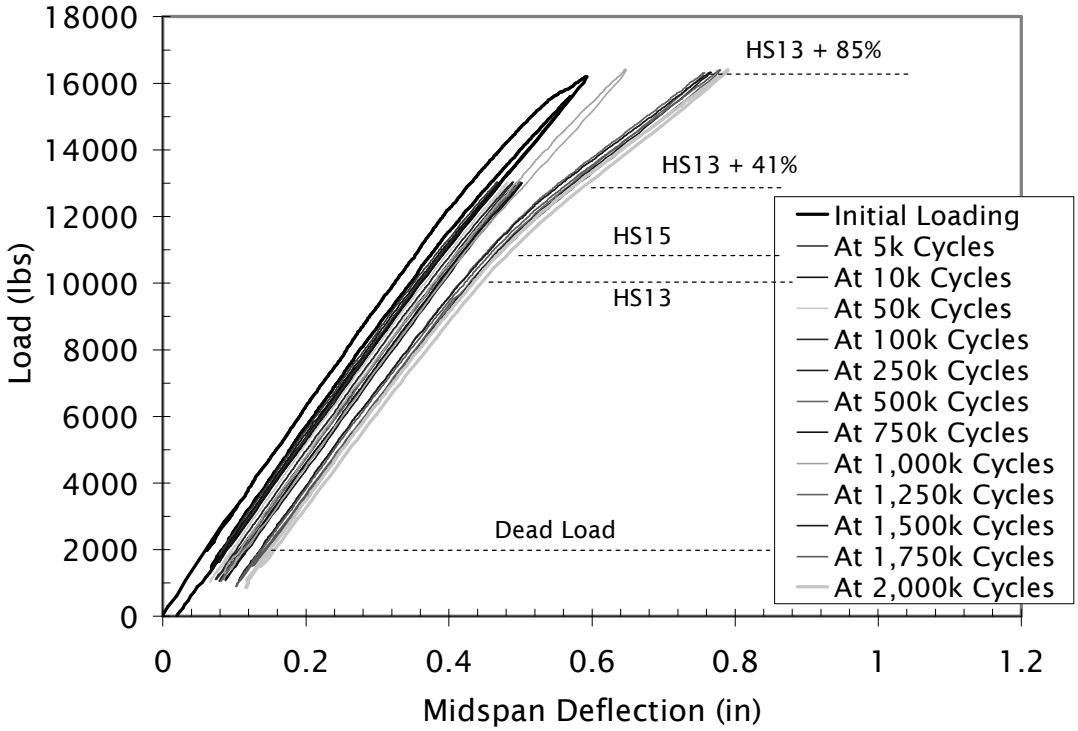

Figure 5.17 Load versus deflection for girder EB4F

Stress Ratio in Lower Prestressing Strand – Based on an extensive literature review of the behavior of prestressed concrete in fatigue (see Section 2.4 and 2.5), the prestressing strands have been identified as the most critical component affecting the fatigue life of a prestressed concrete member. The stress ratio in a prestressing strand during fatigue cycling can be defined as:

$$SR_{ps} = \frac{f_{ps2} - f_{ps1}}{f_{pu}} \times 100 \tag{5.5}$$

where f_{ps2} and f_{ps1} are the upper and lower stress values in the prestressing strand as a result of the fatigue loading, and f_{pu} is the ultimate tensile strength of the strand. The stress ratio in the lower prestressing strand was determined from experimental data by first determining the strain present in the strand from measured values:

$$\varepsilon_{ps} = \varepsilon_i + \varepsilon_{psPI} \tag{5.6}$$

where ε_i is the initial strain in the prestressing strand after losses (determined from the effective prestress force) and ε_{psPI} is the strain in the strand determined from PI gauge readings at a specific load level. Once the strain in the strand was determined for the upper and lower fatigue loads for any given girder, the stress in the strands can be determined by applying the Ramberg-Osgood function (Equation 3.1) with the appropriate material constants A, B and C (see Section 3.2.2). The stress ratio in the lower prestressing strand versus the number of cycles is shown in Figure 5.18.

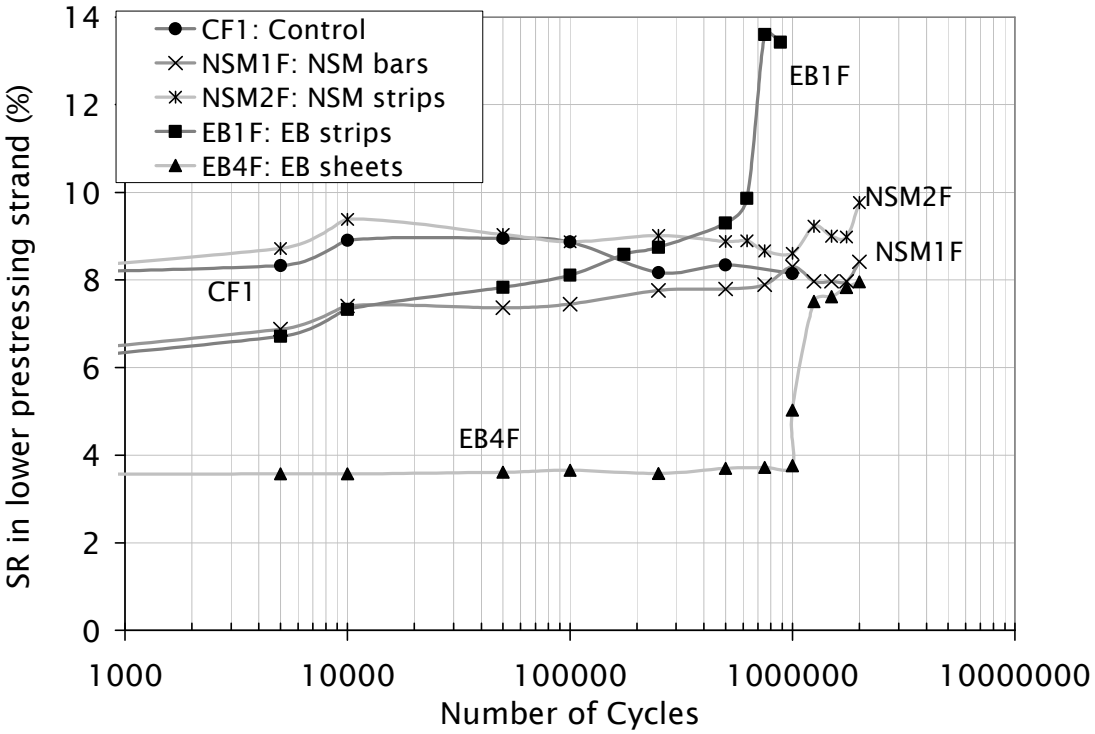

Figure 5.18 Stress ratio in lower prestressing strand versus number of cycles for Type I girders

At midspan, the stress ratio for the lower prestressing strand is typically higher because of the higher eccentricity with respect to the neutral axis. However, since the lower prestressing strands are straight in this prestressing configuration, they may not rupture first. At the hold

down points at midspan, the inclined strands are subjected to high stress concentrations and therefore they may rupture first under the effect of the applied stress ratio, as observed for girder EB4F. Since the stress ratio in the first inclined strand is typically the highest, this is the strand which was analyzed.

The stress ratios for the lowest prestressing strand and for the first inclined prestressing strand can be determined using a Response 2000© analysis and are given in Table 5.4 for each of the Type I girders tested in fatigue. A detailed procedure for this determination is provided in Appendix A. The stress ratios applied in girders NSM1F, NSM2F, EB1F, and CF1 were accurately predicted using the Response 2000© analysis. The stress ratios given by the Response analysis for girder EB4F were conservative. For girder EB1F it can be seen that the applied stress ratio in the applied to the third prestressing strand from the bottom was close to the limit of 3.5 percent recommended by Muller and Dux (1994) and could have caused a rupture event in the inclined strands.

Table 5.4 Stress ratios in prestressing strands of Type I girders from Response 2000© analysis

Specimen Designation	CF1	NSM1F	NSM2F	EB1F	EB4F*
Stress Ratio in lower prestressing strand	7.0	7.6	8.4	7.9	4.7 & 10.4
Stress Ratio in first inclined prestressing strand	0.9	3.2	3.6	3.6	1.5 & 3

* The two values are the stress ratios for the first and second fatigue loading conditions used for girder EB4F.

The stress ratios induced in lower prestressing strands for all of the Type I and Type II girders tested in fatigue versus the number of cycles achieved are shown in Figure 5.19 along with three S-N curves to predict fatigue life, as discussed in Section 2.4. The four girders that survived 2 million cycles are shown with arrows. The early rupture of girder EB5F was due to rupture of an inclined prestressing strand. The early rupture of girders CF1 and EB1F was

mainly due to corrosion of the straight prestressing strands. The behavior shows that both Naaman (1991) and Collins (1991) provide good estimation of the fatigue life behavior of a prestressed member with straight prestressing strands, while Muller and Dux (1994) gives a lower bound estimation of the life of a prestressed member with inclined prestressing strands.

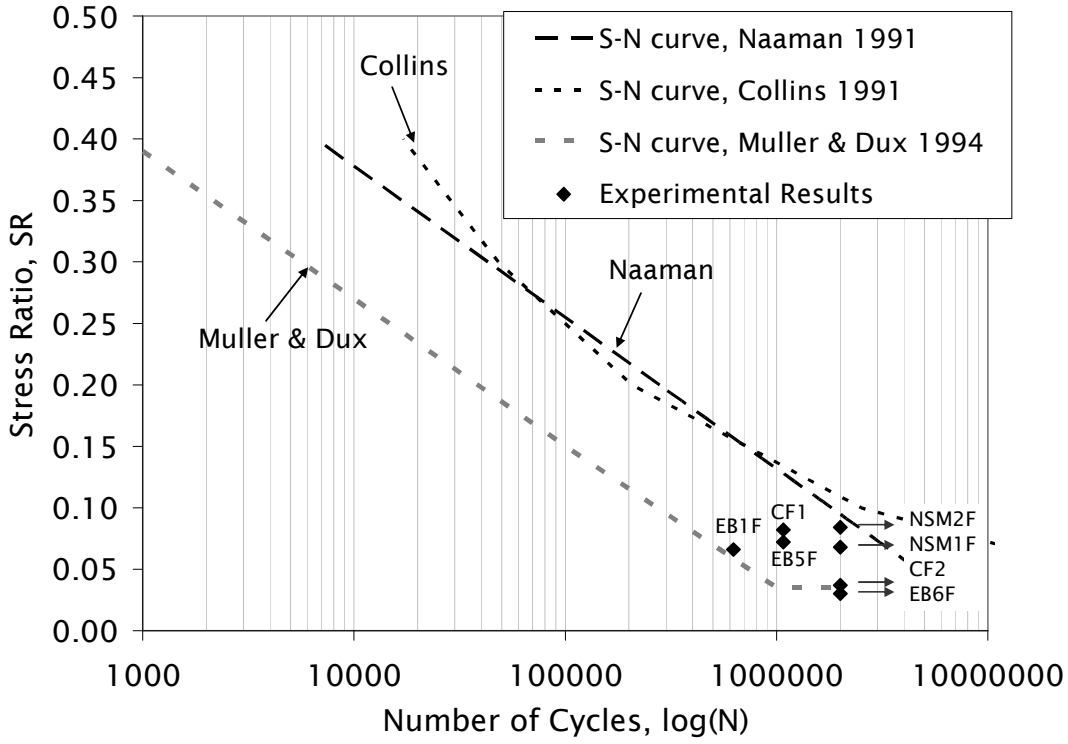

Figure 5.19 Stress ratio in lower prestressing strand versus number of cycles

Stress Ratio in Extreme Compressive Fiber of Concrete – The fatigue behavior of concrete in compression is discussed in Section 2.5 and the behavior in compression fatigue can be estimated using Equation 2.1 (Aas-Jacobsen 1970). In order to determine the minimum and maximum range of the compressive stresses in the extreme compression zone of the concrete, the initial compressive stress in the concrete, f_{ci}, due to the dead load and the applied effective

prestress force can be evaluated from the value of effective prestress force per strand for each girder, P_f,

$$f_{ci} = \frac{n \times P_f}{A} - \sum \frac{P_f e_i}{S_b} + \frac{\omega_D L}{8} \times \frac{1}{S_b} \tag{5.7}$$

where n is the number of cycles. The maximum and minimum compressive stresses in the concrete, $f_{c\max}$ and $f_{c\min}$ respectively, can be determined using measured strain data:

$$f_{\min} = f_{ci} + \varepsilon_{c\min} \cdot E_c \tag{5.8}$$

$$f_{\max} = f_{ci} + \varepsilon_{c\max} \cdot E_c \tag{5.9}$$

For the Type I girders, the average values of $f_{\min}$ and $f_{\max}$ for girders strengthened for a 20 percent increase in ultimate capacity are:

$f_{\min}$ = -0.0817 ksi (565 MPa)

$f_{\max}$ = 1.343 ksi (9529 Mpa)

These values were lower than $f_{\min}$ and $f_{\max}$ values of 0.362 ksi and 2.061 ksi (2496 MPa and 14210 MPa) determined from calculations based on prestressed concrete theory, because the analysis assumes the girder is uncracked.

Using the conservative predicted values for $f_{\min}$ and $f_{\max}$, a prediction of the fatigue life of the concrete can be evaluated using the Aas-Jacobsen equation. For the girders strengthened to achieve a 20 percent increase in ultimate capacity, the fatigue life is $7.75 \cdot 10^{12}$ cycles, and for the girder strengthened to achieve a 60 percent increase in ultimate capacity the fatigue life is $7.62 \cdot 10^{9}$ cycles. Based on the results, it was concluded that compression-compression concrete fatigue is not a concern, even at a loading 84.6 percent higher than HS-13 truck loading.

Behavior of the strengthened girders under fatigue loading indicated some signs of degradation, even in the girders which survived 2 million cycles. This degradation was most likely due to tension-tension fatigue in the concrete. As was discussed in Section 2.4, the tensile strength of concrete subjected to tension-tension fatigue can be reduced up to 27 percent of its original value. (Ahmad 2004). The degradation could also be due to concrete creep effects, both in compression and tension (ACI 215 1997).

The compression stress ratio of concrete, SR_{conc}, can be calculated from the experimental results from:

$$SR_{conc} = \frac{f_{c\max} - f_{c\min}}{f'_c} \tag{5.10}$$

Where $f_{c\max}$ and $f_{c\min}$ are the experimental values for concrete stress in extreme compressive fiber corresponding to the upper and lower load levels. The compression stress ratio versus the number of cycles is shown in Figure 5.20. Due to the impact loading exerted on the girder CF1, the concrete stress ratio shown is artificially high.

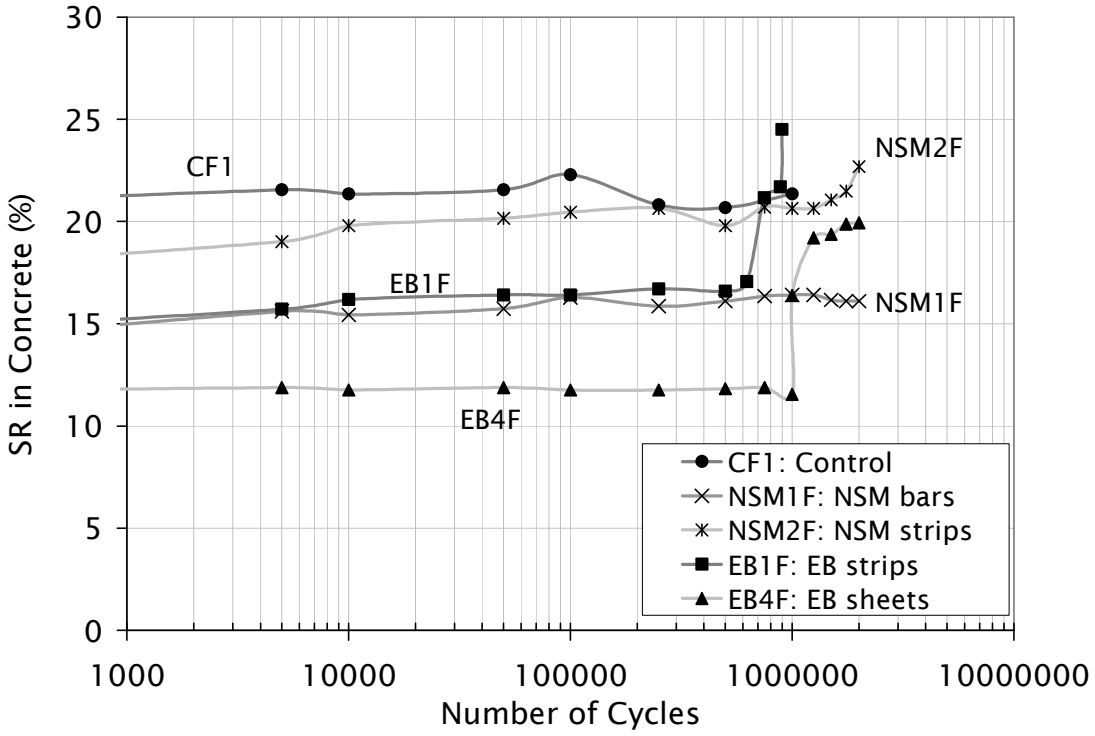

Figure 5.20 Stress ratio at extreme compressive fiber of concrete versus number of cycles for Type I girders

Stress Ratio in FRP – The stress ratio in the extreme tensile fiber of the CFRP material at midspan, defined as:

$$SR_{FRP} = \frac{f_{FRP\max} - f_{FRP\min}}{f_{uFRP}} \tag{5.11}$$

where $f_{FRP\max}$ and $f_{FRP\min}$ are the measured values for stress in the CFRP corresponding to the upper and lower fatigue loading values. f_{uFRP} is the ultimate tensile strength of CFRP as determined from material testing.

One of the more recent studies on the topic of fatigue of CFRP (Adimi et al 2000) has shown that CFRP pre-cured laminates can withstand over 4 million cycles subjected to a stress ratio of 35 percent of their ultimate tensile strength. From Figure 5.16, the stress ratio in the FRP for all strengthened girders is less than 35 percent and therefore the fatigue rupture of the FRP should not be a concern. The degradation in the stress ratio of FRP for girder EB1F shown in

Figure 5.21 is a result of ruptured prestressing strands which induce a larger demand on the FRP during the remaining fatigue cycles.

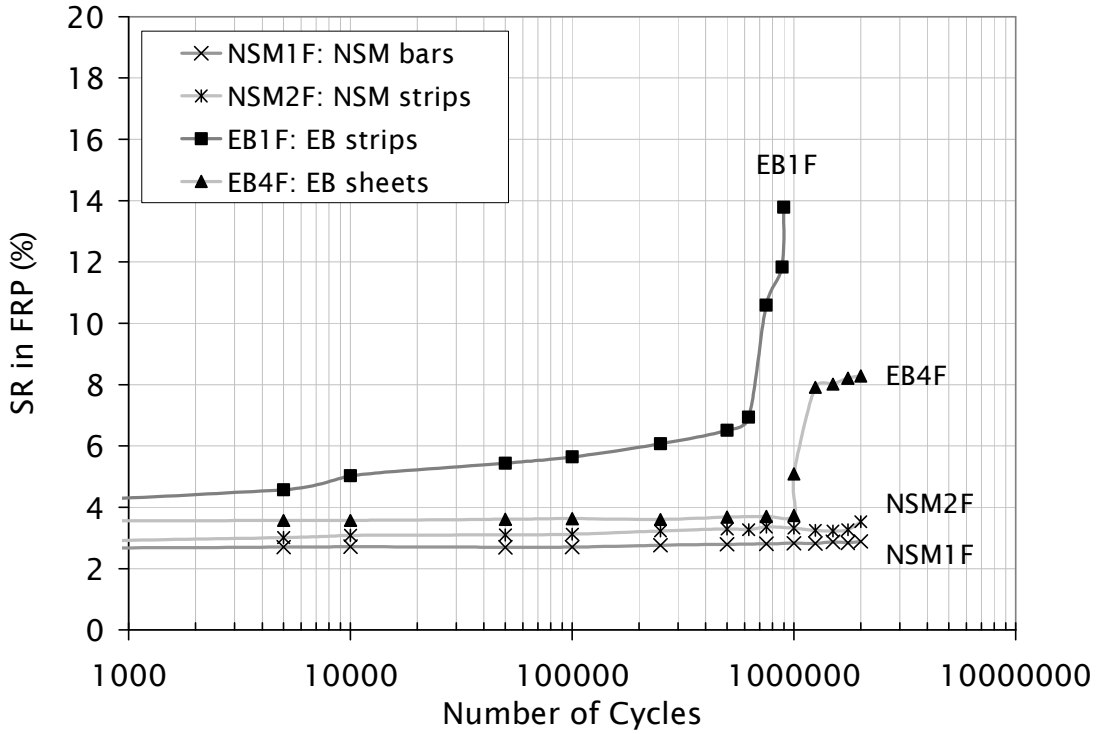

Figure 5.21 Stress ratio in FRP versus number of cycles for Type I girders

Residual Strength – Of the Type I girders which failed due to ruptured prestressing strands (CF1 and EB1F) neither was brought to catastrophic failure. A final static test to failure was performed on the other three strengthened Type I girders. Compared with their counterparts tested under static loading conditions, the behavior of the fatigue cycled girders was nearly identical. The measured ultimate load varied by -1.5, 10.2 and 4.1 percent for girders NSM1F, NSM2F, and EB4F, respectively, compared to the girders tested under static loading. The variation could be attributed to variations in the cross-sectional dimensions, effective prestress forces or slight misalignment of the CFRP material in the externally bonded girder.

5.5.3 Type II Girders

Load Displacement Hysteric Response – The load versus displacement hysteric relationships for each of the Type II girders tested under fatigue loading are shown in Figures 5.22 through 5.24. Test results are also given in Table 5.5.

Table 5.5 Summarized test results for Type II girders tested under fatigue loading conditions

Specimen Designation	CF2	EB5F	EB6F
Strengthening	-	EB sheets	EB HM sheets
P_{cr}, k	12.5	13.5	14.2
P_{ro}, k	10.2	10.2	10.7
P_e, k	18.7	17.5	18.5
Losses, %	13.8	19.4	14.7
N, number of cycles achieved, thousands	2000	1075	2000
Failure Mode*	C	RPS then D	RFRP
P_{ult}, k (residual)	32.0	31.1**	30.0
% change from virgin	--	-43.8**	-11.0
Initial Stiffness, k/in†	30.5	32.9	36.2

* C = crushing of concrete, RPS=rupture of prestressing strand, RFRP = rupture of CFRP, D = debonding of CFRP
** Residual strength after rupture of prestressing strand during fatigue test
† defined from 2 k to 11 k (9 kN to 44.5 kN)

The control girder CF2 survived 2 million cycles of fatigue loading equivalent to 15.3 percent higher than the original AASHTO HS-13 loading. Very little degradation was observed after completion of 2 million fatigue cycles, as shown in Figure 5.22.

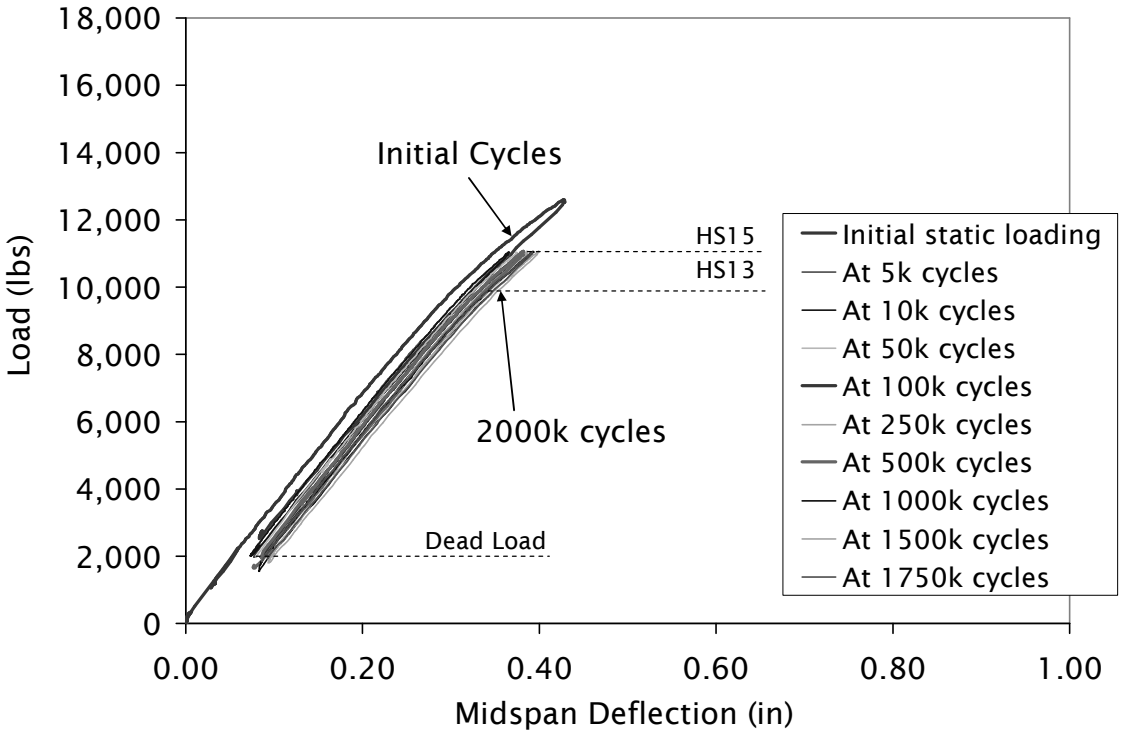

Figure 5.22 Load versus deflection for girder CF2

Girder EB5F, strengthened with three layers of normal modulus externally bonded CFRP sheets, was subjected to a fatigue load equivalent to 84.6 percent higher than the original AASHTO HS13 type loading, as shown in Figure 5.23. Failure was due to the rupture of a prestressing strand after completion of 1,075,000 cycles. After the final static test, a post mortem inspection was carried out which indicated that several of the inclined prestressing strands were also ruptured.

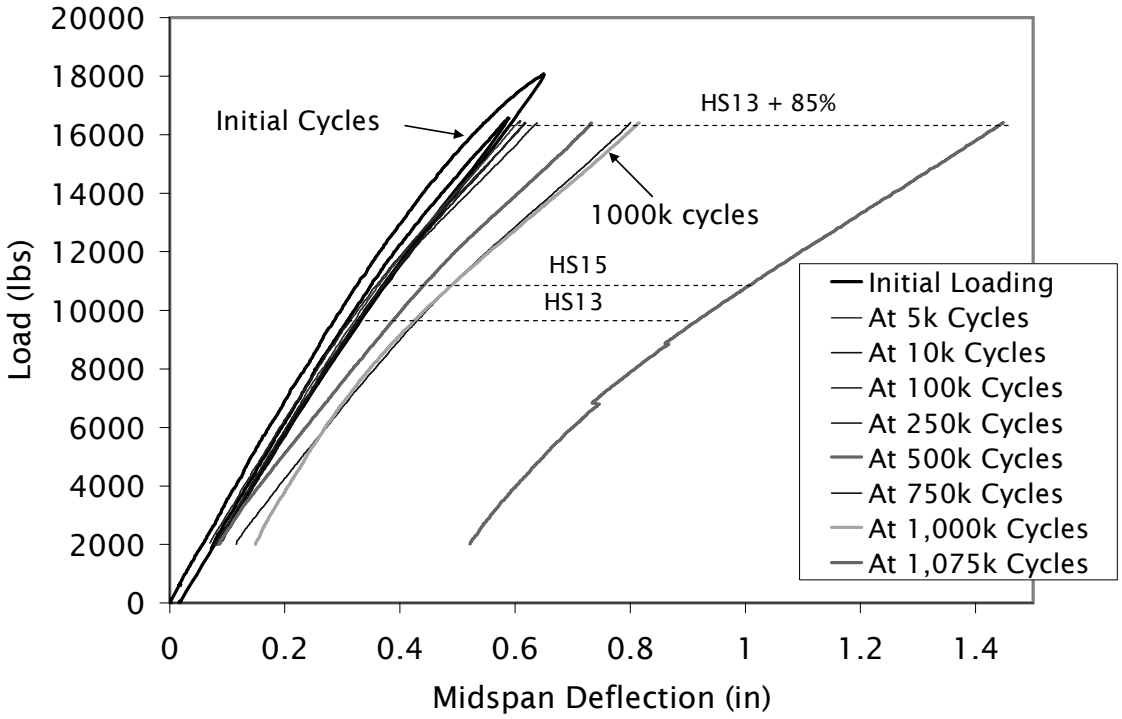

Figure 5.23 Load versus deflection for girder EB5F

Girder EB6F, strengthened with five layers of high modulus externally bonded CFRP sheets, was cycled at a fatigue load 41 percent higher than AASHTO HS-13 type loading and survived 2 million cycles with very little stiffness degradation, as shown in Figure 5.24.

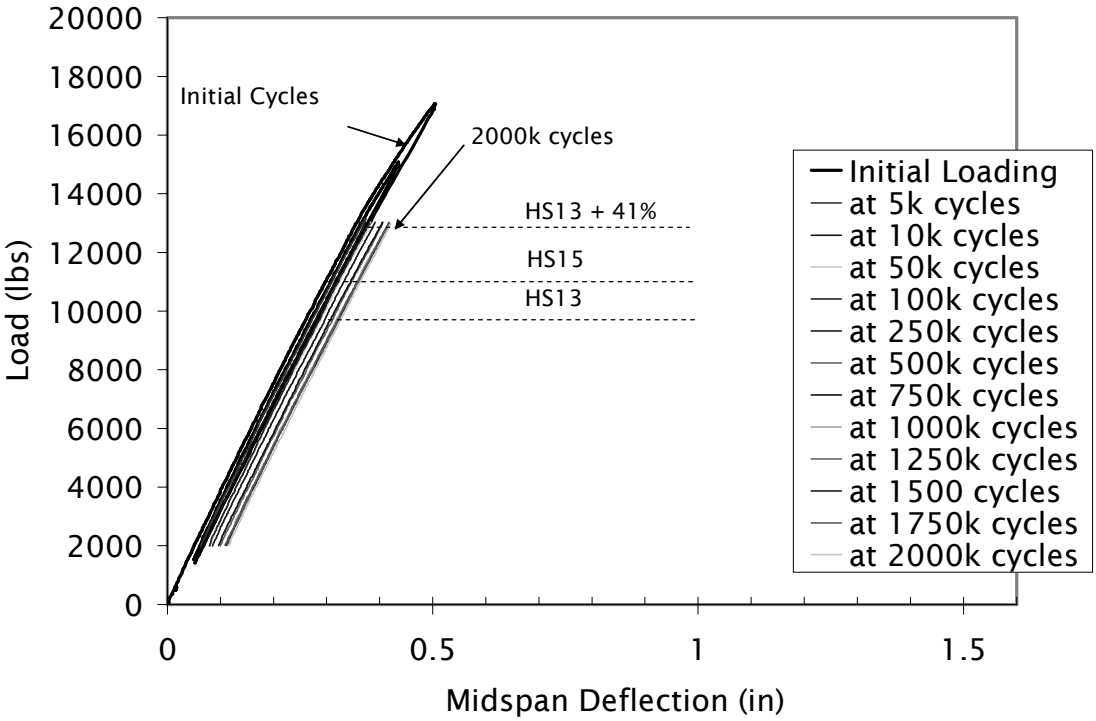

Figure 5.24 Load versus deflection for girder EB6F

Stress Ratio in Lower Prestressing Strand – The Type II girders had a prestressing strand configuration consisting of four 270 ksi (1862 MPa) strands in each web, three inclined with hold down points at midspan. The stress ratio in the lower prestressing strand was determined from Equation 5.5 and is shown versus the number of cycles in Figure 5.25. The magnitude of the observed stress ratio for girder EB5F is high, and lead to the premature rupture of prestressing strands.

The stress ratios determined from a Response 2000© analysis of the Type II girders tested in fatigue are presented in Table 5.6. The predictions closely match the experimental values for girders EB5F and EB6F. The observed stress ratio in lower prestressing strand for girder CF2 is slightly higher than the value predicted by Response 2000©.

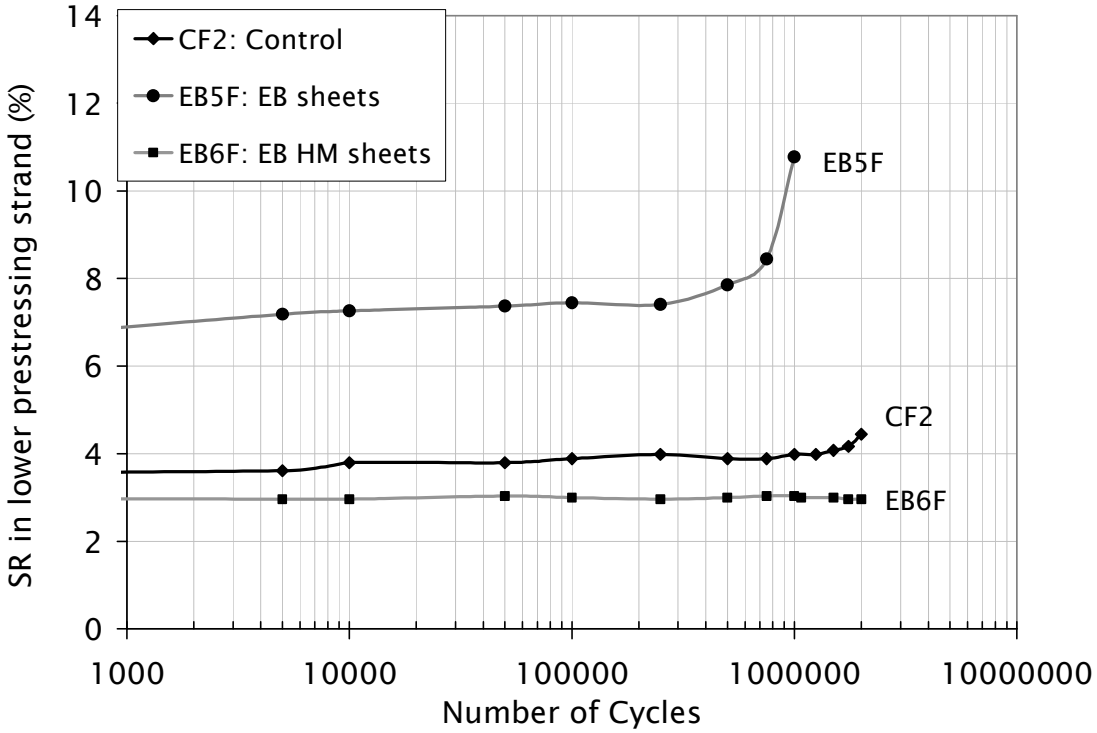

Figure 5.25 Stress ratio in lower prestressing strand versus number of cycles for Type II girders

Table 5.6 Stress ratios in prestressing strands in Type II girders from Response 2000© analysis

Specimen Designation	CF2	EB5F	EB6F
Stress Ratio in lower prestressing strand	2.7	6.7	2.5
Stress Ratio in 3rd prestressing strand from bottom	1.6	3.1	1.3

Stress Ratio in Extreme Compressive Fiber of Concrete – The stress ratio in the concrete for the Type II girders tested in fatigue was determined from Equation 5.10 and is plotted versus the number of cycles and shown in Figure 5.21. After 500,000 cycles, the stress ratio in the concrete for girder EB5F experienced a large increase, as shown in Figure 5.26. This was likely due to the rupture of several wires of the inclined prestressing strand. Due to the low value of stress ratio in concrete for this girder, fatigue failure of the concrete did not occur.

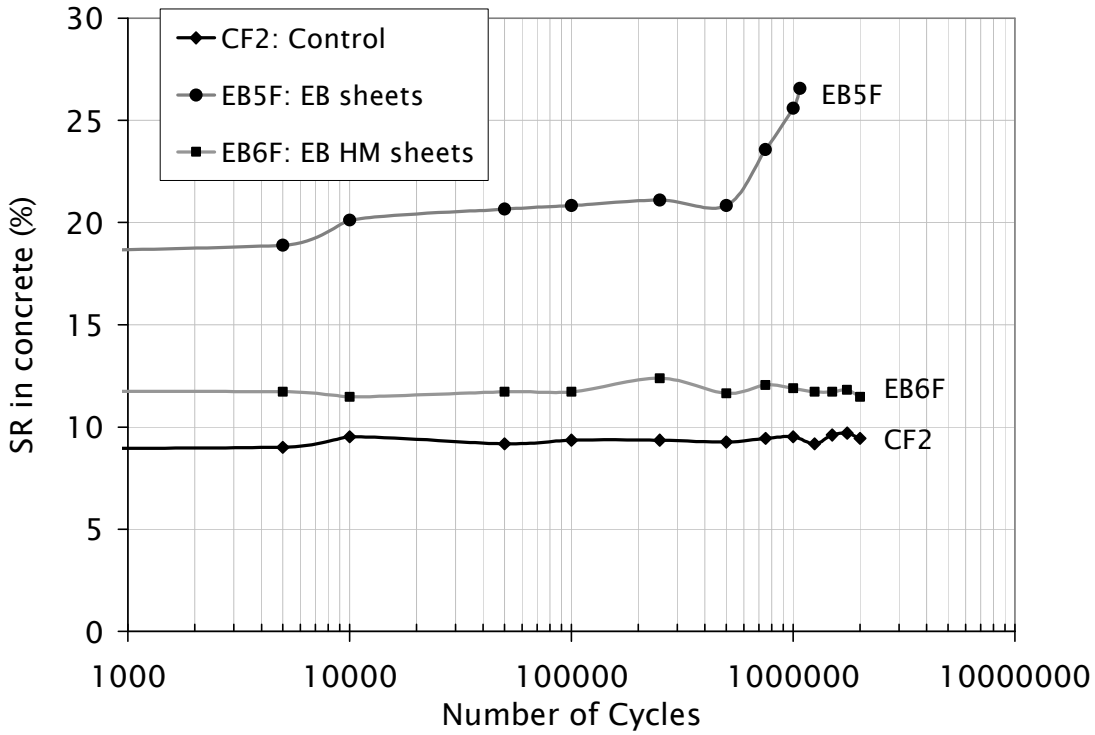

Figure 5.26 Stress ratio in extreme compressive fiber of concrete versus number of cycles for Type II girders

Stress Ratio in FRP – The stress ratio in the CFRP for the Type II girders tested in fatigue was determined from Equation 5.11 and is plotted versus the number of cycles in Figure 5.27. The large increase in stress ratio for girder EB5F, corresponding to initiation of rupture of the inclined prestressing wires is evident in the figure. The high modulus material in girder EB6F showed very little change in the applied FRP stress ratio over time.

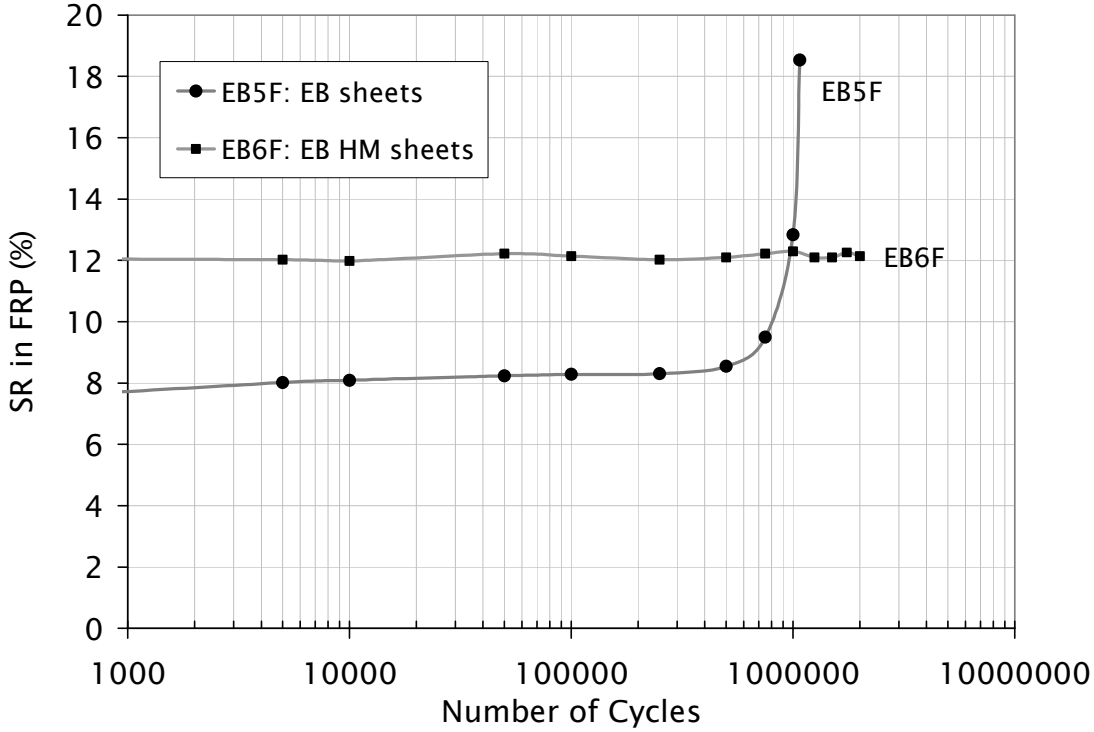

Figure 5.27 Stress ratio in FRP versus number of cycles for Type II girders

Residual Strength – After 2 million cycles of loading equivalent to a 15.4 percent increase in live load above AASHTO HS-13 type loading, the control girder, CF2, was tested statically to failure and used as a control girder for the Type II girders.

A final static test was performed on girder EB5S after rupture of a prestressing strand, and the catastrophic failure in this case was due to debonding of the CFRP sheets. The loss of prestressing reinforcements in the web placed an increased load demand on the CFRP system and caused debonding rather than rupture of the CFRP sheets due to the increased curvature of the beam at high load levels.

Girder EB6F experienced little degradation after completion of 2 million cycles of fatigue loading. Failure was due to rupture throughout the five layers of high modulus CFRP at the edge of a U-wrap provided near midspan. The ultimate load achieved was 11.6 percent less than an

equivalent girder tested under static loading conditions (EB5S). The measured tensile strain at rupture for girder EB6F was 0.24%, lower than the 0.26% observed in the static test. This difference could be due to the effect of fatigue loading on the high modulus material; although misalignment of the fibers could also have caused this modest decrease.

5.6 AASHTO Girder Test

Load Displacement Hysteric Response – The applied load versus midspan displacement relationship for the fatigue loading ranging between the load values 18.7 k to 45.2 k (83.2 kN to 201.1 kN) for the repaired AASHTO girder is shown in Figure 5.28. The girder survived 2 million cycles with very little degradation or crack propagation in the repaired region after the initial cycles. Fatigue creep of concrete (ACI 215 1997) caused small amounts of displacement degradation totaling 0.11 in (2.8 mm) after 2 million cycles of loading. No stiffness degradation in the girder was observed after 2 million cycles of fatigue loading.

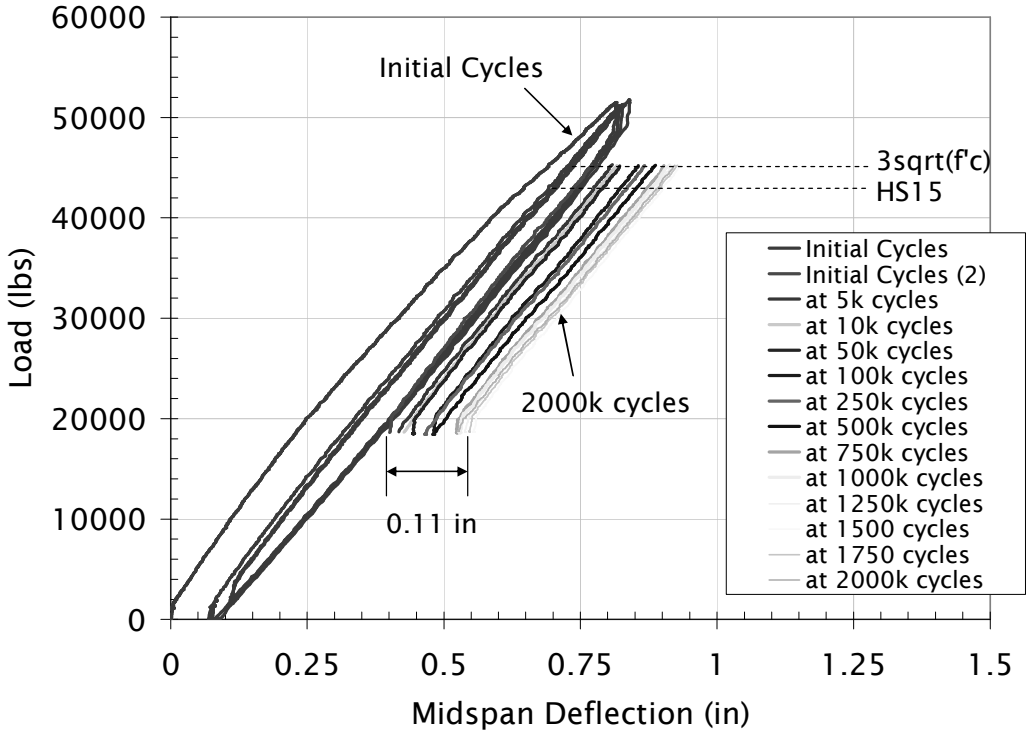

Figure 5.28 Load versus deflection for repaired AASHTO girder under fatigue loading

Stress Ratio in Lower Prestressing Strand – Due to the impact damage imparted on the AASHTO girder and the concrete restoration process, a good estimate of the effective prestress force in the prestressing strands was difficult to obtain. Using an estimate of prestress losses of 24.0 percent calculated using the AASHTO specification (2004) lump-sum method, the stress ratio in the lower prestressing strands at midspan was determined using the procedure outlined in Section 5.5.2 and found to be 1.7 percent. The stress ratio in the lower prestressing strands was also determined using a Response 2000© analysis and was found to be 2.6 percent, slightly higher than the observed value. It should be noted that all of the prestressing strands were straight in the AASHTO test girder. Previous work demonstrates that fatigue rupture of prestressing strands is rare at such low stress ratio values in straight prestressing strands (Naaman 1991, Collins & Mitchell 1991) therefore no degradation was observed after completion of 2 million cycles, as shown in Figure 5.29.

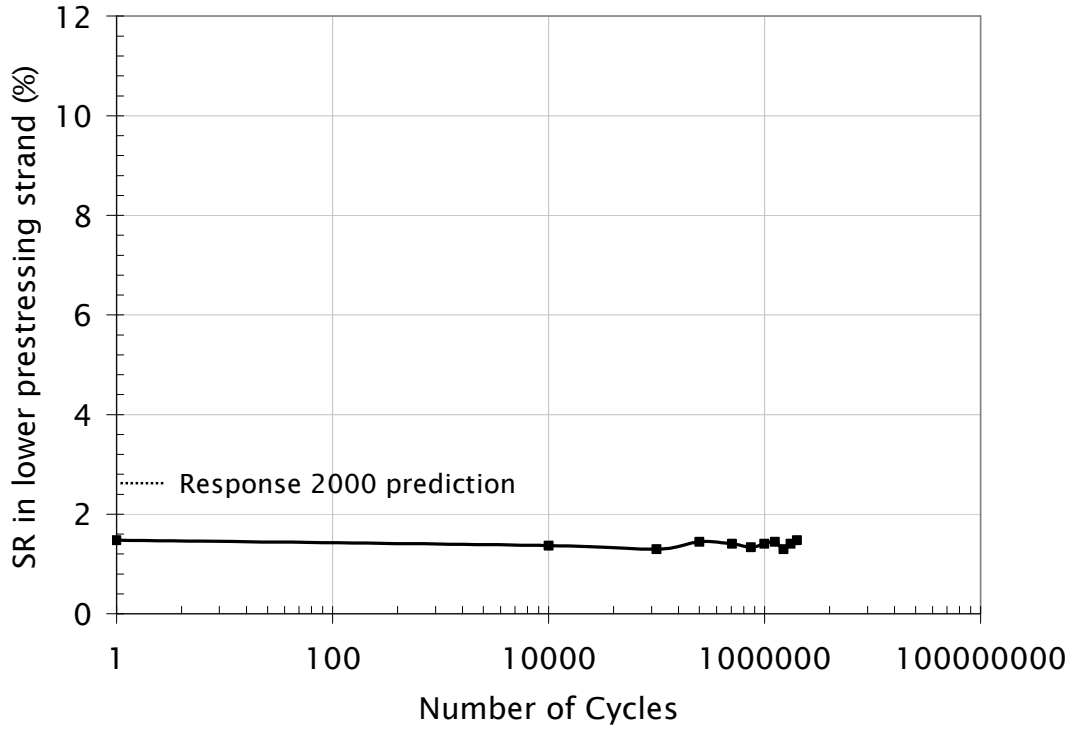

Figure 5.29 Stress ratio in lower prestressing strand versus number of cycles for repaired AASHTO girder

Final Static Test – A full description of the final static test on the repaired AASHTO girder is provided in Section 4.6. Flexure-shear cracks which initiated outside the termination point of longitudinal CFRP in the undamaged region propagated in an inclined fashion towards the compression zone and eventually caused failure of the girder near midspan. Test results indicated that the presence of the main longitudinal CFRP in the configuration shown in Figure 4.3 significantly increased the flexural capacity of the damaged zone of the girder causing the failure outside this region. The presence of the tension-strut CFRP reinforcement and transverse U-wraps controlled crack propagation within the damaged zone as well as enhancing the shear capacity of the strengthened section. The overall behavior of the repaired girder far exceeded the predicted strength of the undamaged girder in both strength and ductility, as shown in Figure 5.30.

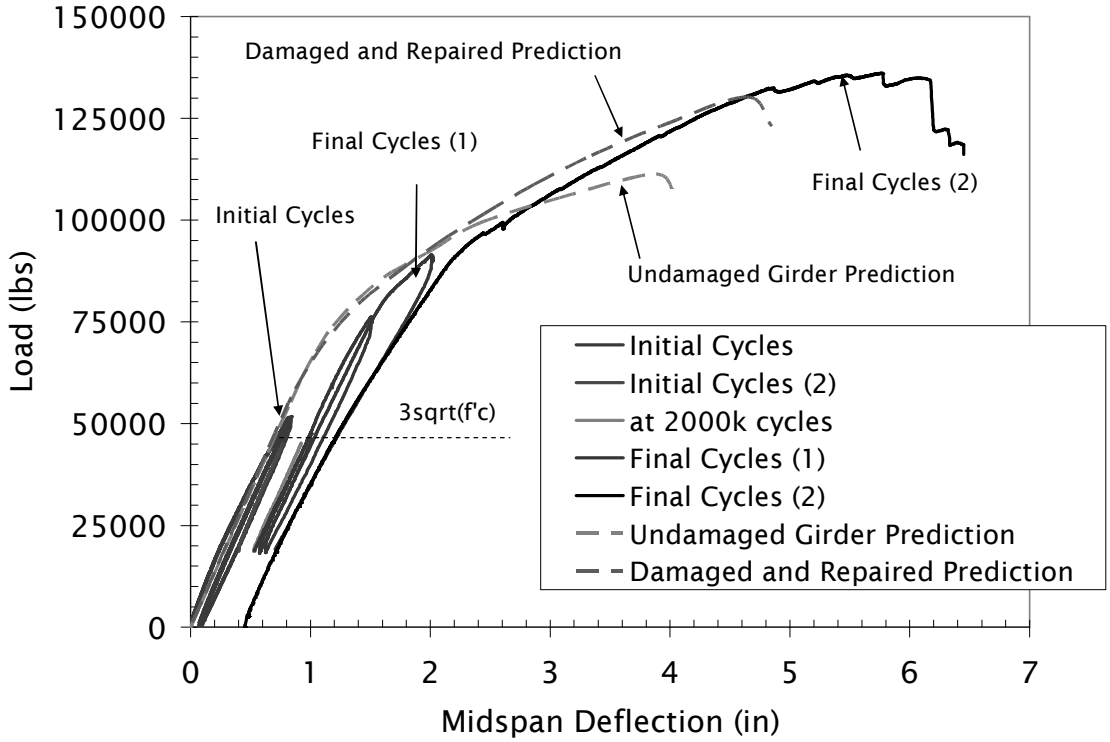

Figure 5.30 Load versus deflection during final cycles for repaired AASHTO girder

The tensile strains in the repaired AASHTO girder during the final static test measured from various PI gauges is shown in Figure 5.31. Several items that should be noted in the figure include:

1) Residual tensile strains in the CFRP of 0.07 percent can be seen in the repaired region after the fatigue cycling due to crack opening and aggregate interlock in the restored concrete.
2) Flexural cracks first formed at the undamaged section at an applied load of 94.4 k (420 kN).
3) The stiffness of the damaged region and the undamaged region were almost the same after flexural cracking occurred in the undamaged region.

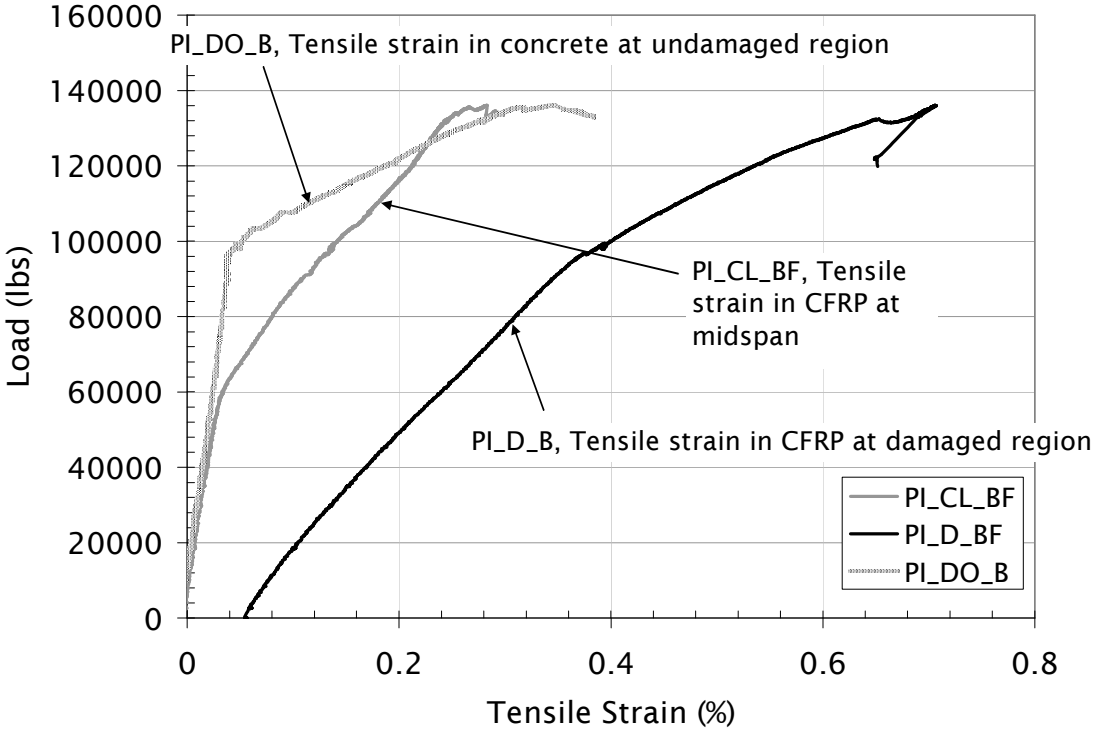

Figure 5.31 Load versus tensile strain during final static test of repaired AASHTO girder

Experimental v. Predicted – A prediction using Response 2000© (see Section 5.1) was performed on the undamaged girder as well as the repaired girder, and is shown with the experimental results in Figure 5.31. Due to the difficulties in assessing the cracking load of the girder, the value for effective prestress used was determined from calculations (AASHTO 2004). In the analysis, the following scenarios were included: 1) All the longitudinal CFRP was modeled (including tension strut CFRP reinforcing), 2) A prestressing strand on the bottom layer was removed and considered to be ineffective throughout the length of the girder, and 3) One average value for the width of the composite deck of 14.9 in (379 mm) was used in the analysis in spite of the fact that the width varied throughout the length of the girder.

Response 2000© predicted concrete crushing failure for the damaged and repaired girder at an applied load of 130.4 k (580 kN) which corresponds well to the measured load at failure. The measured ultimate load was 22.2 percent higher than the ultimate load predicted for the undamaged girder.

6 COST-EFFECTIVENESS AND VALUE ENGINEERING

6.1 Introduction

One of the major research goals is to provide the NCDOT Bridge Maintenance Department a complete evaluation including a cost-effectiveness and value engineering analysis of different FRP repair and strengthening techniques. Each FRP system was thoroughly analyzed to provide a comparison among the different techniques used in this study. It shall be noted that since the research project has been granted an extension for one year for further study, the analysis presented in this chapter can be considered a full evaluation only alongside the future report. In spite of the fact that the near surface mounted strengthening technique has proven to be the most structurally efficient (see Section 5.4.2), the preliminary findings show that the most cost-effective systems are the ones which use externally bonded CFRP sheets. Aspects considered in the value engineering analysis corroborate these findings.

6.2 C-Channel Strengthening

6.2.1 Cost Analysis

To closely resemble field conditions, the girders were placed side by side, as they would be on a bridge, on top of a steel substructure provided by the Department of Bridge Maintenance approximately 8 ft (2.5 m) off the ground. The strengthening of the girders began in the winter of 2004 when temperatures at night dropped below recommended values for curing of the epoxy by the manufacturer. Therefore a plastic enclosure and a propane heater were provided to increase the surrounding temperature. This cost was assumed to be similar for all types of bridges repaired under these conditions and was not included as a parameter in the analysis.

To determine the cost-effectiveness of each strengthening technique, the following items were considered: (1) labor costs of the professional FRP applicators, (2) time taken to complete all tasks, (3) material costs, (4) equipment used for strengthening. The material costs include all primers, adhesives and CFRP required for field application for each technique. Equipment items include the rental of sandblasting pot, compressor, sand, and the special diamond bit saw blades used for cutting of the grooves for the NSM strengthened girders. Also included in the equipment cost are items such as latex gloves, Tyvek© suits and plastic mixing buckets. For the externally bonded sheet systems, installation involved the use of paint rollers – so these are included. All other equipment (such as grinders, mixers, safety equipment, etc) is either assumed to be provided by the contractor or used equally in each of the strengthening systems. A summary of the labor tasks and time required for the installation of each of the strengthening systems is provided in Table 6.1. The results of the cost-effectiveness analysis are shown in Table 6.2. The labor costs were determined using a wage of $45 per hour. Consultation with several FRP installers produced this value which is commonly used for cost estimation in FRP strengthening work. Although both strengthening systems using high modulus material (EB3 and EB6) did not achieve the desired level of strengthening, the girder EB3S was not included in the cost-analysis because of a difficulty in determining the cost of the material, which changed substantially after the discrepancies were addressed in the manufacture of the laminate.

Table 6.1 Labor Summary for C-Channel CFRP strengthening systems (in hours)

System Designation	NSM1	NSM2	EB1	EB2	EB4	EB5	EB6
Strengthening	NSM bars	NSM strips	EB strips	EB sheets	EB sheets	EB sheets	EB HM sheets
Gluing Strips	--	1	--	--	--	--	--
Concrete Repair	0.95	0.95	0.95	0.95	0.95	1.5	1.5
Groove cutting	5.5	5.5	--	--	--	--	--
Grinding / chipping	5.5	5.5	4	2	3.75	2	2
Sandblasting	0.3	0.3	0.93	0.93	0.75	0.5	0.5
Cutting of fiber	--	--	0.5	1	1.59	1.75	2.25
CFRP lay-up	5.63	5.63	10	8.75	11.59	9.95	14.3
Total hours / girder	17.88	18.38	13.88	13.63	18.63	15.70	20.55
Total hours / ft*	0.66	0.68	0.51	0.50	0.69	0.58	0.76

* length of strengthening = 27 ft (8.23 m)

Table 6.2 Cost-Effectiveness Analysis for C-Channel CFRP Strengthening Systems (in US dollars)

System Designation	NSM1	NSM2	EB1	EB2	EB4	EB5	EB6
Strengthening	NSM bars	NSM strips	EB strips	EB sheets	EB sheets	EB sheets	EB HM sheets
Main CFRP / ft	8.45	6.42	65.45	3.42	6.14	8.18	16.16
CFRP U-wraps /ft	--	--	3.34	3.34	3.76	3.34	3.17
Main adhesive /ft	7.43	7.43	4.24	1.49	Included	3.58	7.46
U-wrap adhesive /ft	--	--	1.47	1.47	above	1.46	1.46
Equipment / ft	3.54	3.54	3.39	3.85	3.85	3.85	3.85
Labor / ft	30.44	31.28	23.71	23.29	31.70	26.79	35.07
Total cost / ft	49.85	48.66	98.85	36.85	45.46	47.21	67.17
% increase in strength*	22.9	22.6	19.3	10.5	60	72.8	5.3
Cost-Effectiveness**	0.459	0.464	0.195	0.285	1.320	1.542	0.079

* for girders tested under static loading condition

** based upon (percent increase in strength) / (total cost per meter)

The cost analysis indicates that the most cost-effective system, when comparing the variables described previously and combined with the percent increase in strength, were the girders which were strengthened using normal modulus CFRP sheets (systems EB4 and EB5). The NSM systems also performed well using these criteria. The only system with poor cost-effectiveness was the externally bonded CFRP strips used for girders EB1S and EB1F, due to the high costs of the CFRP material.

When CFRP was used to increase the ultimate flexural capacity by 20 percent (NSM1, NSM2 and EB1), the labor required for installation of a NSM system was substantially higher than for installation of an externally bonded system at the same strengthening level. If a NSM system was used to strengthen a girder by 60 percent, an appropriate increase in labor costs would be noted, most likely much higher than for the two systems strengthened to that level or higher with externally bonded CFRP sheets (EB4 and EB5).

The difference in labor costs between EB5 (EB Sheets) and EB6 (EB HM Sheets) should be noted. Although the girders strengthened with system EB6 had more material, it wasn't only the amount of material that caused in increased labor costs. The contractors also said that the material itself was harder to work with and install than equivalent normal modulus CFRP sheets.

6.2.2 Value Engineering Analysis

Various items were considered in the strengthening of C-Channel girders from a value engineering perspective. The cost analysis cannot be used in a stand alone manner in deciding which CFRP strengthening system to apply. Many aspects particular to a certain project or design problem could lead to a decision making the use of certain systems unfeasible. The ability to provide guidance and forethought to the design problem from an engineering viewpoint is the goal of the value engineering analysis.

One of the most important items that need to be considered prior to strengthening a C-Channel bridge is the condition of the bridge. The research team visited four C-Channel bridge sites in the course of the research. All bridges consisted of two simply supported spans with C-Channel girder superstructure systems.

Figure 6.1a Corrosion of bearing plate at support

Figure 6.1b Typical timber substructure

Figure 6.1c Concrete spalling repair

Figure 6.1d Corrosion of lower prestressing strand

Figure 6.1 C-Channel bridge conditions

Fiure 6.1a is from Bridge 70 in Catawba County, NC. Figure 6.1b and 6.1c are from Bridge 43 in Carteret County, NC. Figure 6.1d is from Bridge 14 Pamlico County, NC.

From limited observations and from information given in the literature it can be concluded that some common problems encountered at C-Channel bridge sites are: 1) corrosion of lower prestressing strands near midspan resulting in longitudinal cracking and spalling (shown in Figure 6.1d), 2) corrosion of the bearing plate at the support, resulting in spalling of concrete around bearing region (shown in Figure 6.1a), 3) shear cracks extending from area near support into the deck and 4) cracking of deck near midspan as a result of incorrect lifting maneuvers during original girder installation. In addition to these items observed with the superstructure elements, various other poor conditions can be found in the timber substructure (Figure 6.1b). Since strengthening may increase the posted capacity of the bridge, the timber substructure must be carefully evaluated to ensure that these increased loads do not lead to poor performance or deterioration. Therefore it is highly recommended to monitor the structural performance of any bridge strengthened using CFRP systems, especially the timber substructure. It is also essential to evaluate the efficiency of the timber substructure prior to installation of any strengthening technique.

The condition of the C-Channel girders may also lead to the use of particular systems which may be more effective. If the soffits, or webs, of a girder span have spalled concrete over a substantial length on either side of midspan, the use of NSM systems could be problematic. If the concrete is damaged in the cover concrete below the lower prestressing strand, corrosion treatment of the strands and careful restoration of the concrete section should be performed prior to installation of the CFRP system. In the case of significant concrete damage, NSM systems may not be the best systems because of a danger of debonding failures despite their structural efficiency. An externally bonded system, with sufficient transverse CFRP U-wrap reinforcements would be the most effective choice.

It should be noted for C-Channel girders: even if the condition of the soffits is good, spalling of concrete may occur during the groove cutting process. If the two-bladed saw typically used for this purpose becomes slightly off-center, the groove could extend towards the edge of the soffit and spall off the concrete. This incident occurred numerous times during the installation process, since the width of the C-Channel soffit was only 2.5 in (63.5 mm) and the width of the groove is 0.75 in (19 mm). One of the reasons the concrete saw bounced off the groove line was because of the presence of regular steel reinforcing stirrups which extended farther down than was specified on the plans. In some cases these stirrups were exposed at the bottom of the C-Channel girder, which had lead to corrosion in the stirrups and in the lower prestressing strand. Installation of a NSM system would be much more difficult if the bridge had many of these exposed stirrups which are in the region reserved for the NSM groove.

The width of the soffit may also control the configuration and level of strengthening since the geometry of the groove and width of the soffit often dictates the amount of NSM strengthening – whereas with externally bonded sheets an increase in ultimate load capacity of 73 percent was reached by increasing the number of sheet layers. The 20 percent increase in ultimate capacity was achieved using the NSM configurations; strengthening beyond this level was not feasible because of the width of the soffit.

Strengthening using NSM systems could be extremely useful and effective for increasing the negative moment capacity for continuous span bridge decks located over the supports since many grooves can be cut efficiently in the concrete deck and the CFRP bars or strips inserted inside. For similar reasons, the strengthening of one-way slabs using NSM systems can be very effective (Hassan and Rizkalla 2002a).

Since all the strengthening work was performed under simulated field conditions, an evaluation of the difficulty of overhead installation can be made. Cutting of the NSM with the saw overhead can be a challenging task. If large numbers of girders are being strengthened using a NSM system, a guidance system should be constructed to locate the groove cutting in the correct position and to alleviate the weight burden on the installer. The easiest and simplest system to install overhead was the externally bonded strips. The installation of externally bonded sheets systems was slightly more challenging due to the need to apply pressure to the saturated sheets to ensure good adhesion.

Installation of the systems using externally bonded strips were the most straightforward among the various systems considered in this investigation. In light of the possible debonding problems that could be encountered in this system, as well as the high cost of the material, it might not be the most effective solution to strengthening girders of this type. In addition, in order to control debonding of the CFRP plates, transverse CFRP U-wrap sheets are highly recommended.

The high modulus (HM) CFRP material, installed as either strips or sheets, are not the most effective material due to their limited ultimate strain capacity. Due to their brittle characteristics, handling and installation of the material requires careful attention to transportation and handling which increases the overall cost associated with this strengthening system.

Due to the fact that C-Channel type bridges typically span small streams and estuaries, the impact of a repair using CFRP must take into account its effect on the environment. It is recommended that the mixing of all the materials used in the repair be performed at a flat location away from streams and other environmentally sensitive areas due to the undesirable

environmental problem which could occur due to a possible spill. Each of the strengthening systems in this investigation has their own set of drawbacks for the environment that may need to be considered in the selection process. The NSM systems use the least amount of adhesive during installation and therefore may be the safest option. However, it is recommended to isolate the superstructure of the bridge during cutting of the grooves required for the NSM system to prevent large quantities of concrete dust being released into the surrounding areas. Special precaution should be taken when mixing and applying the various primers, bonding agents and adhesives used in a wet lay-up type repair to prevent site contamination and health concerns. Safety precautions and environmental guidelines published in the recent NCHRP document (Mirmiran et al 2004) should be followed.

6.3 AASHTO Repair

6.3.1 Cost Analysis

The cost analysis of the repair of the AASHTO girder was similar to the C-Channel cost analysis since the installation of the CFRP repair system was carried out in a similar manner. All materials involved in the concrete repair and restoration were included: the concrete repair mortar, rust inhibitors, epoxy injection cost and the cost of the materials involved in the building of formwork.

At the site, a plastic enclosure was used and heated to provide comfort for the contractors and providing adequate curing temperatures for the adhesive. An equipment charge that was believed to be relevant for inclusion in the cost analysis was the rental of the sandblaster, sandblasting pot, compressor and sand. In addition, items such as Tyvek© suits, plastic gloves, mixing buckets and plastic rollers were also included. Items such as grinders, safety equipment

and mixers were not included as it is assumed that their cost is covered by the contractors. Since the goal of the project in this case was to restore the original capacity of an undamaged girder, the cost-effectiveness cannot be evaluated. However, since the repair was successful in achieving its goals, the labor summary shown in Table 6.3 and the cost analysis shown in Table 6.4 could be of use and beneficial as an estimate of the expenses involved in a repair of this type. It should be noted that the labor cost per meter and total cost per meter should be used carefully because the actual length of repair depends on many different factors including the amount of concrete damage and number of ruptured prestressing strands.

Table 6.3 Labor Summary of CFRP Repair of AASHTO Girder (in hours)

Task Description	AASHTO1
Chipping damaged concrete	4
Applying rust inhibitors	2.5
Constructing and installing formwork	3.2
Pouring concrete	19.83
Epoxy injection	5
Grinding	20
Sandblasting	9
Cutting fiber	3
Installing all longitudinal CFRP reinforcement	15
Installing U-wrap CFRP reinforcement	12
Total hours / girder	93.53
Total hours / ft*	3.23

* length of repair = 29 ft (8.84 m)

Table 6.4 Cost-Effectiveness Analysis for CFRP Repair of AASHTO Girder (in US dollars)

System Designation	AASHTO1
Repair system	EB CFRP sheets
Repair Mortar	500
Rust Inhibitors	60
Epoxy Injection	700
Formwork Materials	100
Main Longitudinal CFRP	456
Tension strut CFRP	391.5
CFRP U-wraps	564
Equipment	265.5

Labor total ($45/hour)	4208.85
Total cost	7245.85
Total cost / ft*	249.9

* length of repair = 29 ft (8.84 m)

In the repair of the AASHTO girder, the time required to restore the concrete section (34.53 hrs) was substantially less than the time required to install the CFRP repair system (59.00 hrs). The cost of the main longitudinal CFRP reinforcement was only 32 percent of the total cost of the CFRP material, the remaining material being used for transverse U-wraps and tension struts – representing the importance of proper detailing.

At this stage of research, information is not available to provide comparisons between different repair systems or levels of repair work. The approved project extension (NCDOT Project 2006-10) may provide and confirm the above cost analysis since the project includes the repair of four additional impact damaged AASHTO Type II girders.

6.3.2 Value Engineering Analysis

Most of the findings presented in the value engineering analysis for the C-Channel girders in Section 6.2.2 strengthened with externally bonded CFRP wet lay-up systems are applicable for the repair of the AASHTO girder. Some other items specific to the AASHTO girder repair are discussed below.

In some cases, where the impact damage occurs near the supports, the desired length of development of CFRP sheets beyond the damaged region may not be possible. It would be recommended to provide for additional anchorage systems in this instance. Barnes and Mays (1999) have described a mechanical anchorage detail for CFRP plates which could be adapted for this purpose. The research team will study this problem as part of the project extension where one AASHTO Type II girder will be damaged near the supports and repaired using CFRP sheets.

In order to restore the original serviceability after an impact event resulting in a loss of prestress, the girder may have to have additional prestressing added – either in the form of external post-tensioning, splicing of the ruptured strands or application of prestressed CFRP sheets. The original ultimate capacity of the girder can be restored by repair using CFRP sheets.

Although the examination of different types of CFRP repair for impact damaged AASHTO girders is not being explored in the project extension, with a greater number of CFRP repair systems under field conditions, a better understanding of aspects related to value engineering can be obtained.

7 DESIGN GUIDELINES

7.1 Introduction

This chapter provides general design guidelines which should be followed in the design and construction of CFRP strengthening or repair systems for prestressed concrete bridge girders. In addition to the proper selection of CFRP material and appropriate adhesive, the performance of the CFRP system is highly dependent on the method of installation. In the design of a CFRP system to regain lost strength due to loss of reinforcements or strengthening the girder to increase the strength of a bridge member, the following structural design recommendations should be considered by the bridge maintenance engineer. The guidelines include selection of an appropriate system, selection of the required flexural reinforcement, and providing appropriate detailing to prevent debonding type failures and to achieve full utilization of the system. The design guidelines also address proper surface preparation and installation procedures.

7.2 CFRP Repair and Strengthening Systems

7.2.1 Carbon Fiber Reinforced Polymer (CFRP) Materials

Carbon Fiber Reinforced Polymer (CFRP) materials consist of carbon fiber filaments embedded in an adhesive matrix. There are various types of CFRPs that are commonly used for structural strengthening of concrete members including pre-cured laminates and wet lay-up systems.

Pre-cured laminate CFRPs are normally available commercially in the form of a bar or strip. The pre-cured laminate is manufactured by impregnation of carbon fibers with adhesive, which is then pultruded and cured by the manufacturer. The controlled environment used in

manufacturing of the pre-cured laminate can create laminates which are stronger and stiffer per unit volume than equivalent wet lay-up laminates.

The laminates typically used for concrete strengthening are unidirectional and have all of the fibers oriented in the longitudinal direction. A laminate can come in various shapes and sizes. A typical pre-cured laminate is shown in Figure 7.1.

Figure 7.1 A CFRP pre-cured laminate strip

An externally bonded wet lay-up system consists of a carbon fiber sheet which is typically field impregnated with a structural adhesive. A unidirectional carbon fiber sheet consists of bundles of carbon fibers held together by thin pieces of plastic material. Carbon fiber sheets typically come in rolls 24 in by 300 ft (610 mm by 91.4 m). Typical properties of CFRP pre-cured laminates and wet lay-up systems are presented in Table 3.5.

7.2.2 Adhesive

Adhesives, or epoxies, are used to bond the CFRP material to the concrete surface. The tensile strength and flexural strength of the adhesive are typically much higher than the shear strength of the concrete. Therefore, most of the failures occur within the concrete substrate during a debonding type failure. The adhesives are typically shipped to the site in two-parts and mixed at the site. There is quite a difference between the adhesives used during a wet lay-up type application, where the dry fiber CFRP filaments are field impregnated with the adhesive, and an installation of near surface mounted (NSM) CFRP or externally bonded laminates, where the adhesive is bonding a pre-made CFRP to the concrete. The different types of adhesives used in

the strengthening of the C-Channels are given in Table 3.4. The adhesive used for the CFRP repair of the AASHTO girder was a Tyfo© Type S two part structural epoxy. The manufacturer of the pre-cured laminate or wet lay-up system is required to supply the appropriate adhesive to match the CFRP material being used.

7.3 Installation Recommendations

Proper installation of the CFRP system is essential in ensuring the performance desired by the designer. Correct techniques must be employed from the surface preparation to the application of the final protective coating, to ensure effective behavior of the CFRP system. The recommendations provided in this chapter are based on the sizeable experience gained by conducting this research, as well as state-of-the-art installation procedures and guidelines found in the literature (Mirmiran et al 2004, JSCE 2001, The Concrete Society 2004). Use of experienced contractors to perform the installation is essential and required for the proper installation of the system.

Proper scheduling of any repair or strengthening operation using CFRP is essential. Typical repair projects require preparation of the surface, protection of the exposed steel reinforcement, and restoration of the concrete section which calls for a two-part mortar to be properly cured. The application of a CFRP system is also highly time dependent, including the use of a two-part structural epoxy with a specific pot-life. When using proper materials and techniques, a CFRP installation can take less time compared to a conventional repair or strengthening operation, and far less time than total bridge or girder replacement.

7.3.1 Shipping, Storage and Handling

FRP materials, in particular pre-cured laminates, should be shipped in impact resitant containers. All components of the FRP system must be stored properly in clearly marked containers in ambient temperatures 50-75° F (10-24° C). The shelf life of the FRP system components should be specified by the manufacturer and marked on containers.

Correct handling of components of the FRP system is important to prevent damage or fiber misalignment. After cutting of CFRP sheets, it is recommended that the sheets are rolled at a radius no tighter than 12 in (305 mm) (Mirmiran et al 2004). This is especially important for CFRP sheets made of a high modulus material. Rolling of high modulus CFRP pre-cured laminate strips is not recommended.

7.3.2 Section Restoration

The restoration of a damaged prestressed concrete section can be a large task involving formwork and shoring or simply routine patching of lost cover concrete in the region below the lower prestressing strand. Before beginning restoration, all defective concrete should be removed in accordance with ACI 546 (1996) using an appropriate jack-hammer or electric saw, to a depth of ½ in (13 mm) beyond the repair area in order to expose sound aggregates.

Prior to application of the concrete repair material, the condition of the regular reinforcement and prestressing needs to be carefully evaluated. Discovery of corroded prestressing strands was found in some of the C-Channel bridges as discussed in Section 6.2.2. In the flexural design of a CFRP strengthening system, it might be required to reduce the area of the prestressing strands in response to corrosion damage. To prevent further corrosion, application of a corrosion inhibitor is highly recommended.

Cementitious, epoxy-modified products such as Sika Armatec© 110 EpoCem acts as an anti-corrosion coating in addition to a bonding agent for repairs to concrete and steel. An alternative, the two layer spray-on corrosion inhibitor Tyfo© CIS can be used for restoration of the strands.

Figure 7.2 Application of corrosion inhibitor

Selection of the correct material to use in concrete repair is important. The repair material should have a compressive strength equal to or greater than the original concrete. Small areas of damage may be repaired with the same adhesive used in CFRP installation, and can be thickened by mixing with silica sand material. Any concrete voids larger than ½ in (13 mm) in diameter, should be repaired with an appropriate two-component polymer modified cementitious mortar. For overhead patching work, to be used in lifts of 1 to 2 in (25 to 50 mm), the material Tyfo© P or SikaTop© 123 Plus is recommended. For large areas of concrete damage, where some amount of formwork is needed, the material Tyfo© PF or SikaRepair© 222 can be used in lifts up to 4 in (102 mm).

One technique recommended by Shanafelt and Horn (1980) and Klaiber et al (1999) is to preload the bridge span with an appropriately sized truck during the concrete repair and curing. Once the truck is removed, this simple procedure can induce compressive stresses in the repaired concrete within the impacted region.

7.3.3 Surface Preparation

Once the engineer has approved the concrete repair and restoration, the surface preparation of the section may begin. The importance of a flat, smooth or convex surface is paramount in the performance of a FRP system to provide good bond characteristics and to prevent irregularities in the FRP from forming.

Surface grinding should be performed on the concrete surfaces on which the FRP system will be applied, eliminating "all irregularities, unevenness and sharp protrusions" (Mirmiran et al 2004). All surface paint, sealant or any other surface substance should be removed using a disk grinder.

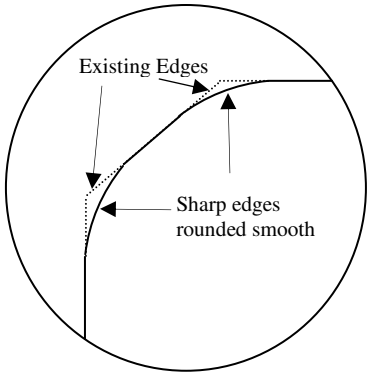

Figure 7.3 Chamfering Corners (adapted from Mirmiran et al 2004)

All sharp corners should be rounded to a minimum radius of ½ in (13 mm) (ACI 440R-02). All surface cracks in concrete larger than 0.01 in (0.25 mm) should be injected with epoxy.

The size of the groove used in NSM applications should be specified on the design specifications. For NSM bars, the width and depth of the groove should be twice the bar diameter (Hassan 2002b). For NSM strips, the width of the groove should be approximately 3 times the width of the strip, and the height 1.5 times the width of the strip (Sena Cruz and Barros 2004).

Figure 7.4 Cutting of NSM groove

An electric saw with two diamond bit blades aligned to the correct width and depth should be used for cutting of NSM groove, as shown in Figure 7.4. After the two saw cuts are made, the concrete within the cuts can be removed using an electric chipper. Groove cutting for NSM systems should take care not to fracture any of the surrounding concrete. If concrete becomes damaged it may be repaired with structural two-part epoxy mixed with sand or an appropriate material.

For externally bonded CFRP system, surface cleaning of the concrete substrate after surface grinding is important in order to remove all dust and to open the pores of the concrete to guarantee good adhesion between the concrete and CFRP system. Sandblasting using Black Beauty© abrasive sand on all surfaces to be applied with CFRP is recommended. For NSM systems, sandblasting of the interior surfaces of the groove is recommended, although cleaning of the inside of the groove with compressed air or similar is sufficient.

7.3.4 NSM CFRP System Installation

The installation of a NSM system is straightforward. The adhesive should first be mixed in the appropriate ratios using an electric mixer for the specified duration in ambient temperatures specified by the manufacturer. The CFRP bar or strip should be cut to the specified length, cleaned and placed at mid-depth of the NSM groove.

Figure 7.5 NSM bar in groove

The bar should then be lightly pressed to allow the adhesive to flow around the bar/strip cross section. The groove shall then be completely filled with additional adhesive and the surface leveled.

7.3.5 Externally Bonded Pre-cured CFRP Laminate Installation

The installation of an externally bonded CFRP pre-cured laminate should begin by cutting the laminate to the specified dimensions and cleaning the CFRP surface. The adhesive should then be mixed in the appropriate ratio using a suitable electric mixer for the specified duration at ambient temperatures specified by the manufacturer.

Using an adhesive bed, or guide is the best way to apply the adhesive to the CFRP laminate surface. The strip is placed longitudinally in the bed and the adhesive placed on one side of the metal plate. When the strip is pulled though the bed, a thin layer of adhesive is deposited on the CFRP strip in a triangular cross-section.

Figure 7.6 Adhesive bed for externally bonded CFRP laminate installation

The thickness of adhesive to be used should be specified by the laminate manufacturer. After adhesive application, the strip can be placed on the concrete substrate and pressed firmly to release entrapped air and change the dimension of the triangular adhesive cross section to a uniform thickness. Placement of clamping or shoring systems may be necessary in overhead applications for the duration of curing. After placement, the excess adhesive around the edges of the laminate should be wiped clean.

7.3.6 Externally Bonded Wet Lay-up CFRP Installation

All primers, putties and saturants should be mixed in the appropriate ratios with an electric mixer for the correct duration in ambient temperatures specified by the manufacturer.

Figure 7.7 Application of putty for wet lay-up

A primer coat is usually applied first to the concrete surface to penetrate open pores. Next, a bonding agent or putty is applied using a trowel to smooth the concrete surface and fill in small voids or gaps not adequately filled in during concrete repair and surface preparation.

The saturation of the CFRP sheets is an integral part of the installation – impregnating the fibers of the sheet within an adhesive matrix. This is best performed with a resin-impregnating machine to ensure uniform saturation, but can be performed by hand using the following procedures: 1) impregnate one side of the sheet with saturant by using a paint roller, 2) flip the sheet over and saturated the other side similarly, 3) roll up the saturated sheet and let stand until the sheet becomes slightly hot to the touch.

Once the primer and putty applied to the concrete surface have become tack-free (depends on ambient temperatures) the saturated CFRP sheet may be installed as shown in Figure 7.8. The sheet is put in place by hand and rolled in the direction of the fibers using a plastic serrated roller.

Figure 7.8 Installation of CFRP sheets

Rolling in a direction perpendicular to the fibers or with excessive force may fracture the fibers. Care must be taken to apply sufficient pressure to the sheets to release entrapped air and prevent sagging in overhead applications. Sufficient adhesive should be used around the edges of the CFRP sheets when wrapping around a soffit to prevent ponding effects.

Successive layers may be added by applying an additional layer of bonding agent or putty and installing another saturated sheet. Designs of more than five layers of CFRP wet lay-up sheets should be avoided. The manufacturer of each CFRP wet lay-up system may specify their own installation procedures that may differ slightly from the guidelines provided here.

7.4 CFRP Strengthening Design Philosophy

7.4.1 Introduction

The design of a CFRP strengthening system should begin after a desired increase in the posted capacity of a bridge has been identified by the owner. Based on the findings of this research, including an analysis of the test results from the experimental program, and analytical approaches to evaluate the effectiveness of the various parameters, a maximum increase in service load of 40 percent is recommended. A typical value of 30 percent may be adequate for most bridge girders. Once a level of strengthening has been identified, other components in the bridge system should be carefully inspected and evaluated at the increased service loads, including the precast cap beams, timber substructure and bearing plates. If the performance of the constituent bridge components are deemed satisfactory at the increased service load, the flexural design of the CFRP strengthening can proceed as outlined in the following sections.

7.4.2 Design for Flexural CFRP Strengthening

There are five criteria which need to be considered in the design of the CFRP strengthening system to increase the capacity of the bridge girder:

1) The stress range in the prestressing strands should be kept within limits specified in AASHTO Section 5.5.3.3 (2004), which for our girders is 18 ksi (125 MPa) for straight and 10 ksi (70 MPa) for harped prestressing strands. This fatigue strength design criteria controls the posted capacity for operation of the bridge.
2) The presence of the CFRP system at the extreme tension fibers of the girder will constrain crack opening and spacing, therefore the tensile stress limit specified in AASHTO code is not crucial, provided that the design satisfies the criteria related to the stress ratio in prestressing strands.
3) The increase in ultimate flexural strength should satisfy the ultimate strength requirement using the proper AASHTO (2004) specified load and impact factors.
4) The ultimate flexural strength of the unstrengthened girder should exceed the unfactored summation of dead and live loads. This criterion ensures the safety of the bridge if the CFRP strengthening system is compromised by unintentional or intentional damage, and guarantees that the bridge can operate under the increased service loading conditions with reduced serviceability.
5) Deflections and crack widths of the strengthened girder should be determined under the effect of the increased service load and held within the acceptable limits specified by AASHTO (2004).

In addition to the design criteria presented above, several detailing and specific design rules are recommended:

1) The material properties of the CFRP system should be reduced using the environmental reduction factor, C_E, specified in ACI 440F (2002), "Design and Construction of Externally Bonded FRP Systems for Strengthening Concrete Structures."
2) Transverse CFRP wet lay-up U-wraps should be provided at most 3 ft (914 mm) spacing with the appropriate length into the depth of the girder to prevent any possible debonding in externally bonded CFRP strengthened girders. In addition, U-wraps should also be provided at all termination points of longitudinal externally bonded CFRP.
3) If the engineer wishes to use externally bonded CFRP plates, the bond reduction factor, κ_m, defined in ACI 440F (2002) Article 9.2 should be used.
4) Due to the limitations of the ultimate strain of high modulus CFRP materials, they are not recommended for use in increasing the flexural strength of prestressed concrete members. However, due to their high stiffness they are recommended to enhance girder serviceability requirements.

7.5 CFRP Repair Design Philosophy

The design philosophy for repairing AASHTO girders with CFRP should follow the same criteria used in strengthening of C-Channel girders. An extension of the project, NCDOT Project 2006-10, will include the testing of additional AASHTO girders damaged due to impact load. The design guidelines for CFRP repair will be presented in the final report of the project extension.

8 CONCLUSIONS

8.1 Summary

A research project funded by the North Carolina Department of Transportation (NCDOT) was initiated to evaluate the cost-effectiveness and value engineering of various Carbon Fiber Reinforced Polymer (CFRP) repair and strengthening systems for prestressed concrete bridge girders. A comprehensive literature survey was conducted; including published research and field applications of CFRP strengthening for concrete structures. The research team completed an experimental program involving static and fatigue testing of seventeen prestressed concrete C-Channel girders strengthened with various CFRP systems and fatigue testing of an impact damaged AASHTO girder. All the CFRP systems used in the research program were evaluated to determined their cost-effectiveness and value engineering aspects of the various systems. An analytical technique was devised to aid in the design of the flexural CFRP strengthening for prestressed concrete bridge girders. Design guidelines, selection criteria and construction specifications of CFRPs for use in flexural strengthening have been recommended, as well as a means for technology transfer and future field applications with continuous structural monitoring.

8.2 Conclusions

8.2.1 Strengthening of C-Channel Girders

Based on the experimental program and analysis of the test results of the C-Channel girders, the following conclusions can be made:

1) Proper design and installation of a CFRP strengthening system can lead to the failure mode of crushing of concrete in the compression zone, preserving the ductile structural response of the unstrengthened girders.
2) Externally bonded CFRP sheets are the most cost-effective strengthening technique and are the most applicable technique for these types of girders.
3) The most structurally efficient strengthening technique used is the near surface mounted (NSM) CFRP bars or strips system.
4) The ultimate flexural capacity of prestressed concrete can be increased substantially using CFRP materials. The flexural capacity of the C-Channel girders tested in this research program could be increased by as much as 73 percent with the use of externally bonded CFRP sheets.
5) The use of transverse CFRP U-wraps delayed debonding failures in externally bonded CFRP systems.
6) For externally bonded CFRP wet lay-up systems, the experimental tensile strain in the CFRP outperformed the manufacturer's provided value. Therefore, the use of a bond reduction coefficient, κ_m in ACI 440F 2002, would be very conservative.
7) The crack spacing and crack widths at ultimate can be substantially reduced using CFRP strengthening. Crack widths observed during the testing of the C-Channels were reduced by as much as 400 percent using CFRP materials in comparison to the unstrengthened girder.
8) The initial and secondary stiffness of C-Channel girders can be increased by the use of high modulus CFRP materials. Using strictly a serviceability criterion, high modulus CFRP materials outperformed the normal modulus CFRP materials.

9) Strengthening using CFRP materials can reduce the stress ratio in the prestressing strands due to their effectiveness in controlling crack widths and increasing the overall stiffness.

10) The most fatigue critical component in a CFRP strengthened prestressed concrete bridge girder are the prestressing strands. The level of the induced stress ratio in the prestressing strands under the effect of the increased live load, including impact factor, should be kept below limits specified in AASHTO Section 5.5.3.3 (2004), which for the C-Channel girders is 18 (125 MPa) ksi for straight and 10 ksi (70 MPa) for harped prestressing strands.

8.2.2 Repair of AASHTO Girder

Based on the experimental program and analysis of the test results of the AASHTO Type II girder, the following conclusions can be made:

1) An impact damaged AASHTO Type II girder with one ruptured prestressing strand and significant loss of concrete section can be repaired using externally bonded CFRP sheets to restore its original flexural capacity.
2) The detailing of the CFRP repair system should be carefully considered to restrain crack opening in the damaged region and to prevent debonding failures.
3) At ultimate, the section repaired with CFRP material outperformed the original section.

Due to the approval of a project extension which involves further testing and analysis of several impact damaged AASHTO girders, the conclusions above can be considered complete only in conjunction with the future report.

8.3 Future Work

Approval has been granted for an extension of the research project for one year. Items to be examined in the future research work, as approved by the NCDOT, include: 1) Evaluation of an additional technique for the strengthening of C-Channel girders and 2) Assessment of additional items in the restoration of impact damaged AASHTO girders including various levels of damage and damage locations.

RECOMMENDATIONS

The main objective of this research was to evaluate the cost-effectiveness and value engineering of various CFRP repair and strengthening systems for prestressed concrete bridge girders. As a result of the study, the following recommendations can be made:

1) When properly designed, CFRP systems are a viable, practical, and cost-effective strengthening technique that can be used to increase the live load of prestressed concrete bridge girders up to 40 percent.

2) When properly designed, CFRP systems can be used effectively as a repair technique to regain the original capacity of impact damaged AASHTO Type II bridge girders with one ruptured prestressing strand and significant loss of concrete section.

IMPLEMENTATION

This research has shown that the Response 2000© program is an accurate analysis tool adequate to design any CFRP repair and strengthening system for prestressed concrete bridge girders. Using the design recommendations presented in Chapter 7, CFRP systems are a practical and cost-effective strengthening technique. Field application of the systems using existing bridges is highly recommended. The bridge should be instrumented and structurally monitored to observe behavior under real field conditions, including environmental effects.

REFERENCES

1. Aas-Jakobsen, K., (1970) “Fatigue of Concrete Beams and Columns”, Trondheim NTH Institutt for Betonkonstruksjoner, Bulletion No. 70-1, pp. 148.

2. Adimi, R.M., Rahman, A.H., Benmokrane, B., (2000) “New Method for Testing Fiber-Reinforced Polymer Rods under Fatigue”, Journal of Composites for Construction, Vol. 4, No. 4.

3. ACI Committee 215, (1997) “Considerations for Design of Concrete Structures Subjected to Fatigue Loading (ACI 215R-74 revised 1997)”, ACI Manual of Concrete Practice, American Concrete Institute.

4. ACI Committee 440, (1996) "State-of-the-Art Report on FRP for Concrete Structures (ACI 440R-96)”, ACI Manual of Concrete Practice, American Concrete Institute.

5. ACI Committee 440F, (2002) “Design and Construction of Externally Bonded FRP Systems for Strengthening Concrete Structures (ACI 440F-02)”, ACI Manual of Concrete Practice, American Concrete Institute.

6. ACI Committee 546, (1996) “Concrete Repair Guide”, (ACI 546R-96), ACI Manual of Concrete Practice, American Concrete Institute.

7. Alkhrdaji, T., Barker, M., Chen, G., Mu, H., Nanni, A., Yang, X. (2001) “Destructive and Non-Destructive Testing of Bridge J857, Phelps County, Missouri”, MoDOT Report RDT01-002A.

8. American Association of State Highway and Transportation Officials, (2004) “AASHTO LRFD Bridge Design Specifications”, AASHTO.

9. Arduini, M., Nanni, A., and Romagnolo, M., (2002) “Performance of Decommissioned RC Girders Strengthened with FRP Laminates,” ACI Structures Journal, Vol. 99, No. 5.

10. Asplund, S. O., (1949) “Strengthening Bridge Slabs with Grouted Reinforcement”, ACI Structural Journal V.20, No. 4, pp.397-406.

11. Barnes, R.A., Mays, G.C., (1999) “Fatigue Performance of Concrete Beams Strengthened with CFRP plates”, Journal of Composites for Construction, Vol. 3, No. 2.

12. Bentz, E. C., (2000) “Section Analysis of Reinforced Concrete Members”, Ph.D. Thesis, University of Toronto, 2000.

13. Breña, S.F., Kreger, M.E., Wood, S.L., (2005) “Fatigue Tests of Reinforced Concrete Beams Strengthened using Carbon Fiber Reinforced Polymer Composites”, ACI Structural Journal, Vol. 102, No. 2.

14. Canadian Standards Association, (2000) "Design and Construction of Building Components with FRP", Canadian Standards Association Report S806-00.

15. Carolin, A. Nordin, M. and Taljsten, B. (2001) “Concrete Beams Strengthened with Near Surface Mounted Reinforcement of CFRP.” Proceedings of the International Conference on FRP Composites in Civil Engineering, Hong Kong, China, pp. 1059-1066.

16. Carolin, A. (2003) “Carbon Fiber Reinforced Polymers for Strengthening of Structural Elements”, Doctoral Thesis, Luleå University of Technology.

17. Collins, M.P. and Mitchell, D., (1991) “Prestressed Concrete Structures”, Prentice Hill, New Jersey.

18. Concrete Society, The, (2004) “Design Guidance for Strengthening Concrete Structures using Fibre Composite Materials”, Technical Report 55, The Concrete Society, United Kingdom.

19. De Lorenzis L. and Nanni, A., (2001a) “Shear Strengthening of Reinforced Concrete Beams with Near-surface Mounted Fiber Reinforced Polymer Rods”, ACI Structural Journal, Vol. 98, No. 1, pp.60-68.

20. De Lorenzis L. and Nanni, A. (2001b) “Characterization of NSM FRP Rods as Near-Surface Mounted Reinforcement,” Journal of Composites for Construction, May 2001, pp. 114-121.

21. De Lorenzis L. and Nanni, A., (2002) “A Bond Between Near-surface Mounted FRP Rods and Concrete in Structural Strengthening”, ACI Structural Journal, Vol. 99, No. 2, pp. 123-132.

22. Di Ludovico, M., (2003). “Experimental Behavior of Prestressed Concrete Beams Strengthened with FRP.” Report CIES 03-42, University of Missouri-Rolla, MO.

23. Di Ludovico, M., Nanni, A., Prota, A., & Cosenza, E. (2005). Repair of Bridge Girders with Composites: Experimental and Analytical Validation. ACI Structural Journal, 102(5), 639-648.

24. El-Hacha, R., Filho, J., Rizkalla, S., and Melo, G., (2004a) "Static and Fatigue behavior of Reinforced Concrete beams strengthened with different FRP Strengthening techniques", Proceedings of the 2nd International Conference on FRP Composites in Civil Engineering (CICE 2004), Adelaide, Australia.

25. El-Hacha, R., Rizkalla, S. (2004b) “Near-Surface-Mounted Fiber-Reinforced-Polymer Reinforcements for Flexural Strengthening of Concrete Structures,” ACI Structural Journal, Vol. 101, No. 5, September-October 2004.

26. El-Tawil, S. and Okeil, A. M. (2002) "LRFD Flexural Provisions For PSC Bridge Girders Strengthened with CFRP Laminates," ACI Structural Journal, 99(2), pp. 300-310.

27. Hassan, T., and Rizkalla, S., (2002a) “Flexural Strengthening of Prestressed Bridge Slabs with FRP Systems”, PCI Journal, V. 47, No. 1, pp. 76-93.

28. Hassan, T., (2002b) “Flexural Performance and Bond Characteristics of FRP Strengthening Techniques for Concrete Structures”, PhD. Thesis, University of Manitoba, Winnipeg, Canada.

29. Hassan T. and Rizkalla, S. (2003) “Investigation of Bond in Concrete Structures Strengthened with Near Surface Mounted CFRP Strips”, ASCE, Journal of Composites for Construction, Vol. 7, No.3, pp.248-257.

30. Hassan, T., Rizkalla, S., (2004) “Bond Mechanism of NSM FRP Bars for Flexural Strengthening of Concrete Structures”, ACI Structural Journal, Vol. 101, No. 6, November-December 2004.

31. Heffernan, P.J., Erki, M.A., (2004) “Fatigue Behavior of Reinforced Concrete Beams Strengthened with Carbon Fiber Reinforced Plastic Laminates”, Journal of Composites for Construction, V. 8, No. 2.

32. James, R. G., (1997) “ANACAP Concrete Analysis Program Theory Manual”, Version 2.1. Anatech Corp., San Diego, CA.

33. Japan Society of Civil Engineers, (2001) “Recommendations for Upgrading of Concrete Structures with use of Continuous Fiber Sheets”, Concrete Engineering Series 41, Japan.

34. Klaiber, F. W., Wipf, T.J., Kempers, B.J., (1999) “Field Laboratory Testing of Damaged Prestressed Concrete (P/C) Girder Bridges”, Iowa Department of Transportation Report HR-397.

35. Malek, A.M., Saadatmanesh, H., Ehsani, M.R., (1998) “Prediction of Failure Load of R/C Beams Strengthened with FRP Plate due to Stress Concentration at the Plate End”, ACI Structural Journal, V. 95, No.1.

36. Mirmiran, A, Shahawy, M., Nanni, A., Karbhari, V., (2004) “Bonded Repair and Retrofit of Concrete Structures using FRP Composites”, National Cooperative Highway Research Program (NCHRP) Report 514, Transportation Research Board.

37. Muller, J.F. and Dux, P.F., (1994) “Fatigue of prestressed concrete beams with inclined strands”, ASCE Journal of Structural Engineering, Vol. 120, No. 4.

38. Naaman, A.E., (1991) “Fatigue in partially prestressed concrete beams: summary of ten years of research”, International Symposium on Fatigue and Fracture in Steel and Concrete Structures.

39. Nanni, A, (1999) "Composites: Coming on Strong", Concrete Construction, vol. 44, p. 120.

40. Nanni, A., Di Ludovico, M., Parretti, R., (2004) “Shear Strengthening of a PC bridge girder with NSM CFRP rectangular bars”, Advances in Structural Engineering, Vol. 7, No. 4.

41. Oehlers, D.J., (1990) “Reinforced Concrete Beams with Plates Glued to their Soffits”, Journal of Structural Engineering, V.118, No. 1.

42. Oehlers, D.J., Seracino, R., (2004) “Design of FRP and Steel Plated RC Structures”, Elsevier Press, London.

43. Overman, T.R., Breen, J.E., and Frank, K.H., (1984) “Fatigue Behavior of pretensioned concrete girders”, Research Report 300-2F, Center for Transportation Research, Austin, TX.

44. Rabbat, B.G., Kaar, P.H., Russell, H.G., Bruce, R.N., (1985) “Fatigue tests of pretensioned girders with blanketed and draped strands”, PCI Journal, Vol. 105, No. 4.

45. Rao, C. and Frantz, G.C., (1996) “Fatigue tests of 27-year old prestressed concrete bridge box beams”, PCI Journal, Vol. 41, No. 5.

46. Reed, C.E., Peterman, R.J. (2004) “Evaluation of Prestressed Concrete Girders Strengthened with Carbon Fiber Reinforced Polymer Sheets”, ASCE Journal of Bridge Engineering, Vol. 9, No. 2.

47. Saito, M., and Imai, S., (1983) “Direct Tensile Fatigue of Concrete by the Use of Friction Grips”, ACI Journal, V. 80, No. 5, pp. 431-438.

48. Schiebel, S., Parretti, R., Nanni, A., (2001) “Repair and Strengthening of Impacted PC Girders on Bridge A4845”, Missouri Department of Transportation Report RDT01-017/RI01-016.

49. Schnerch, D., (2005) “Strengthening of Steel Structures with High Modulus Carbon Fiber Reinforced Polymer (CFRP) Materials”, PhD Thesis, North Carolina State University.

50. Sena Cruz, J.M. and Barros, J.A.O. (2004) “Bond Between Near-Surface Mounted Carbon-Fiber-Reinforced Polymer Laminate Strips and Concrete”, Journal of Composites for Construction, November/December 2004, pp. 519-527.

51. Shanafelt, G.O., Horn, W.B., (1980) “Damage Evaluation and Repair Methods for Prestressed Concrete Bridge Members”, NCHRP Report 226.

52. Smith, S.T., Teng, J.G. (2002a) “FRP Strengthened RC Beams. I: Review of Debonding Strength Models”, Engineering Structures, 24.

53. Smith, S.T., Teng, J.G. (2002b) “FRP Strengthened RC Beams. II: Assessment of Debonding Strength Models”, Engineering Structures, 24.

54. Stallings, J.M., Tedesco, J.W., El-Mihilmy, M., McCauley, M. (2000) “Field Performance of FRP Bridge Repairs.” Journal of Bridge Engineering, Vol 5, No. .5, pp. 107-113.

55. Takács, P. F., and Kanstad T., (2002) “Strengthening Prestressed Concrete Beams with Carbon Fiber Reinforced Polymer Plates”, NTNU Report R-9-00, Trondheim, Norway.

56. Teng, J.G., Chen, J.F., Smith, S.T., Lam, L. (2002) “FRP Strengthened RC Structures”, John Wiley and Sons, Ltd, England.

57. Tumialan, J.G., Huang, P.C, Nanni, A. (2001) “Strengthening of an Impacted PC Girder on Bridge A10062.” Final Report RDT01-013/RI99-041, Missouri DOT, St. Louis County, MO, 41 pp.

58. Walton, J.M., Yeung, Y.C.T., (1986) “The Fatigue Performance of Structural Strands of Pultruded Composite Rods”, Mechanical Engineering Publications Ltd.

59. Zobel, R.S. and Jirsa, J.O., “Performance of Strand Splice Repair in Prestressed Concrete Bridges”, PCI Journal v.43 (6) (1998) (72-84).

APPENDIX A – DESIGN EXAMPLE WITH RESPONSE 2000

A.1 Introduction

This appendix provides a design example to illustrate the various steps involved in the design of a CFRP strengthening system for a prestressed concrete bridge girder. The analysis is based on cracked section analysis which is performed using the Response 2000© analysis program. The program is available to download free of cost, along with the instruction manual, at http://www.ecf.utoronto.ca/~bentz/home.shtml.

A.2 Problem Statement

A simply supported 30 ft (9.14 m) concrete bridge girder prestressed with ten 0.4375 in (11.1 mm) diameter 250 ksi (1723 MPa) strands, as shown in Figure A.1, requires a 30 percent increase of its original service load carrying capacity. The bridge is currently rated to carry AASHTO HS-13 type loading. Assume in the design a possible future wearing surface of 2 in (51 mm).

Testing of core samples taken from the girder indicate a concrete compressive strength of 6000 psi (41.37 MPa). The cross sectional area of each strand is A_{ps} = 0.1089 in^2 (70.26 mm^2). Assume an initial prestress level of 0.7f_{pu} and a total prestress loss of 16 percent. Use the Ramberg-Osgood equation for the stress strain relationship of the strand:

$$f_p = E_p \varepsilon_{ps} \left[A + \frac{1 - A}{\left[1 + \left(B\varepsilon_{ps}\right)^C\right]^{1/C}} \right]$$

with constants with constants A = 0.025, B = 139, C = 6, E_p = 29000 ksi (200 GPa). Assume a rupture strain of 0.06 in/in.

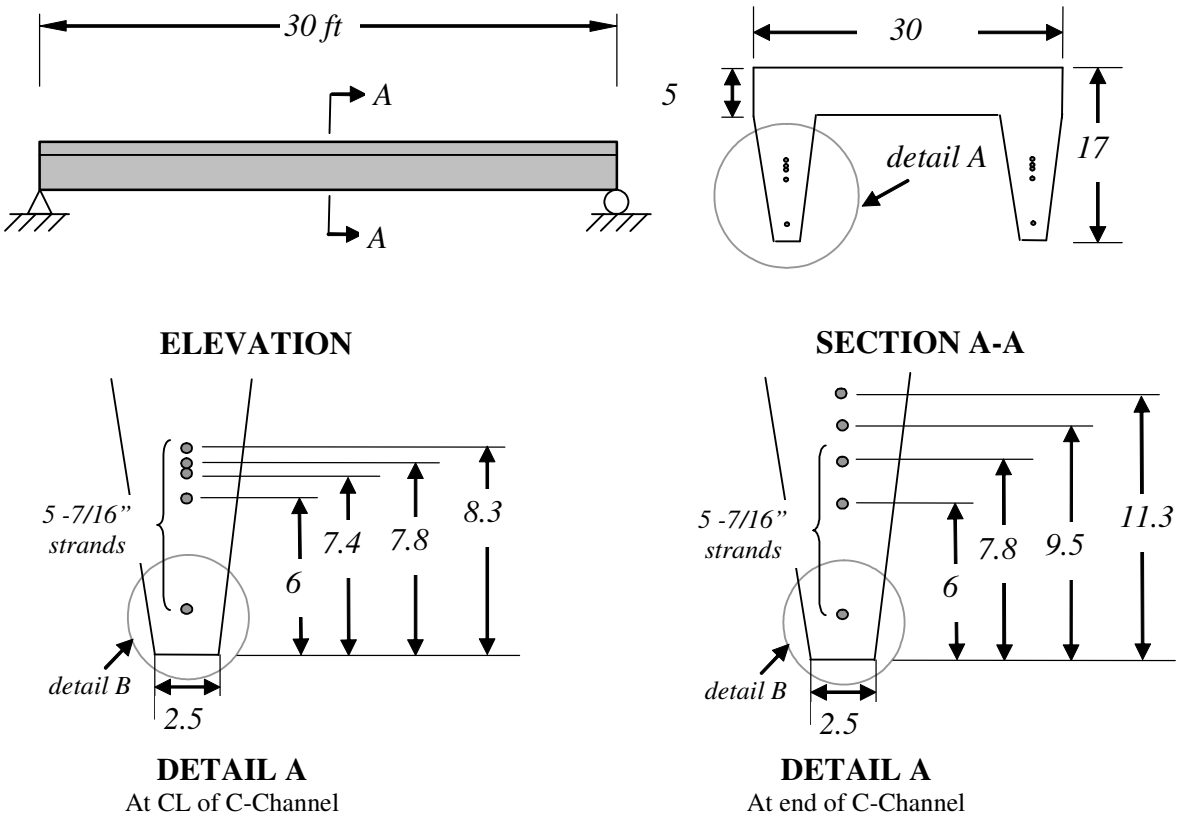

Figure A.1 Elevation and cross section of C-Channel girder to be strengthened with CFRP (in inches)

Non-prestressed reinforcement in the C-Channel consists of: four #3 (D10) bars in the deck and #4 (D13) open-leg stirrups spaced at 13 in (330 mm).

It is proposed to use externally bonded CFRP wet lay-up sheets as the strengthening system. The material properties provided by the manufacturer are:

Ultimate tensile strength $f^*_{fu} = 143$ ksi (986 MPa)

Rupture strain $\varepsilon^*_{fu} = 0.0103$ in/in

Laminate thickness $t = 0.04$ in (1.0 mm)

A.3 Analysis of the Unstrengthened Section

The first step in the design is to conduct a flexural analysis of the existing section in order to predict the behavior, including the ultimate flexural strength of the unstrengthened girder.

Input of the Material and Geometric Properties – It is assumed that the reader is familiar with the Response 2000© Instruction Manual. Additional recommendations for input are described below:

1) Due to limitations of the user-defined cross section tool of the program, the C-Channel girder must be input as a T-beam cross-section with equivalent sectional properties.
2) The material properties of the concrete can be automatically calculated by Response 2000© based on the stress-strain characteristics discussed in Section 5.3 for the given value of f'_c.
3) The material constants of the Ramberg-Osgood equation are required to define the characteristics of the type of prestressing steel used.
4) The prestrain in the prestressing strands can be calculated using the Ramberg-Osgood equation by first calculating the stress in one of the prestressing strands after losses:
   $f_{ps} = 0.7 \cdot f_{pu}(1 - 0.16)$
5) The slope of the three layers of inclined prestressing strands can be input as a percentage.

Moment-Curvature Response of the Section – Using Response 2000©, the moment versus curvature behavior of the prestressed section is easily obtained by clicking SOLVE >> SECTIONAL RESPONSE. The section response is shown in Figure A.2.

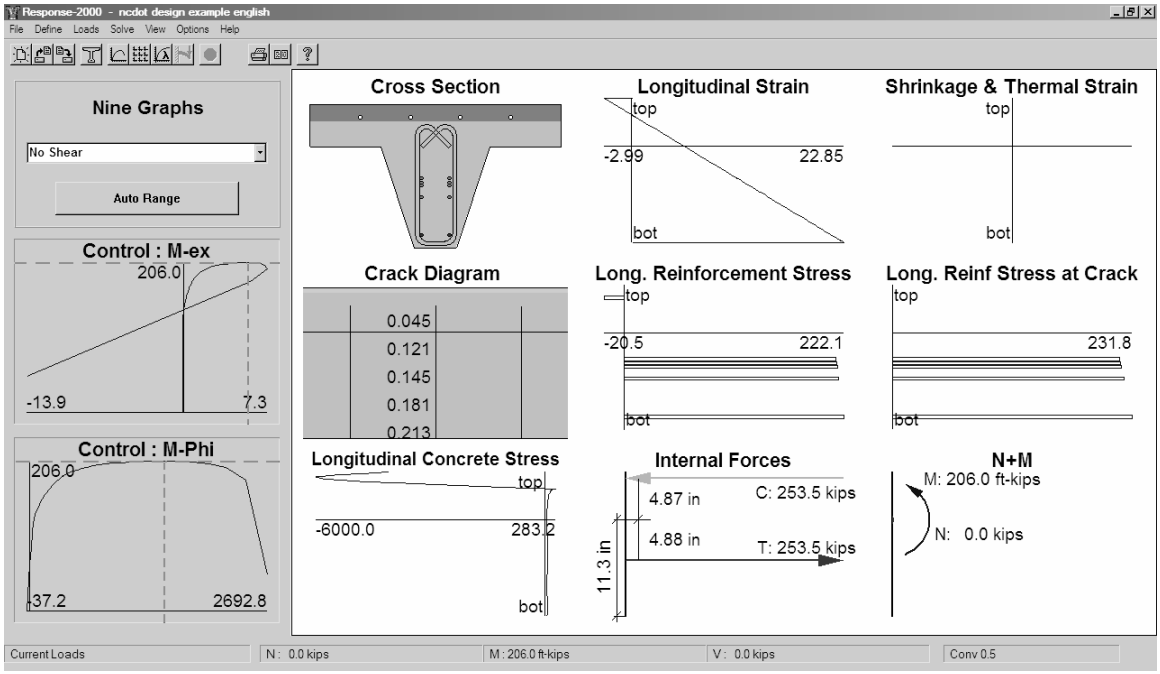

Figure A.2 Section analysis from Response 2000© of unstrengthened section

A.4 Design of Longitudinal CFRP

Design Material Properties – The properties provided by the manufacturer should be considered initial properties and should be appropriately reduced to account for environmental degradation. ACI 440F (2002) recommends an environmental reduction factor, C_E, of 0.85 to be applied to the ultimate tensile strength, f_{fu}^*, and rupture strain, ε_{fu}^*, provided by the manufacturer for Carbon Fiber Reinforced Polymer Materials subjected to exterior exposure. Therefore, the design ultimate strength, f_{fu}, and rupture strain, ε_{fu}, can be calculated as:

$$f_{fu} = C_E f_{fu}^*$$

$$= 0.85 \cdot (143)$$

$$= 121.5 \text{ ksi (838 MPa)}$$

$$\varepsilon_{fu} = C_E \varepsilon^*_{fu}$$

$$= 0.85 \cdot (0.0103)$$

$$=0.00876 \text{ in/in}$$

using the reduced properties, the elastic modulus of the CFRP, E_f, can be calculated:

$$E_f = \frac{f_{fu}}{\varepsilon_{fu}}$$

$$= \frac{121.5}{0.00876}$$

$$= 13880 \text{ ksi } (95700 \text{ MPa})$$

Input Material and Geometric Properties of CFRP– In consultation with the developer of the Response 2000© program, the procedure below should be followed for input of the material characteristics of CFRP.

1) The CFRP material properties should be input as "Longitudinal Reinforcement".
2) The "Elastic Modulus" should be input as E_{FRP}. The "Yield Strength" and "Ultimate Strength" should both be input as f_{fu}. The "e-Strain Hardening" can be entered as $1000 \times \varepsilon_{fu}$. The "Rupture Strain" should be entered as $2 \times 1000 \times \varepsilon_{fu}$, a value recommended by the developer of the program.
3) When defining the FRP as "Longitudinal Reinforcement", the appropriate area and location of the FRP should be specified, even if it is located outside the concrete cross-section.
4) Response 2000© will unrealistically predict a large horizontal shear crack in the cover concrete below the lower prestressing strand if the transverse non-prestressed reinforcement is terminated at the bottom of the web. The transverse steel should

extend to the centroid of the FRP to eliminate this problem; even though it will be located outside of the concrete cross-section.

Design of Longitudinal CFRP – The task of this step is to determine the amount of CFRP required to increase the ultimate capacity of the section by 30 percent. Based on the section analysis of the unstrengthened section, the ultimate moment capacity was found to be 206.0 k-ft (279.5 kN-m). We need to add sufficient CFRP to obtain an internal moment capacity of 267.8 k-ft (363.4 kN-m). After several trials, it was found that 1.5 layers of CFRP sheets per soffit, 4 in (102 mm) wide gives an area of CFRP, $A_{FRP} = (2.5)(0.04)(4)(2) = 0.48$ in^2 (516 mm^2) which satisfies our required moment capacity with a value of 266.2 k-ft (366.4 kN-m) as shown in Figure A.3. It should be noted that the mode of failure predicted by Response 2000© was concrete crushing for the unstrengthened section and FRP rupture for the strengthened section.

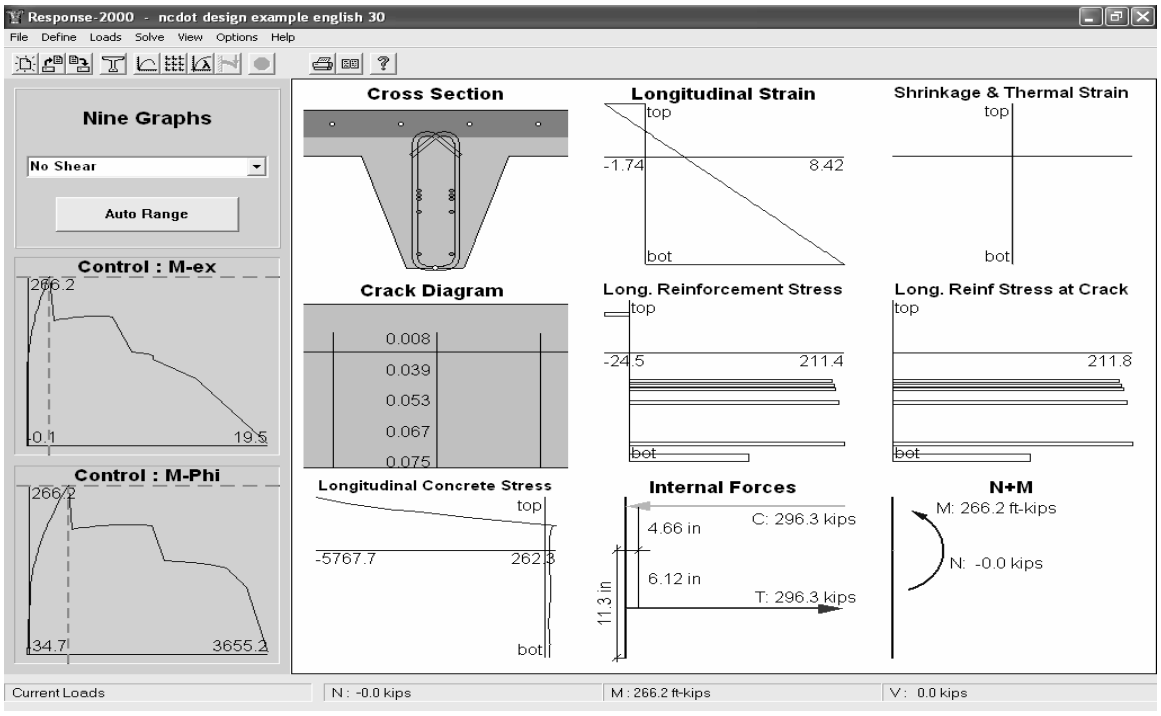

Figure A.3 Section analysis from Response 2000© of CFRP strengthened section

Stress Ratio in Prestressing Strands – According to design guidelines presented in this report, the stress ratio in the prestressing strands should be kept within limits specified in AASHTO Section 5.5.3.3 (2004), which for this girder is 18 ksi (125 MPa) for straight and 10 ksi (70 MPa) for harped prestressing strands. The dead load moment due to the self weight and the 2 in (51 mm) wearing surface can be determined assuming that the unit weight of concrete is 150 lbs/ft^3 (23.56 kN/m^3) as follows:

$\omega_{DLg} = 0.269$ k/ft (3.92 kN/m)

$\omega_{DLws} = 0.0628$ k/ft (0.916 kN/m)

$$M_{DL} = \frac{(0.269 + 0.0628)(30^2)}{8}$$

= 37.3 k-ft (50.5 kN-m)

AASHTO HS-13 loading was determined and the live load moment was found to be 58.4 k-ft (79.3 kN-m), including an impact factor of 1.33. For the girder strengthened with CFRP, since the live load is 30 percent higher, the fatigue moment range will vary between a minimum value of:

$M_{DL} = 37.2$ k-ft (50.5 kN-m)

and a maximum value of:

$M_{DL+LL} = 113.2$ k-ft (153.6 kN-m)

From the "Section Response" screen in the lower left corner is the "Control: M-Phi" plot. The cursor in this plot can be moved to show the corresponding strains, stresses and forces acting on the section at any given value of moment. At values of moments equal to the DL and the DL+LL shown above, the stress in the reinforcing can be determined using Response 2000© and is given in Table A.1. For the dead load plus live load moment, the stress shown at the cracked location

should be used. Using Equation 5.5, the stress ratio in the prestressing can be calculated for the 250 ksi (1723 MPa) prestressing strands.

Table A.1 Stress range in prestressing strands of strengthened C-Channel (from Response 2000©)

Prestressing strand location	bottom	3rd from bottom
Type of strand	straight	inclined
Stress at DL, ksi	140.0	142.4
Stress at DL+LL, ksi	152.9	146.4
Stress range, ksi	12.9	4
SR limit from AASHTO, ksi	18	10

The analysis indicates that the stress range in prestressing strands of the strengthened girder at the increased live load are below the specified values recommended in the design guidelines.

Ultimate Limit State – According to design guidelines recommended in this report, the factored moment due to the increased live load and dead load should not exceed the ultimate flexural moment resistance of the strengthened section. Since this design is solely concerned with the loads determined in Section 3.5.2, the limit state to be considered from AASHTO (2004) Article 3.4.1 is Strength I, the basic load combination relating to normal operation of the bridge without additional loads. From Table 3.4.1-2 the maximum dead load factor, α_D, for permanent component loads is 1.25, and similarly from Table 3.4.1-1 the live load factor, α_L, is 1.75. The dynamic load allowance, IM, is taken from Table 3.6.2.1-1 and is equal to 1.33 for the ultimate limit state. Therefore the total factored moment can be calculated as:

$$M_F = \alpha_D \cdot D + (\alpha_L + IM) \cdot L$$

$$= (1.25) \cdot (37.2) + (1.75 + 1.33) \cdot (58.4)$$

= 226.4 k-ft (307.4 kN-m)

The nominal moment resistance of the strengthened section should be reduced by the resistance factor, ϕ, which is 1.0 for prestressed concrete in flexure. For limit state Strength I, the ultimate moment resistance is $\phi \cdot M_n = (1.0)(270)$ which is larger than the factored moment, $M_f = 226.4$ k-ft (307.4 kN-m), therefore the strengthened section satisfies the ultimate limit state.

Intentional or Unintentional Damage Limit State – According to design guidelines presented in this report, the capacity of the original undamaged section should be more than the unfactored moment capacity, M_{UF} ,which can be calculated as:

$$M_{UF} = 37.2 + 58.4$$

= 95.6 k-ft(129.8 kN-m)

This is much less than the nominal moment resistance of the unstrengthened section, 203.9 k-ft (276.6 kN-m), so the girder is not in danger of collapse in case of intentional or unintentional damage causing sudden loss of the CFRP system under service load conditions.

Check Deflections – AASHTO (2004) specifies in Article 2.5.2.6.2 a maximum deflection, $\Delta_{\max}$, due to dead load and vehicular load of:

$$\Delta_{\max} = \frac{l_g}{800}$$

where l_g is the girder span. For our girder span this corresponds to 0.45 in (11.4 mm). The dead and live load moments found earlier can be resulting into concentrated loads at midspan from:

$$P_{DL} = \frac{(37.2)(4)}{30}$$

= 5.0 k (22.1 kN)

$$P_{LL} = \frac{(58.4)(4)}{30}$$

= 7.8 k (34.7 kN)

The service load level, P_s, at which the deflection should be calculated should include the dead load, P_{DL}, and the live load, P_{LL}, multiplied by the impact factor, IM, as follows:

$$P_s = 5.0 + 1.33 \cdot (7.8)$$

= 15.4 k (68.25 kN)

In Reponse 2000©, the full member response can be calculated by entering various properties under LOAD >> FULL MEMBER PROPERTIES. The values given below correspond to a simply supported girder, 30 ft (9.14 m) clear span, loaded with a concentrated load at midspan.

1) "Length subjected to shear" equal to half of the girder span, 14.6 ft (4570 mm).
2) "Constant Moment zone on right" equal to zero.
3) Use "Constant shear analysis", "support on bottom", and "Load on continuous beam, load on top", to create a simply supported girder.

The full member response of the girder can be calculated by clicking on SOLVE >> MEMBER RESPONSE. Due to symmetry, Response 2000© only calculates the response of half of the member, so the load versus deflection plot shown in the lower left hand corner is half of the actual member response. The deflection at half the service load, $P_s/2$, is 0.13 in (3.3 mm), therefore the AASHTO deflection criteria is satisfied.

A.5 CFRP Detailing

To control premature failures due to debonding as discussed in Section 2.9, the following detailing should be added:

1) The longitudinal CFRP sheets should be extended along the length of the girder. They should be terminated as close to the supports as possible during installation.

2) To control plate-end type debonding, transverse CFRP sheet U-wraps, 6 in (152 mm) wide, should be provided at the termination point of the longitudinal CFRP. The U-shape should extend to the top of the web on both sides.
3) Additional transverse U-wraps, identical to the ones described above, should be provided at 3 ft (330 mm) spacing along the length of the girder to control possible intermediate crack debonding.

APPENDIX B – PARAMETRIC STUDY

Using the design procedures outlined in Section A.4, a parametric study was performed to evaluate the various parameters believed to effect the CFRP strengthening applied to prestressed concrete C-Channel girders with a Type I prestressing configuration. The results of this parametric study are shown in Table B.1. The stress range relationship versus the level of strengthening is shown in Figure B.1.

Table B.1 Results of C-Channel strengthening parametric study

Level of strengthening	M_{ult}, design, k-ft	M_{DL+LL}, k-ft	A_{FRP}, in^2	Stress Range bottom (ksi)	Stress Range 3rd from bottom (ksi)
0	206.0	95.6	0	7.7	2.7
10	226.6	101.4	0.16	8.4	3.3
20	247.2	107.3	0.32	10.3	3.6
30	267.8	113.1	0.48	12.9	4.0
40	288.4	119.0	0.64	14.8	4.6
50	309	124.8	0.80	16.8	5.2
60	329.6	130.6	0.96	19.3	6.9
70	350.2	136.5	1.12	20.8	7.0

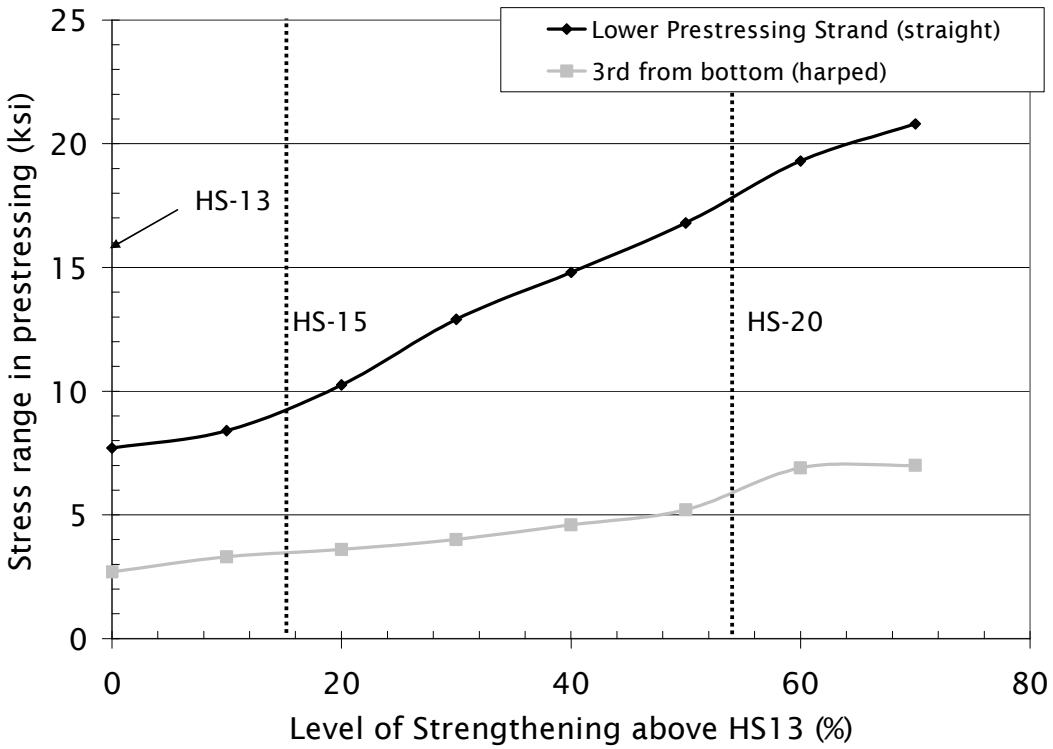

Figure B.1 Level of strengthening v. stress ratio in prestressing strands

The graphs indicates that C-Channel girders with Type I prestressing configuration can be safely upgraded to 50 percent above HS13 loading since the stress ratio for the straight and inclined strands are within the specified limits from AASHTO Section 5.5.3.3.